1966

An Experimental System for Beta and Gamma Ray Spectroscopy

Ora William Leisure

193

AN EXPERIMENTAL SYSTEM FOR BETA AND GAMMA RAY SPECTROSCOPY

By

ORA WILLIAM LEISURE

A thesis submitted
in partial fulfillment of the requirements for the
degree Master of Science, Major in
Physics, South Dakota
State University

1966

AN EXPERIMENTAL SYSTEM FOR

BETA AND GAMMA RAY

SPECTROSCOPY

This thesis is approved as a creditable and independent investigation by a candidate for the degree, Master of Science, and is acceptable as meeting the thesis requirements for this degree, but without implying that the conclusions reached by the candidate are necessarily the conclusions of the major department.

Thesis Adviser Date

Head, Physics Department Date

ACKNOWLEDGEMENTS

The author wishes to thank Dr. Hans G. Graetzer for his guidance and clarifying discussions concerning the work presented herein. It has been a privilege and a great experience to work with him.

The author is indebted to Dr. H. M. Froslie for the opportunity to work as a graduate assistant. The teaching experience was a most enjoyable one. Also, the financial returns were much appreciated by the author's family.

Gratitude is also extended to Dr. G. H. Duffey for the opportunity to have worked on his research program.

owl

TABLE OF CONTENTS

TABLE OF CONTENTS

TABLE OF CONTENTS

LIST OF FIGURES

LIST OF FIGURES

LIST OF FIGURES

LIST OF FIGURES

INTRODUCTION

A nucleus may be left in an excited state following a radioactive decay or nuclear bombardment process. However the lifetime of a nucleus in an excited state is usually very short[1] and the nucleus may undergo an electromagnetic transition to a less excited state. This transition from one nuclear state to another of lower energy can proceed by any one of three processes: gamma ray emission; internal conversion; and internal pair creation. The resulting nuclear state may be stable or further electromagnetic transitions and radioactive decay processes may follow.

Important information concerning nuclear properties can be obtained from experimental observations of the aforementioned nuclear electromagnetic transitions and particles emitted during any accompanying radioactive decay process. These observations, in general, can be put into four categories:

1) Energy and relative intensity measurements of gamma rays and internal conversion electrons determine the energy differences between nuclear levels and yield information concerning transition rates between levels. If sufficient energy is available such that the nucleus may de-excite by internal pair creation, then detection and measurement of the annihilation radiation energy that accompanies internal pair creation is desirable.

---

[1] The lifetime of an excited state is about 10^{-15} sec. but certain excited states called isomeric states have measurably larger lifetimes.

2) Energy and relative intensity measurements of particles emitted during any radioactive decay process preceding electromagnetic transitions yield information concerning transition rates between the product nucleus levels. If the decay process involves beta particle emission, then the beta spectrum and the decay half-life may yield information concerning angular momentum and parity assignments for the product nucleus levels.

3) De-excitation processes of nuclei are, in certain cases, very complex and result in a large number of gamma rays. A process may be such that several gamma rays are in cascade, and there may be several such cascade processes. If an excited nucleus is the product of beta particle decay, different excited nuclear states may result as a consequence of several beta end-point energies. Hence, determination of the various gamma-gamma and beta-gamma coincidences that may exist facilitates construction of an energy level scheme for the nucleus. If internal conversion transitions occur in the complex scheme also, it is then desirable to detect the internal conversion electron-gamma and internal conversion electron-beta coincidences that may exist.

4) Angular correlation between gamma rays emitted in cascade by an excited nucleus yields information concerning angular momentum and parity assignments for the excited levels of the nucleus. Here it is necessary to discern the number of coincidences as a function of the angle between the coincident gammas.

The purpose for the thesis project was to lay the experimental foundation necessary to make the observations noted above. The major part of this paper is devoted to description of the work engendered by this purpose. Preliminary information concerning one of the radioactive sources to be studied at a later date is also included.

CHAPTER I

GAMMA RAY SPECTROMETRY

A variety of methods for the measurement of gamma ray energies have been described in the literature.[2,3,4] Certain of these methods are only suitable for specialized problems; however, several methods merited further study with respect to project requirements and for historical reasons. These methods are:

1) measurement of absorption coefficients of well-calibrated absorbers
2) wavelength measurement by the curved crystal diffraction method
3) magnetic spectrometer analysis for,
   a) atomic electrons liberated during internal conversion
   b) photo-electrons, Compton electrons, and negatron-positron pairs that are liberated when the gamma rays interact with a thin absorber
4) gas-filled type proportional counters
5) scintillation type proportional counters
6) semi-conductor detectors

The main criteria for evaluating these methods concerning project requirements were: resolution; detection efficiency and source

---

[2] C. E. Crouthamel, Beta and Gamma-Ray Spectroscopy, Pergamon Press, New York, 1960.

[3] M. Deutsch and O. Kofoed-Hansen, in Experimental Nuclear Physics III, edited by E. Segre, Wiley and Sons, Inc., New York, 1959.

[4] D. E. Alburger, in Nuclear Spectroscopy, Part A, edited by F. Ajzenberg-Selove, Academic Press, 1960.

activity requirements, experimental complexity; and cost and availability.

An evaluation of the above methods indicated that a sodium iodide (thallium activated) scintillation detector coupled with a pulse height analyzer is the most judicious choice at the present time. As a consequence, a detailed discussion of the scintillation method will ensue next and a discussion of the other methods will be deferred until later in this chapter.

1. SCINTILLATION COUNTERS

Sodium Iodide Scintillation Crystal

A method of scintillation counting was first applied for detection of nuclear radiation by Crookes in 1903. This method required visual detection of the scintillations produced by absorption of alpha particles in thin films of zinc oxide crystals. By 1908, Crookes and Regener had developed an instrument known as the spinthariscope. It consisted of a 30X microscope with an objective of large numerical aperture, a zinc-sulphide copper-activated screen, an alpha particle source, and a vacuum tight box in which the above components, together with the absorbers under study, could be mounted. Despite the relatively unreliable technique of visually counting scintillations, well-known experimenters such as Rutherford and Chadwick utilized the spinthariscope in gathering high quality data and made many important contributions in nuclear research.

The visual scintillation counting method became obsolete in the 1930's with the advent of the gas-filled systems. However, with the increase in interest in gamma rays and the development of photo-multiplier tubes, scintillation techniques were re-considered. In 1948, Hofstadter[5] utilized a sodium iodide thallium-activated crystal to detect gamma rays. Here the scintillations were viewed by a photo-multiplier tube. This basic approach remains as one of the most useful techniques for medium energy gamma ray spectrometry.

A fundamental requirement for a scintillation crystal is that it convert, as fully as possible, the gamma ray energy to photons in the ultra-violet and visible regions. This is a region for which a number of sensitive photo-multiplier tubes have been developed. Just how fully the conversion will take place is dependent upon the basic interaction processes between the incident gamma ray and the scintillation crystal.

Gamma rays can possibly interact with matter by twelve different processes. However, it is found that three of these are adequate to describe absorption and scattering of medium energy gamma rays in matter: photoelectric effect; Compton scattering; and pair production. A discussion of these processes is given in the literature[6] and it is not intended to reproduce this information in detail. It will suffice here to say that the photoelectric effect refers to the complete absorption of a gamma ray when interacting with

---

[5] R. Hofstadter, Physical Review 74, 100 (1948).

[6] See for instance, Wm. F. Hornyak, Nuclear Spectroscopy, Part A, edited by F. Ajzenberg-Selove, Academic Press, 1960.

an atomic electron, Compton scattering refers to elastic scattering of a gamma ray by an atomic electron, and pair production refers to complete absorption of a gamma ray upon production of a negatron-positron pair in the electric field of a nucleus.

The photoelectric effect is mainly responsible for the primary interaction of incident gamma rays and matter for energies less than about 500 Kev. This is true if the material is of high enough atomic number and the gamma ray energy is sufficient to ionize K shell electrons of the material. The Compton scattering process is the predominant primary interaction from about 500 Kev to approximately 5 Mev. Above 5 Mev, pair production comes into prominence as the primary interaction. However, if the crystal is of sufficient volume and density, Compton scattered gamma rays and annihilation radiation following pair production may undergo one or more secondary interactions until absorption occurs by the photo-electric effect. It then appears that the photo-electric effect is largely responsible for the full conversion of the gamma ray energy. Of course, full conversion of gamma ray energies greater than approximately 1 Mev to a single photon pulse would not be possible unless the other two processes occur and the crystal does not resolve the multiple scattering events.

Examination of the absorption coefficient for various materials in the region where the photo-electric effect predominates reveals roughly a Z^5 dependence where Z is the absorbing material's atomic number. Since NaI is approximately 80% iodine by weight, nearly all of the gamma ray absorption takes place in the iodine. Since iodine

has a relatively high Z, scintillator crystals containing iodine have a decided advantage over the organic crystals, plastic phosphors, and many liquid phosphors. Absorption coefficients for the three predominant interaction processes and the total absorption coefficient for NaI are shown in Figure 1.

For reasons to be discussed later in this section, it is important that the photon output for a given incident gamma ray be as large as possible. This is accomplished for inorganic crystals by the addition of a trace impurity to the crystal. For NaI, the trace impurity is thallium in concentrations of about 0.1% to 0.5% by weight. The photon output of NaI for a given gamma ray is essentially constant over this range of impurity concentration. NaI(Tl) photon output is 3 to 4 times larger[7] than that from other inorganic crystals, and 2 to 10 times larger than that from organic crystals, plastic phosphors, and liquid phosphors.

In cases where source activity is very high, it is desirable that the conversion time from gamma energy to photon output be very short. This minimizes accidental summing between non-coincident gamma rays arriving at the crystal at nearly random coincidence. NaI(Tl) has the shortest decay constant[8] among the inorganic crystals but organic, plastic, and liquid phosphors have decay constants 1 to 2 orders of magnitude shorter than NaI. However, the latter scintillators are not useable for full gamma ray energy conversion because of their

[7] Harshaw Scintillation Phosphors, p. 10, The Harshaw Chemical Co., Cleveland, Ohio, 1962.

[8] Ibid., p. 10.

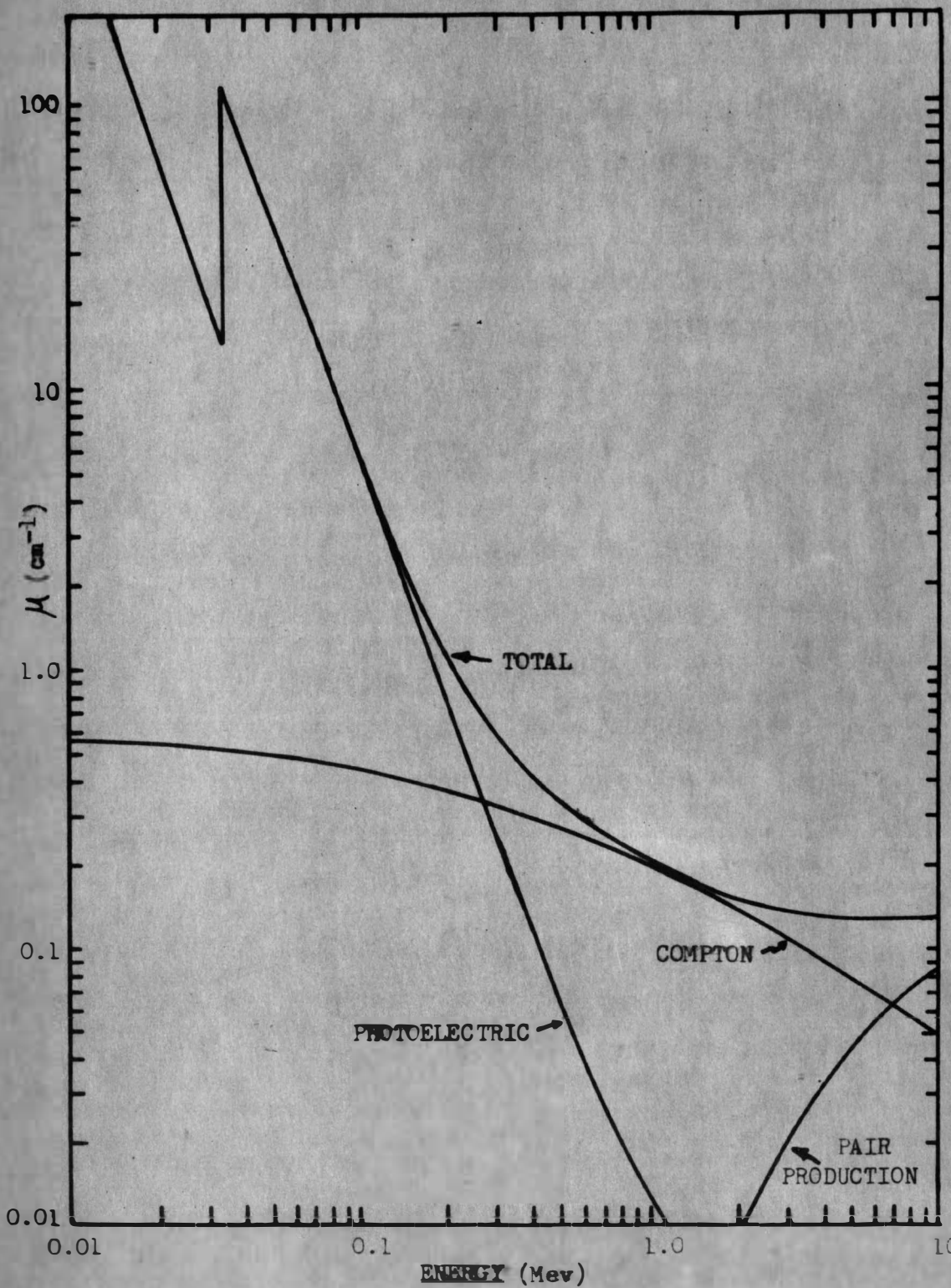

Figure 1. Absorption Cross Section for NaI Scintillation Crystal. From Harshaw Scintillation Phosphors. p. 11

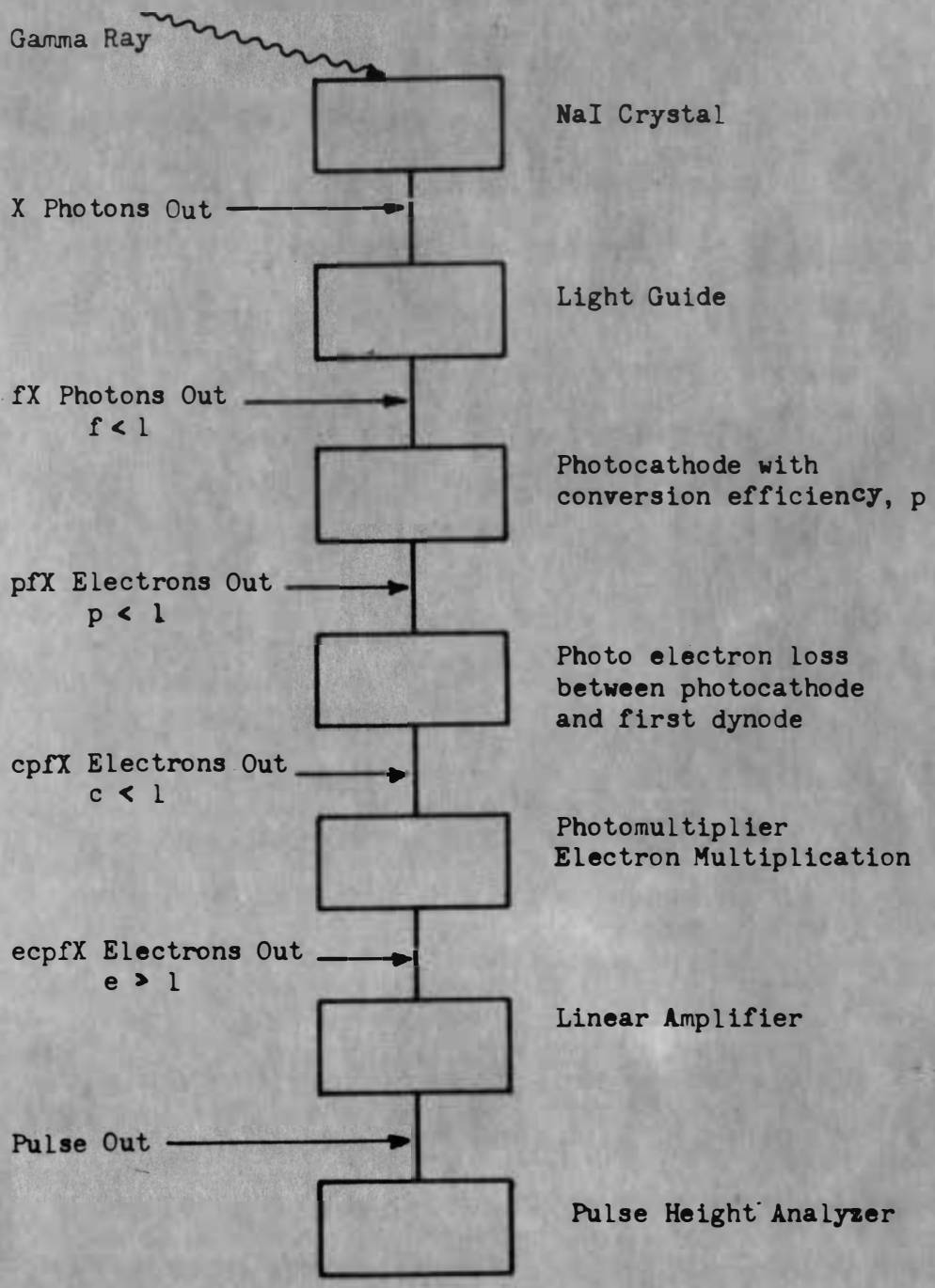

Figure 2. Pulse height reproduction and analysis chain.

Here E represents the energy corresponding to the peak of the distribution, and ΔE represents the full width of the pulse distribution at one-half E.

Breitenberger[9] has performed a theoretical study concerning scintillation spectrometer statistics and has developed the following expression for η.

$$\eta^2 = 8 \ln 2 \left[\frac{1+V_m}{\bar{X}\,\bar{T}} + V_T \right]$$

V_m is the variance due to the characteristics of the photomultiplier while V_T is the variance resulting from non-uniform transfer through each of the stages. Conversion variance due to lack of homogeneity and/or non-linear properties of the crystal, ripple or noise on the high voltage supply for the photomultiplier, non-uniformity of the photo-cathode, and non-uniform reflection of light in different parts of the crystal all contribute to V_T. $\bar{X}$ is the mean number of photons produced by the crystal for one scintillation, and $\bar{T}$ is the transfer efficiency of light photons to photoelectrons for each scintillation. T varies from one scintillation to the next because of the chance nature involved in the transfer stages. The fluctuation in T and X, the appropriate values for a given scintillation, ensures that the pulse height distribution will be nearly Gaussian. This last characteristic is sometimes helpful in deciding whether or not another unresolved

---

[9] E. Breitenberger, Progress in Nuclear Physics, vol. 4, p. 56 Pergamon Press, 1955.

peak may be present under a given pulse height distribution. For example, note the departure from a Gaussian distribution for the 600 Kev peak in Figure 3.

With reference to the expression for η, one notes that $\bar{X}$ and $\bar{T}$ should be maximized while V_M and V_T whould be minimized. The use of NaI (Tl) crystals yields an optimum $\bar{X}$ for presently available scintillators. This was discussed previously in this section. The equipment indicated by the pulse reproduction chain was purchased as a package and represents optimum minimization of factors contributing to V_T and V_M. The factors influencing $\bar{T}$ are optimized and non-adjustable for the same reason given for V_T and V_M with the exception of factors for the photomultiplier. Here a focusing shield (or guard ring) is placed at the periphery of the inner-electrode region between the cathode and first dynode. The voltage of this focusing shield is some fraction of the cathode to first dynode voltage and is usually variable. The variation in η with focus setting and photomultiplier anode voltage is shown in Figures 4 and 5. One notes that the focus setting is not critical.

The linearity of the pulse reproduction chain, including the external linear amplifier and the multi-channel analyzer was examined by noting the channel numbers (pulse height) corresponding to well-known gamma ray energies. This was performed for two frequently used instrument settings. The data is presented in two ways.

1) Channel number vs. gamma ray energy curves are presented in Figure 6.

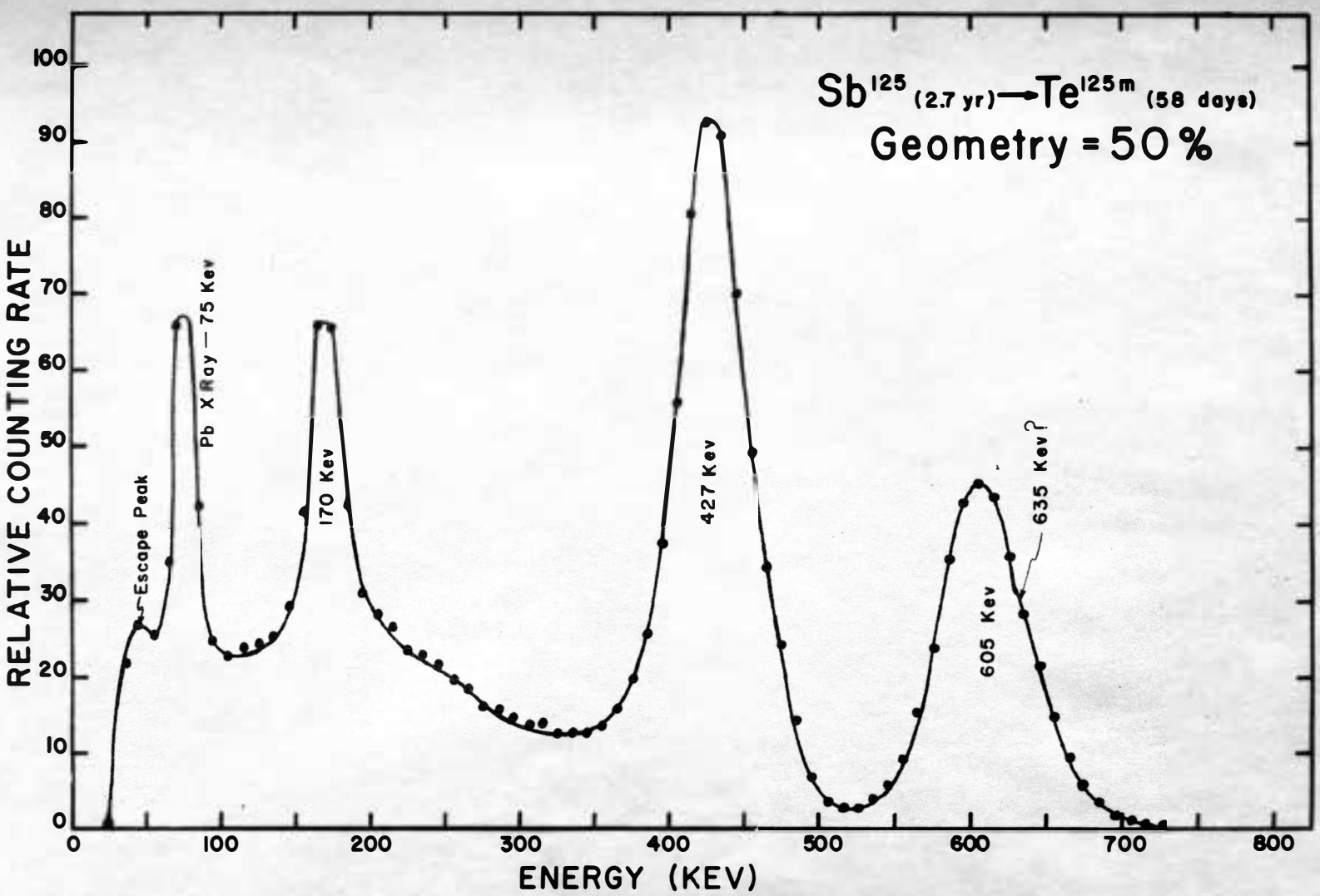

Figure 3. Sb^{125} gamma ray spectrum with radiation incident upon a 3 in. dia. by 3 in. thick NaI crystal.

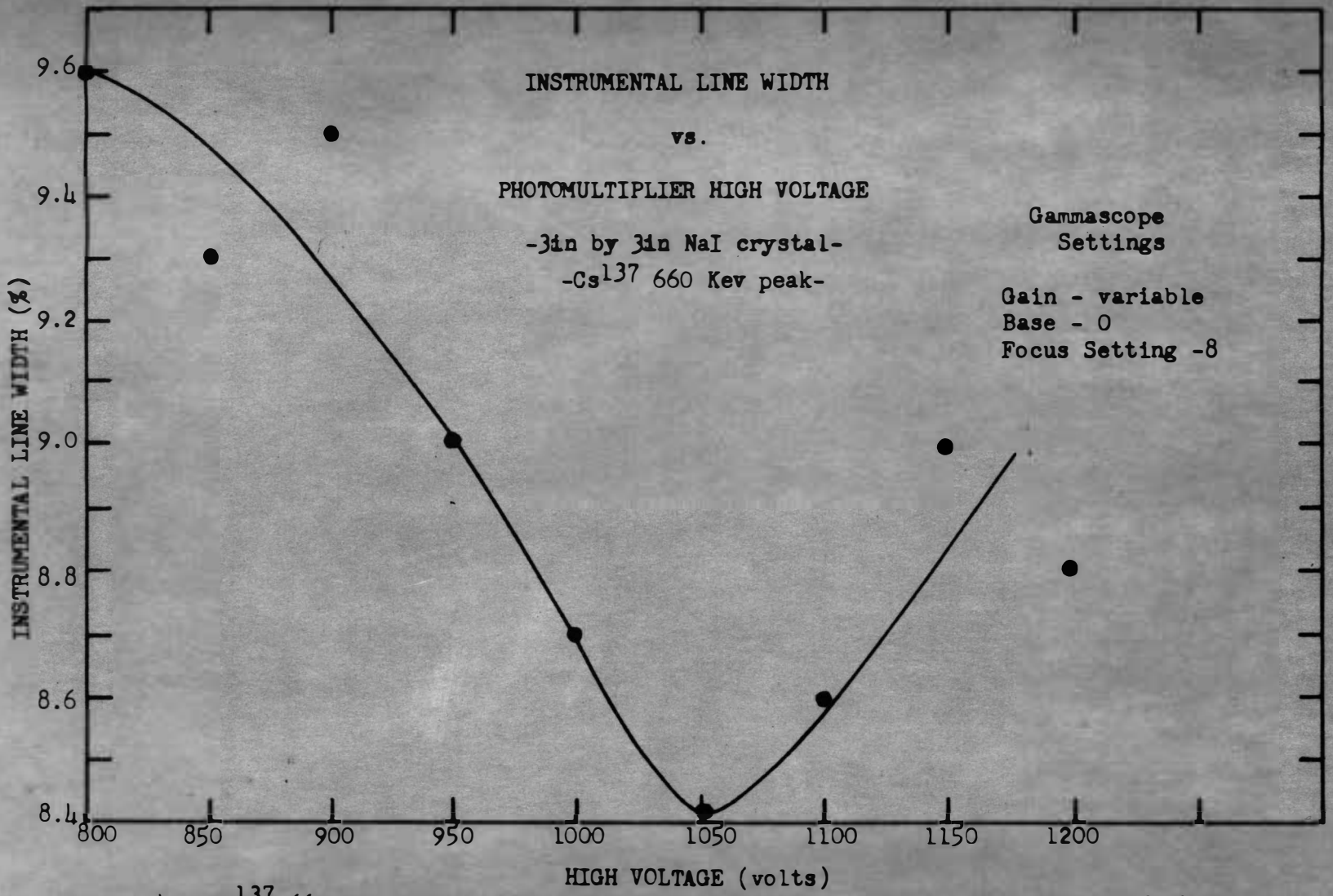

Figure 4. Cs^{137} 660 Kev peak instrumental line width at various anode voltages of photomultiplier for 3 in. dia., by 3 in. thick NaI crystal. Data taken with multichannel analyzer.

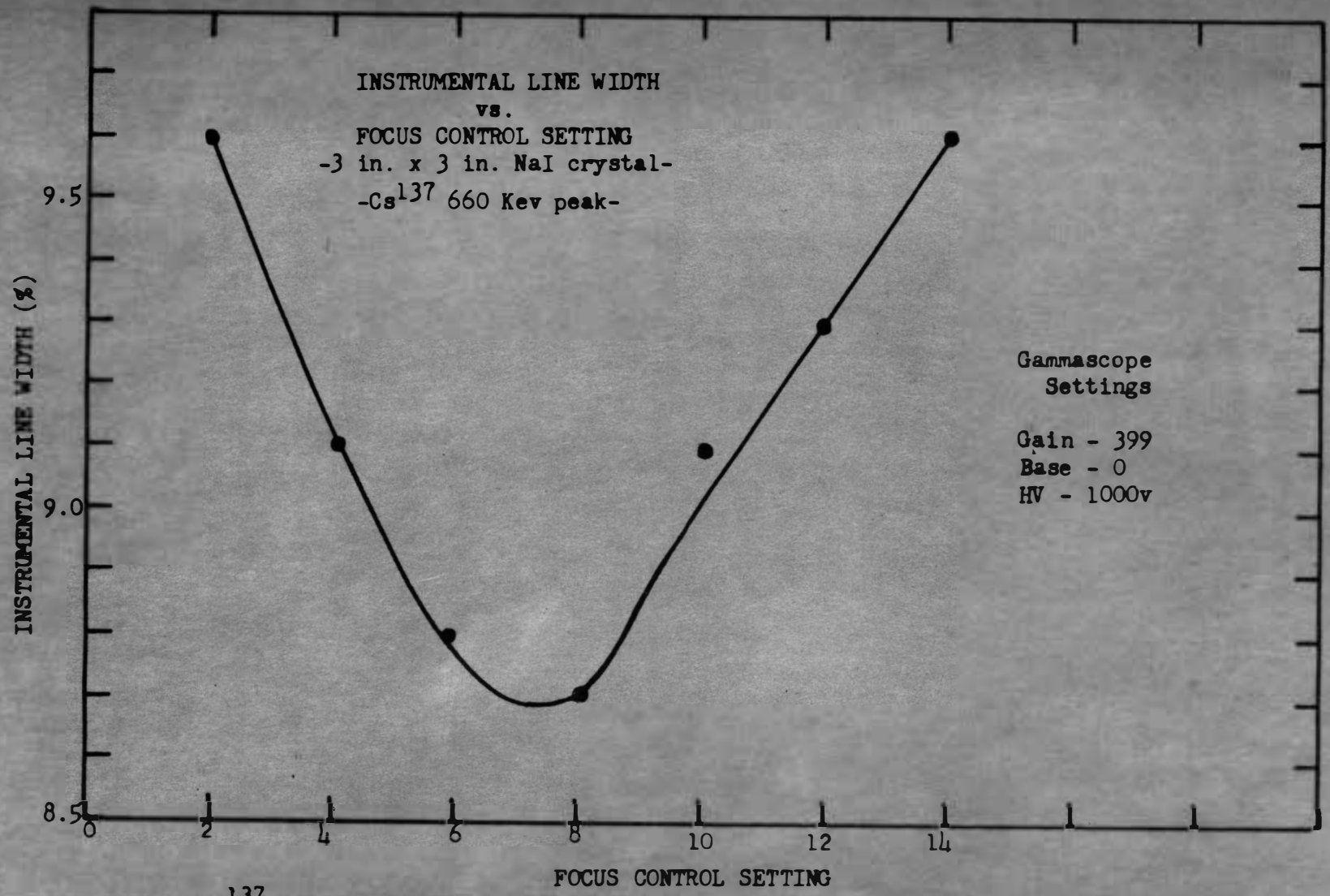

Figure 5. Cs^{137} 660 Kev peak instrumental line width at various focus control settings of photomultiplier for 3 in. dia. by 3 in. thick NaI crystal. Data taken with multi-channel analyzer.

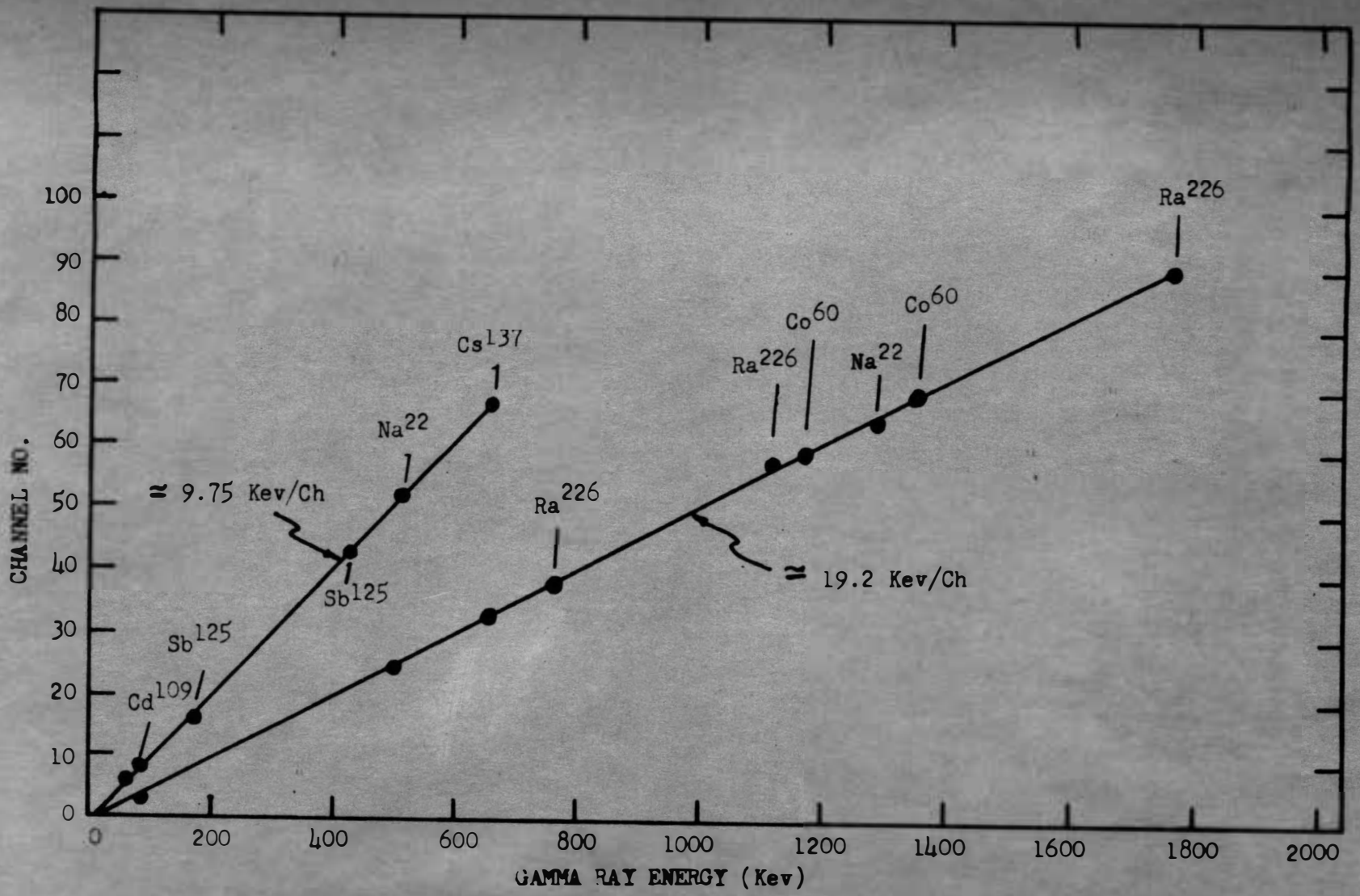

Figure 6. Linearity of NaI Crystal, Amplifier, and Multi-Channel Analyzer

2) Channel number/gamma ray energy vs. gamma ray energy curves are presented in Figure 7.

The curves in Figure 6 show no gross departure from linearity. The curves do not pass through the origin because a reference energy other than zero was used. The curves in Figure 7 are more sensitive to small departures from linearity and show a slight droop at the low energy end. This may indicate a slight deterioration of the crystal surface.

Pulse Height Analysis

The purpose of the pulse height analyzer is to determine the counting rate for a given pulse height increment that is small with respect to the maximum pulse height analyzed. If the pulse height increment (window) is kept constant in width, and its position relative to the pulse height reference is varied along the pulse height spectrum, then one can determine the counting rate for various pulse heights. Consequently all peaks in the counting rate, if any exist, can be identified provided that they are not obscured by background. The gamma ray energies causing these peaks can then be determined.

Two different analyzers which utilize variations of the above approach were employed on the project: a single channel analyzer (S.C.A.); and a multi-channel analyzer (M.C.A.). Description and operating procedures for the analyzers are presented in the instruction manuals provided by the manufacturers. Also, general

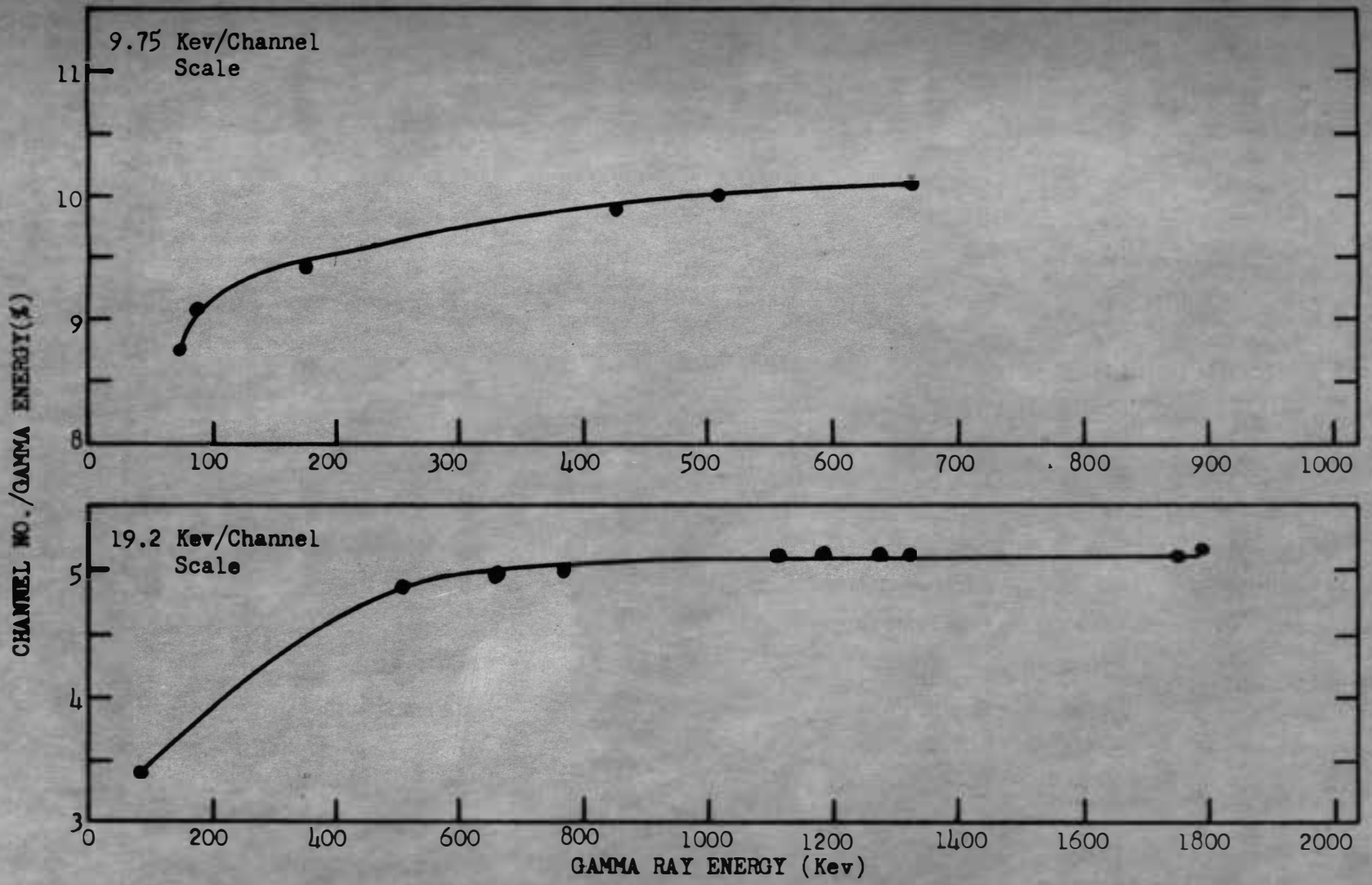

Figure 7. Linearity of NaI Crystal, Amplifier, and Multi-Channel Analyzer

design principles of pulse height analyzer electronic circuitry have been described in the literature.[10] Thus, it will suffice to present a brief, simple description which will emphasize a basic difference between the analyzers.

The operation of the S.C.A. is illustrated in Figure 8. Only pulse heights falling within the window are counted by the scalar. The pulse height corresponding to a given energy can be varied by adjusting the high voltage for the photomultiplier or the gain of the linear amplifier. In effect, this varies the energy scale over which the pulse height analysis occurs. The window, of adjustable width, can be set at different positions along the energy scale used by changing the baseline setting.

The operation of the M.C.A. is illustrated in Figure 9. Ninety-nine windows (channels) are located at fixed distances above the base setting. The distance of each channel above the base is proportional to the channel number, and the proportionality factor is determined by the photomultiplier high voltage and gain setting of the linear amplifier. The base setting determines the reference for the energy scale used and can be varied. It is sometimes desirable to analyze pulse heights over a limited number of channels. For this purpose, a superimposed window is provided whose position and width are adjustable by means of the threshold and upper level controls. The number of pulses falling in each channel are counted

---

[10] Robert L. Chase, Nuclear Pulse Spectrometry, chapters 3, 4, and 5, McGraw-Hill Book Co., Inc., New York, 1961.

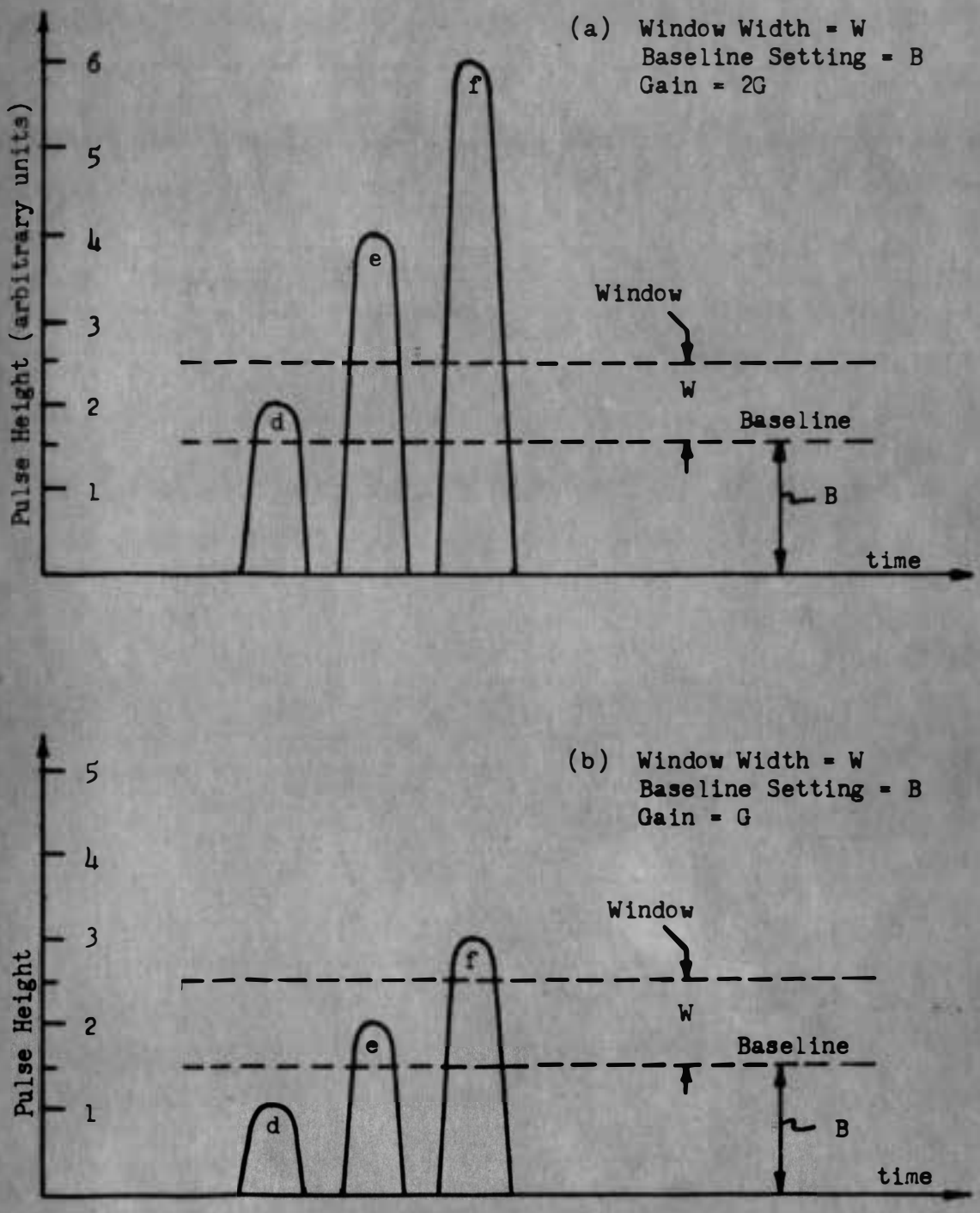

Figure 8. Illustration of Single Channel Analyzer Operation

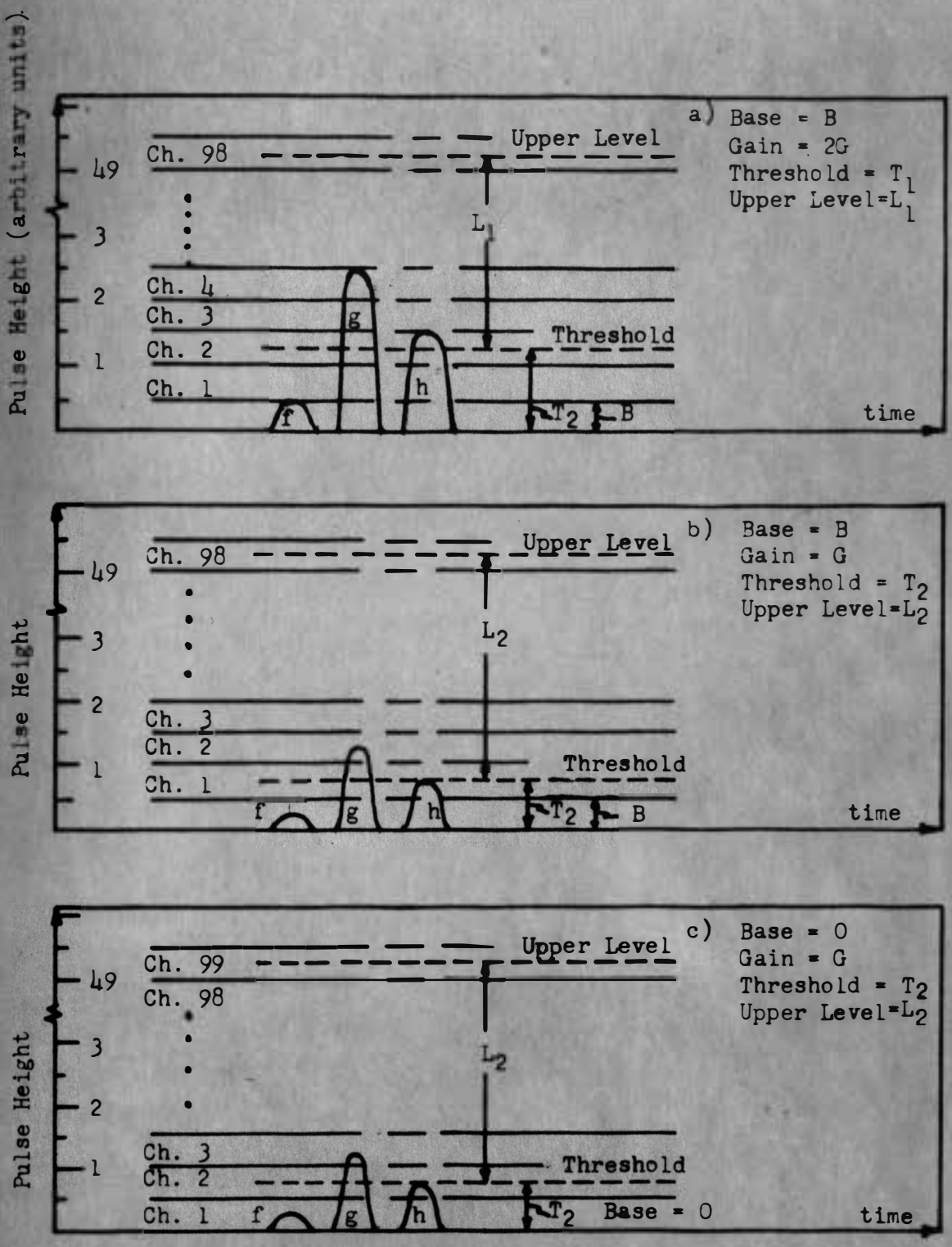

Figure 9. Illustration of Multi-Channel Analyzer Operation

and the information is stored until the end of the counting period. Then the number of counts in each channel is printed out on a paper tape. A cathode ray tube also presents a composite visual display of the information stored in the 99 channels.

The M.C.A. has additional circuitry available for single channel analyzer operation as well. Many other desirable accessories are available also and are adequately described in the instruction manual.

In order to assign energies to peaks in spectra, it is necessary to calibrate the pulse height analysis range used. This is most effectively accomplished by obtaining the spectra for several long half-life sources with peaks of well-known energy that are within the desired energy range. Then a curve similar to those in Figure 5 can be drawn and the conversion from channel number (or baseline setting) to energy can be made. Several good calibration peaks available are: Cd^{109} -- 88 Kev; Sb^{125} -- 175 Kev, 427 Kev; Na^{22} -- 511 Kev; Cs^{137} -- 662 Kev; Co^{60} -- 1.33 Mev, 2.5 Mev; and Ra^{226} -- 1.76 Mev.

The procedure above is tedious, particularly for the single channel analyzer. Thus, if an application does not require a critical calibration, then one peak of well known energy is adequate. However one should recall that, in the case of the M.C.A., the reference energy for a given scale is a function of the base setting and allow for this properly.

2. INTERPRETATION OF GAMMA RAY SPECTRA

The preceding discussion has been concerned mainly with the peaks that are a direct result of complete conversion of the gamma ray energy. However, peaks that are not the direct result of a complete gamma energy conversion arise in several ways.

1) partial gamma energy escape from the detector
2) partial gamma energy escape after interaction with matter surrounding the detector and source
3) atomic electron realignment after internal conversion or orbital electron capture
4) summing of 2 gamma rays in cascade by the detector
5) annihilation of a positron emitted during the radioactive decay of a nucleus
6) background radiation

These six cases are most effectively discussed with reference to spectra where they give rise to "false" peaks and other interesting spectral characteristics.

Internal Conversion X-Ray Peaks

The spectrum of a $Cs^{137} \longrightarrow Ba^{137m}$ decay obtained with the M.C.A. is shown in Figure 10. The 35 Kev peak can be interpreted in the following manner. After internal conversion occurs, realignment of the atomic electrons takes place. This can result in the emission of several x-rays characteristic of the product nucleus and/or Auger electrons. The x-ray emitted in the transition of an L shell electron

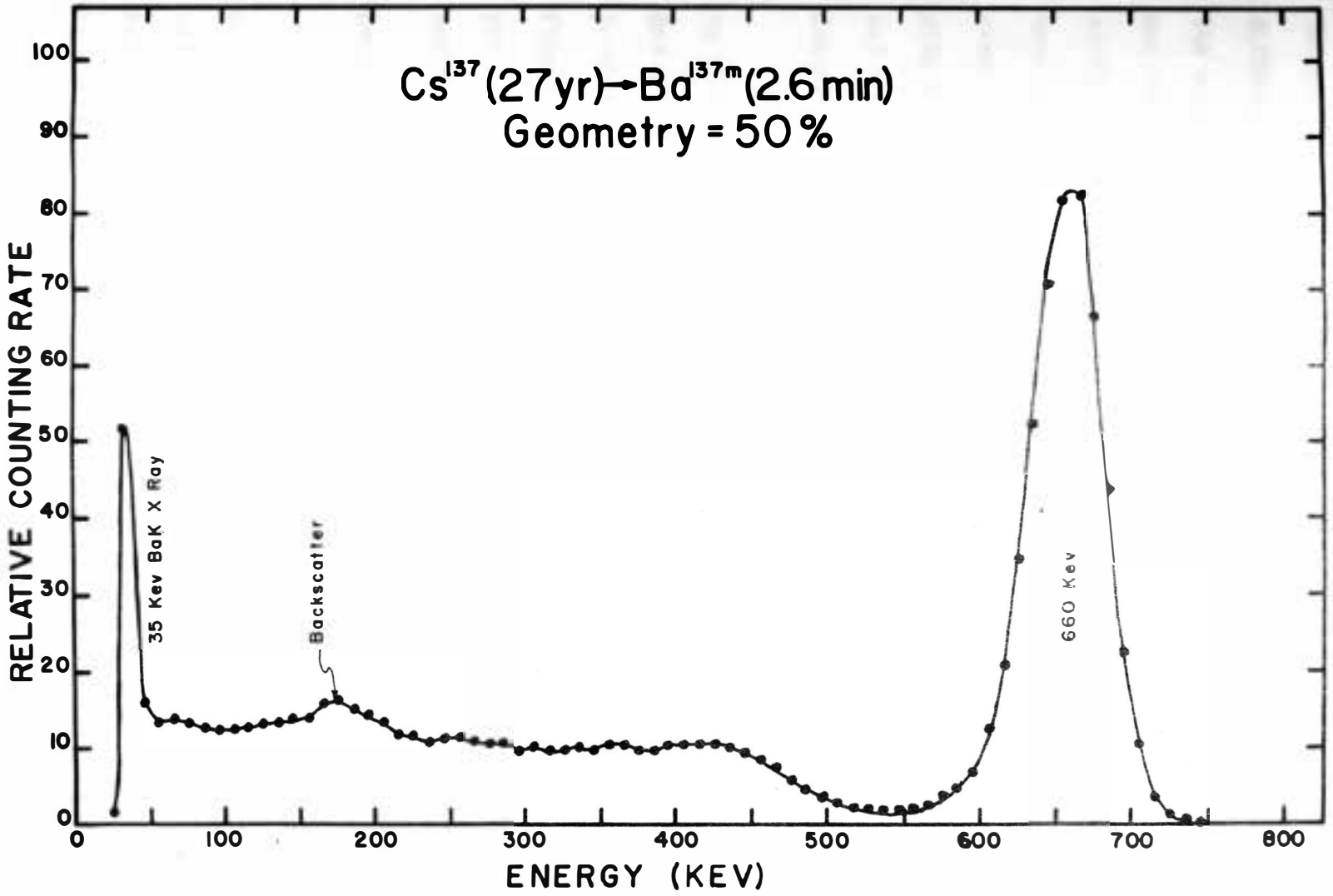

Figure 10. Cs^{137} gamma ray spectrum with radiation incident upon a 3 in. dia. by 3 in. thick NaI crystal.

to the K shell is usually of sufficient energy and intensity for detection by the NaI crystal. From previous knowledge of the difference in K and L shell binding energies, one can then predict the energy at which the product nucleus K x-ray peak should occur, and then determine if the experimental peak is consistent with this prediction. One should note, however, that the preceding discussion does not constitute a sufficient proof for identification as a Ba K x-ray peak. It is necessary to consider any gamma ray interactions with the surroundings, the tentative nuclear energy level scheme, and any conversion electron spectrum present before a positive identification can be made.

Precise determination of K x-ray energies are usually accomplished by other means such as curved crystal diffraction and proportional gas counter methods. The spectrum for the $Cd^{109} \longrightarrow Ag^{109m}$ decay in which Ag^{109} undergoes internal conversion was obtained for Figure 11 with a 3" x 3" NaI crystal and for Figure 12 with a proportional gas counter. Note the improved resolution in this energy region for the proportional gas counter.

Backscatter Peaks

The spectrum shown in Figure 10 contains a "false" peak denoted as a backscatter peak. This peak can be formed when primary gamma rays undergo a Compton scattering process in materials external to the detector. For appropriate scattering angles, the degraded gamma rays enter the detector and are counted. Backscatter peaks are characterized by broad, irregular peak distributions and are normally

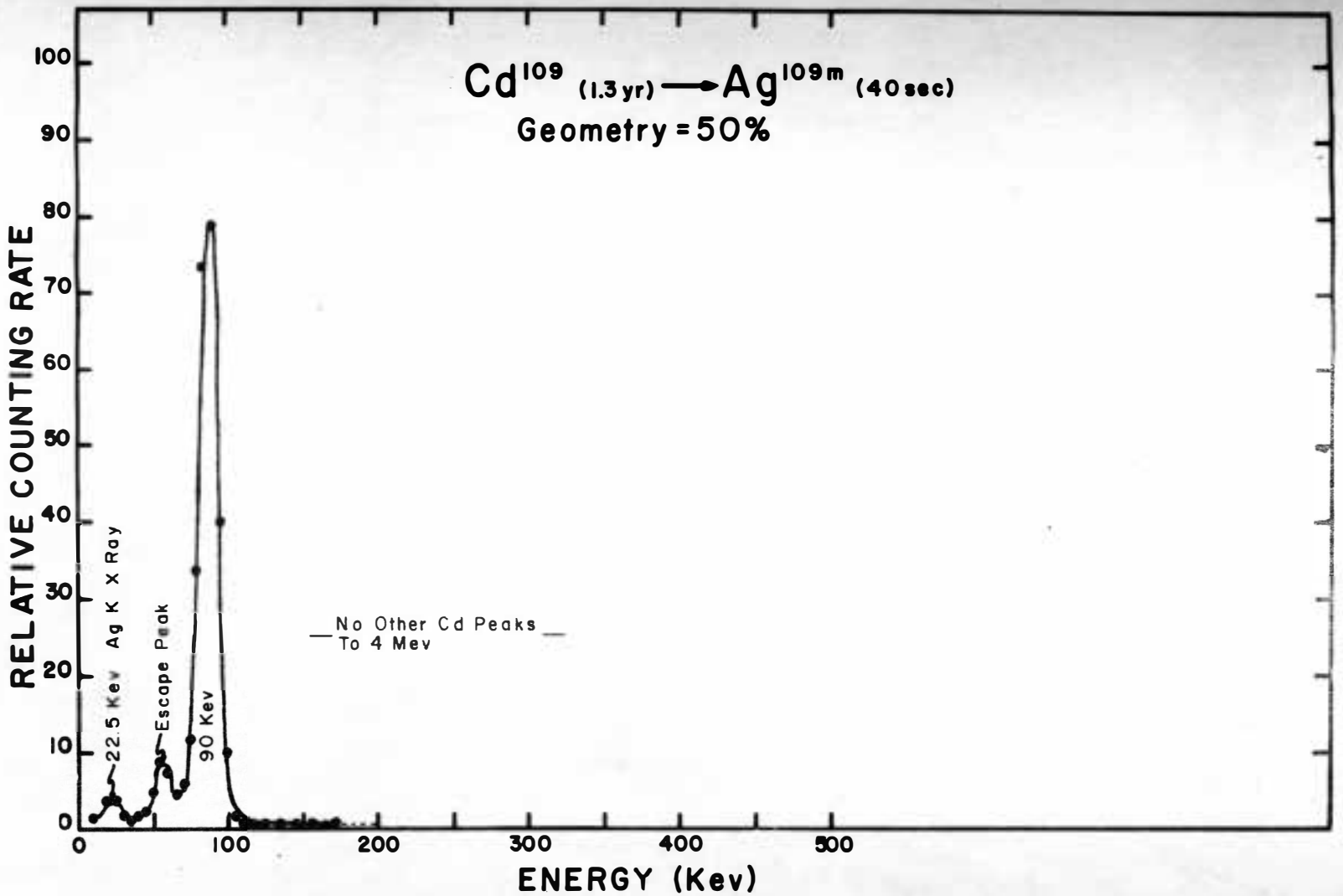

Figure 11. Cd^{109} gamma ray spectrum with radiation incident upon a 3 in. dia. by 3 in. thick NaI crystal.

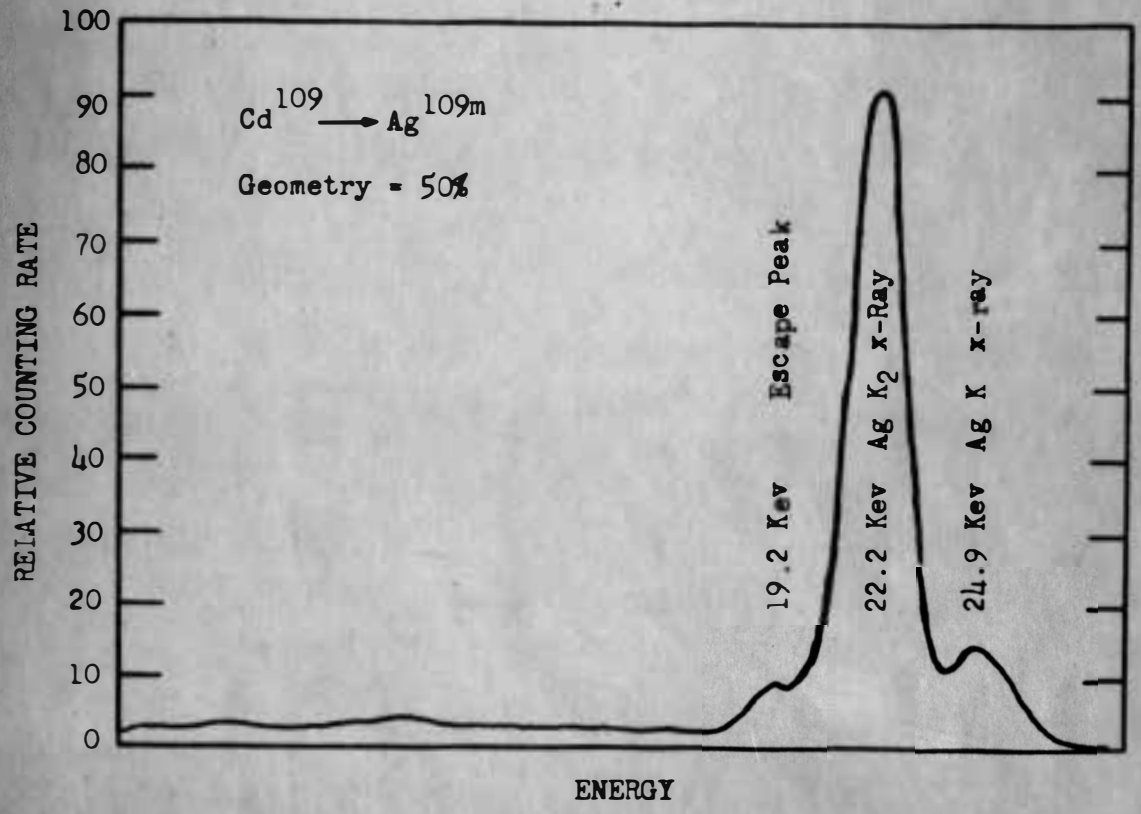

Figure 12. Cd^{109} decay spectrum for internal conversion peaks. Data obtained with proportional gas counter. From Crouthamel, p. 90

found in the 175 Kev to 200 Kev energy region for our experimental arrangement.

The support backings of many sources give rise to 180° back-scatter peaks. Also, preferential backscattering from the walls of the shielding cave and the detector housing may cause peaks and, in any event, raise the general background level. Backscattering from the cave walls may be minimized simply by making the cave dimensions large with respect to detector dimensions. However, availability of shielding materials and space requirements must be considered also in determining the cave dimensions. The cave used on this project is discussed later in this chapter.

Compton Scattering By Crystal

Another feature of any gamma ray spectrum is the crystal Compton scattering continuum that accompanies every full energy peak. While not necessarily a false peak, this continuum merits attention in that it represents an increase in the background for all peaks lower in energy than the full energy peak that it accompanies. This background increase may deteriorate the lower energy peak resolutions and may even obscure low intensity peaks.

The Compton scattering continuum is best discussed with reference to a monoenergetic gamma ray spectrum such as that in Figure 10. One of the prominant features of the spectrum is the pronounced dip in counting rate just before the full energy peak. This can be accounted for mainly by the fact that a maximum exists on the energy

transferred from a photon to a loosely-bound electron in a material during a single Compton scattering process. This is seen by examining the well known expression for an ideal Compton scattering process:

$$h\nu' = h\nu / \left[1 + (h\nu/m_0c^2)(1 - \cos\phi)\right]$$

Here $h\nu'$ is the energy of the scattered photon, $h\nu$ is the energy of the incident photon, m_0c^2 is the rest energy of an electron, and ϕ is the angle that the scattered photon makes with the direction of the incident photon. Maximum energy transfer results when $h\nu'$ is a minimum (when $\phi = 180^o$). Hence a single Compton scattering event will not be detected above this point of maximum energy transfer, and the counting rate should drop rapidly to background level between the Compton "edge" and the start of the full energy peak distribution. In other words, a pronounced dip in the counting rate should occur. Multiple Compton scattering processes in crystals of sufficient density and volume that end with escape of a degraded gamma ray can "fill in the valley" to some extent. However, multiple scattering processes ending with complete absorption by the photoelectric effect are more probable.

The gamma ray spectrum obtained with an anthracene crystal is shown in Figure 13. This spectrum has been included to illustrate the case for small volume and low density crystals where a single Compton scattering event is by far the most predominant process. Note the non-existence of the full energy peak and the sharp termination of the Compton scattering continuum. The slight increase in counting rate just before the Compton edge is sometimes referred

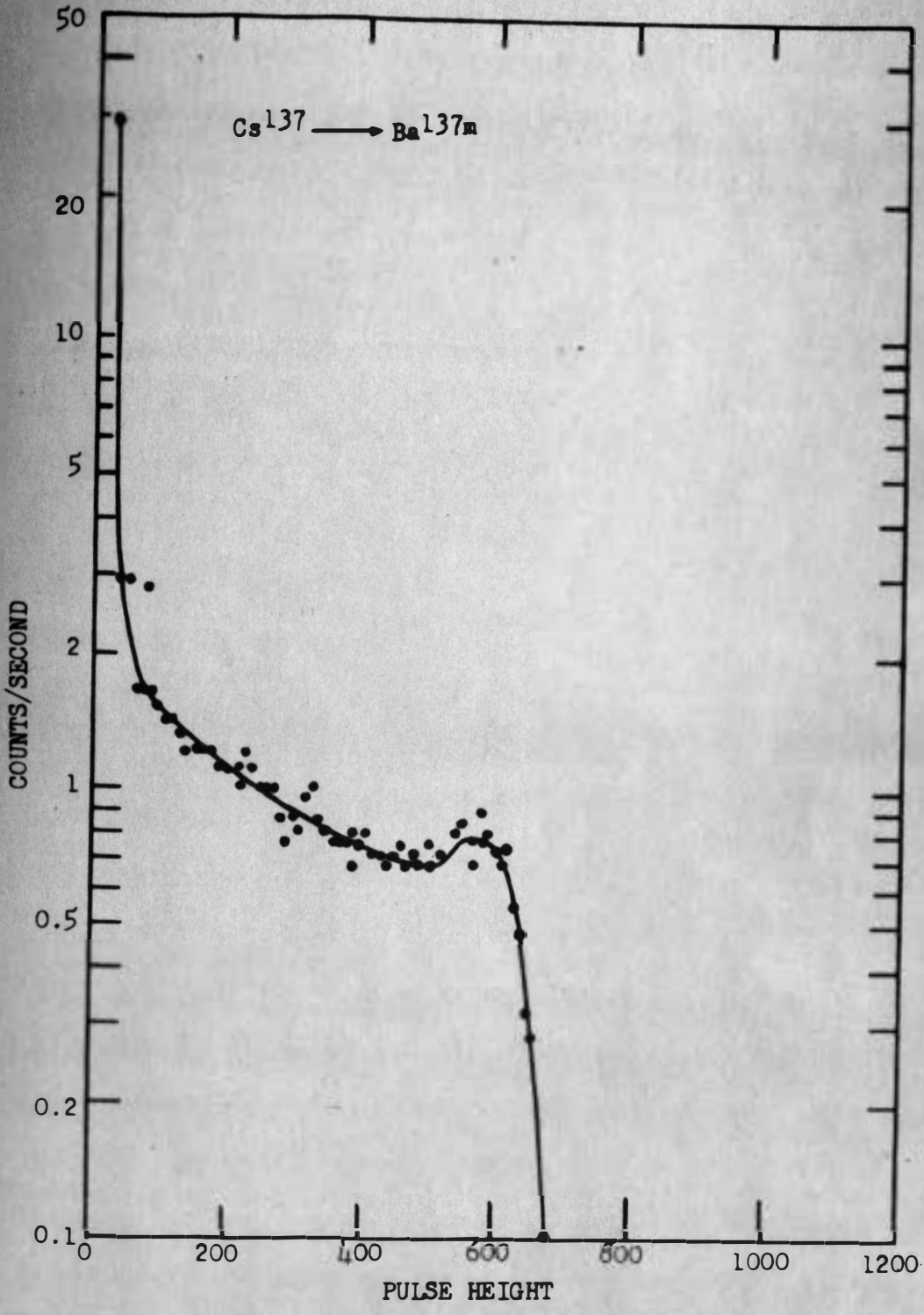

Figure 13. Gamma ray spectrum for Cs^{137} radiation incident upon anthracene crystal. From Harshaw Scintillation Phosphors, p. 21.

to as the "Compton peak" in the literature.

The problems in spectrum analysis that arise because of the Compton scattering continuum can be alleviated somewhat by a method known as spectrum "stripping".[11] Use of this method requires that one first obtain several monenergetic gamma ray spectra with the chosen experimental arrangement. The full energy peaks of these monoenergetic spectra should be well distributed over the energy scale to be used. After the spectrum for the source under study has been obtained, one fits the appropriate monoenergetic spectrum, full energy peak and continuum, to the corresponding peak in the spectrum under study. One starts with the highest energy peak obtained and subtracts out the fitted monoenergetic spectrum from the total spectrum. This procedure is repeated for progressively lower energy peaks. In other words, the spectrum under study is successively stripped away by this procedure. Computer programs for this method have been reported in literature[12] and merit further study with respect to this project.

Detection of the scattered gamma ray with anti-coincident counting techniques have been used also for suppression of the Compton scattering continuum.

---

[11] C. Sharp Cook and others, Physical Review 104, Oct.-Dec., 1956, p. 569.

[12] W. J. Price, Nuclear Radiation Detection, p. 200, McGraw-Hill Book Co., New York, 1964.

Iodine K X Ray Escape From Crystal

It was mentioned in the section on the NaI crystal that the photoelectric effect is the prominent gamma-ray absorption process in the low energy region. After photoelectric absorption of gamma rays, characteristic iodine K X rays are emitted during realignment of the atomic electrons. If the gamma rays are absorbed near the crystal surface, it is very probable that the iodine K X rays may escape from the detector. This has the effect of generating an "escape" peak which is 28 Kev (I K X ray energy) less than the corresponding full energy peak. An escape peak is easily noted in the $Cd^{109} \longrightarrow Ag^{109m}$ spectrum shown in Figure 11.

Escape peaks accompany only full energy peaks less than approximately 200 Kev. For higher energies, the penetration of the detector by the gamma rays is deeper on the average, and the probability of escape for iodine K X rays is lowered accordingly. Hence the escape peak is usually unresolved from the full energy peak for higher energies.

Annihilation Quantum Escape From Crystal

When the incident gamma energy exceeds 1.02 Mev,the energy necessary to create an electron-positron pair, part of the gamma ray energy can escape from the crystal in still a different way. The crystal can normally absorb the kinetic energies of the pair; however, either one or both of the 511 Kev quanta liberated upon annihilation of the positron can escape from the detector. This has

the effect of generating two escape peaks that are less by 511 Kev and 1.02 Mev than the corresponding full energy peak. The spectrum for the $Na^{24} \rightarrow Mg^{24}$ decay for which two quanta escape is easily detected is shown in Figure 14. The probability of just one of the 511 Kev quanta escaping from the detector is higher than that for both escaping simultaneously since they are emitted in nearly opposite directions. This means that if one annihilation quantum has a good chance of escaping, thus indicating a short distance to the crystal surface, then the other has a longer distance to travel before escape is possible. This fact accounts for the difference in counting rate between the two annihilation quantum escape peaks. In many instances, the lower energy escape peak is unresolved.

Detector Sum Peaks

Certain excited nuclei decay by the emission of two or more gamma rays in cascade. This process is illustrated for Co^{60} decay in Figure 15. If the intermediate states have very short half lives such that the total delay in the transition to the ground state is less than the resolving time for the detector, then a peak corresponding to the summation of the gamma energies in cascade will appear in the spectrum. Spectra in which summation peaks occur are shown in Figures 14 and 16. Note that the gamma rays experiencing summation also give rise to single peaks of appropriate energy. Further, these peaks have an appreciably greater counting rate than the summation peak. This effect can be explained by briefly examining the orientation

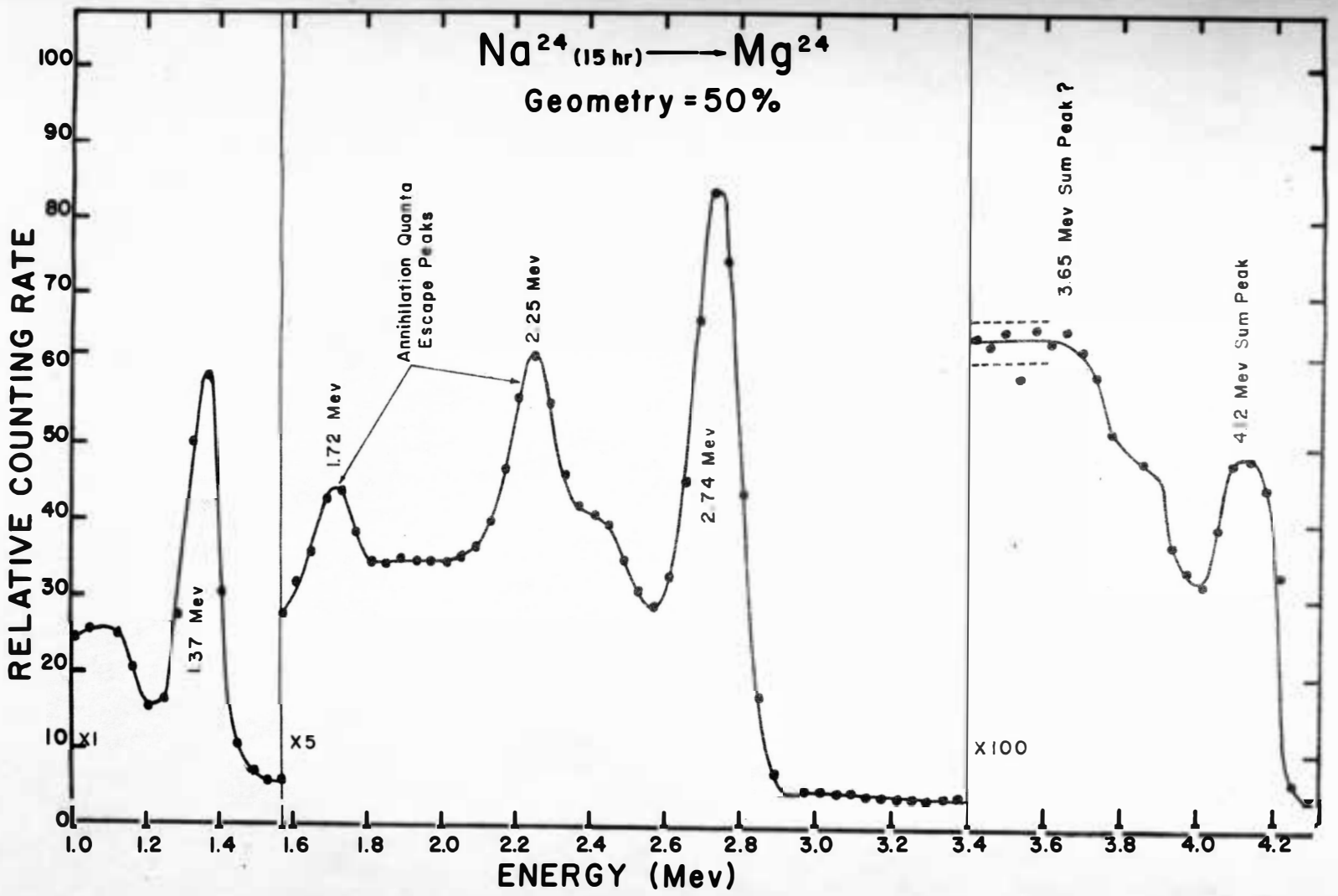

Figure 14. Na^{24} gamma ray spectrum with radiation incident upon a 3 in. dia. by 3 in. thick NaI crystal.

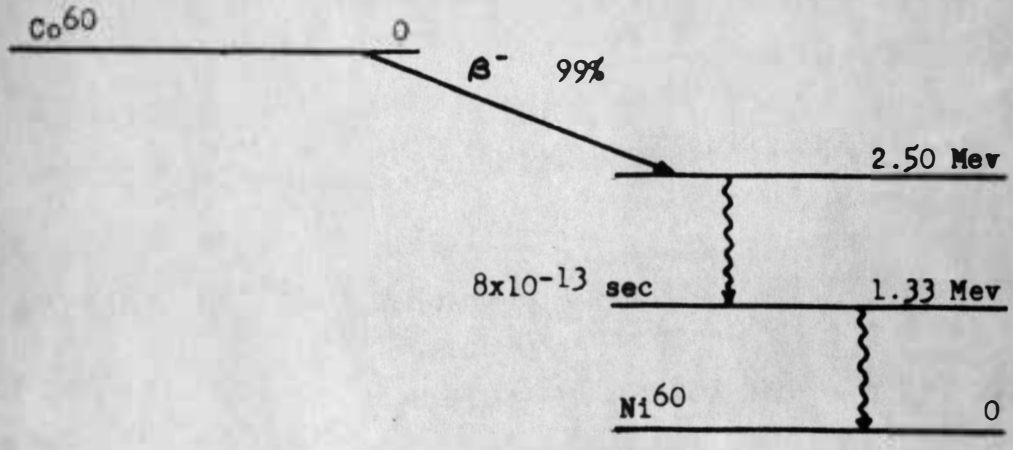

Figure 15. $Co^{60} \longrightarrow Ni^{60}$ Decay Scheme Showing Gamma Rays in Cascade.

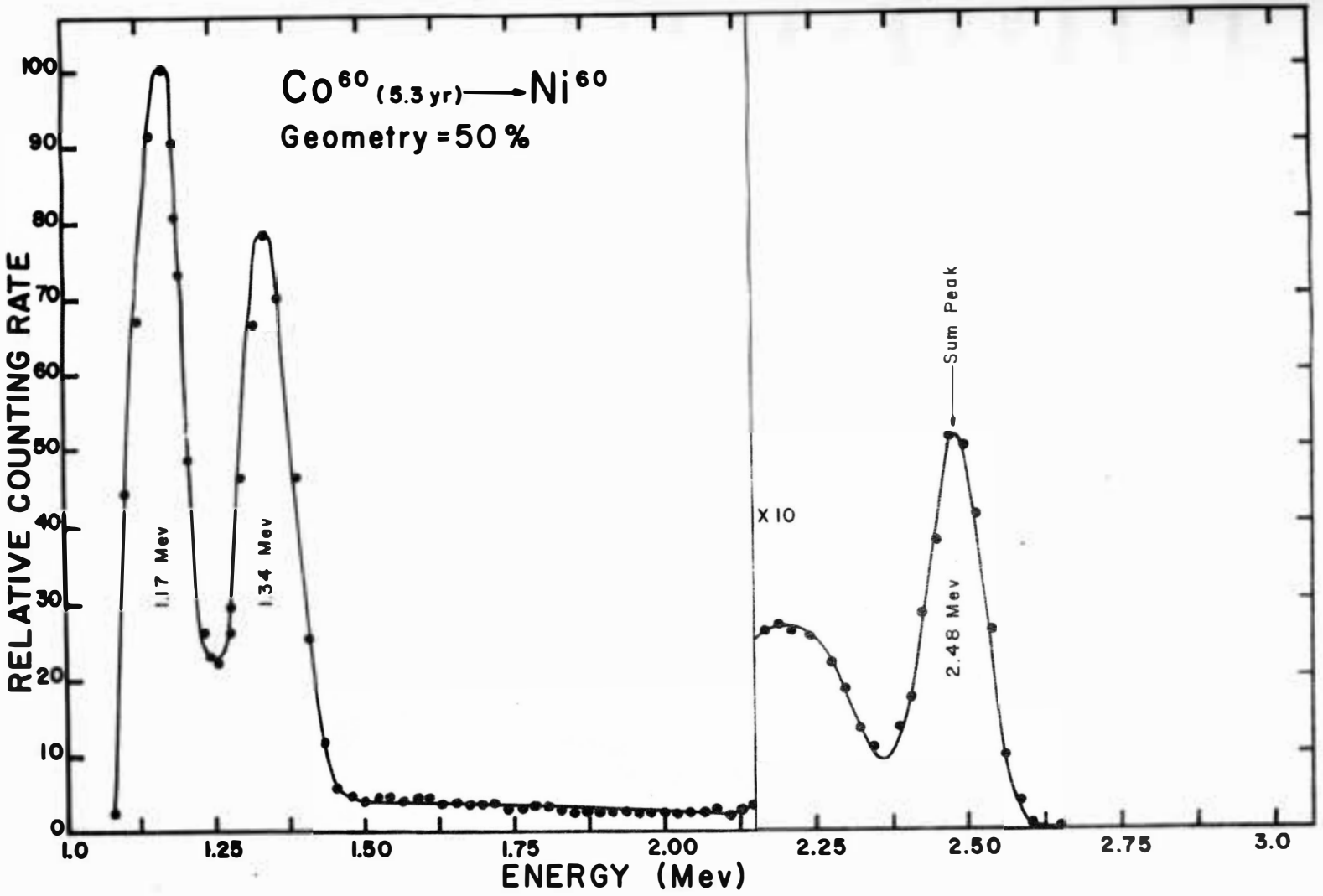

Figure 16. Co^{60} gamma ray spectrum with radiation incident upon a 3 in. dia. by 3 in. thick NaI crystal.

of the emitted gamma rays.

For individual nuclei, it is found that the probability of emission of a gamma ray in a given direction is roughly a function of the angle between the nuclear spin axis and the direction of emission. At room temperature, however, the nuclei in a macroscopic source are randomly oriented and the emitted radiation is isotropic. If each nucleus emits two gamma rays in cascade, the detection rate of each singly is a function of the solid angle subtended at the crystal by the source and the detector efficiency. The detection of one of the cascade gamma rays selects a nucleus with a particular spin orientation. The other cascade gamma ray from the same nucleus has a certain probability for emission in a given direction as discussed previously, and it is found that the probability of both cascade gamma rays being emitted in nearly the same direction is very low. The probability of coincident detection is a complicated function showing dependence on solid angle, detector efficiency, and the emission probability distribution for the gamma rays. Generally, it increases rapidly at first with increasing solid angle but is still appreciably less than the probability for single gamma ray detection. Hence a difference in the counting rates for the single peaks and the sum peak will exist as was noted experimentally.

The above discussion also indicates how a sum peak can be distinguished from a bonafide single energy peak. If the source is moved away from the detector such that the solid angle subtended becomes smaller and smaller, the sum peak height will decrease more

rapidly than the single energy peak heights.

Positron Annihilation Detection

A number of excited nuclei decay by emitting a positron. The shape of the positron's energy spectrum is analogous to that for a B^- particle except that the endpoint energy is 1.02 Mev less than the mass difference of parent and daughter atoms. A positron exhibits the same characteristics as an electron with the exception of charge sign; thus it is stopped fairly easily in any beta absorbing material near the detector. The positron is then annihilated with subsequent emission of two 511 Kev photons in nearly opposite directions. If one of the photons has proper direction for entering the crystal, then the other will not and has at best only a grazing incidence with the crystal. The photon that enters the detector gives rise to a corresponding full energy peak called the annihilation peak in the source spectrum under study. The spectra shown in Figures 17 and 19 contain annihilation peaks which indicates that the two parent isotopes decay, at least in part, by positron emission.

Background Radiation

Many radioactive sources are of low activity and it is frequently necessary to count over long time periods in order to obtain good statistics. However, radiation from other sources external to the sample under study may decrease resolution and introduce extraneous peaks in the spectrum. The spectrum shown in Figure 18 is that

obtained with a 3 inch diameter x 3 inch thick NaI crystal for background radiation in room B02 - Old Engineering Hall. One spectrum is for the detector shielded by iron and lead and the other is for the detector unshielded. Note that a peak is present at approximately 1.46 Mev in both spectra. This peak probably arises from K^{40} activity which is present in many materials as a trace impurity and has a half-life of approximately 10^9 years. The presence of this peak in both spectra may indicate that K^{40} is present in the detection apparatus in trace amounts. This observation has already been noted in the literature.[13] Another resolved peak of low intensity is present at approximately 600 Kev in the spectrum for the detector unshielded. This peak may arise from Ra^{226} activity (1600 year half-life) since Ra^{226} is present in many materials as a trace impurity.[14] Note that the 600 Kev peak is not resolved in the spectrum taken with the detector shielded.

[13] C. E. Crouthamel, op. cit., p. 82.
[14] Crouthamel, op. cit., p. 82.

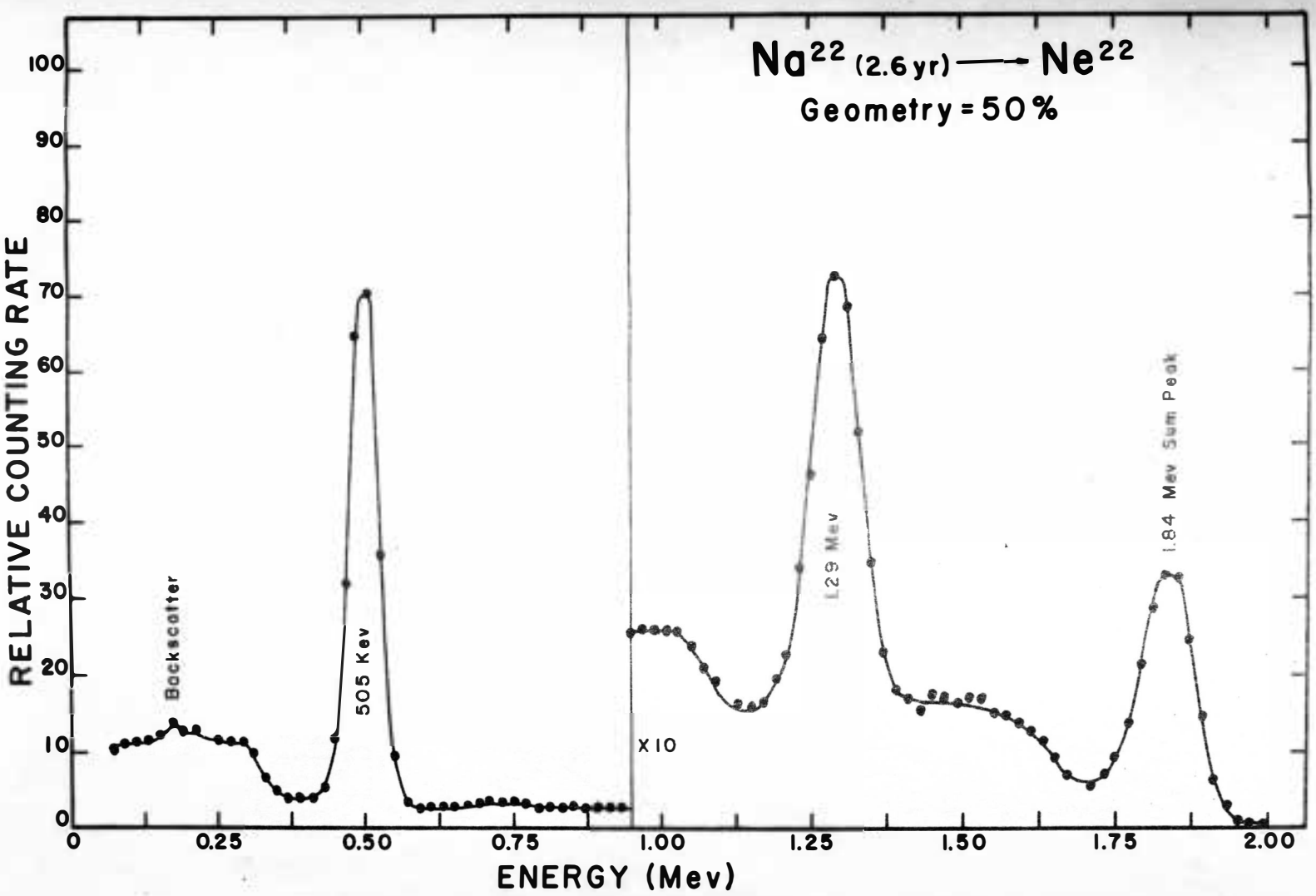

Figure 17. Na^{22} gamma ray spectrum with radiation incident upon a 3 in. dia. by 3 in. thick NaI crystal.

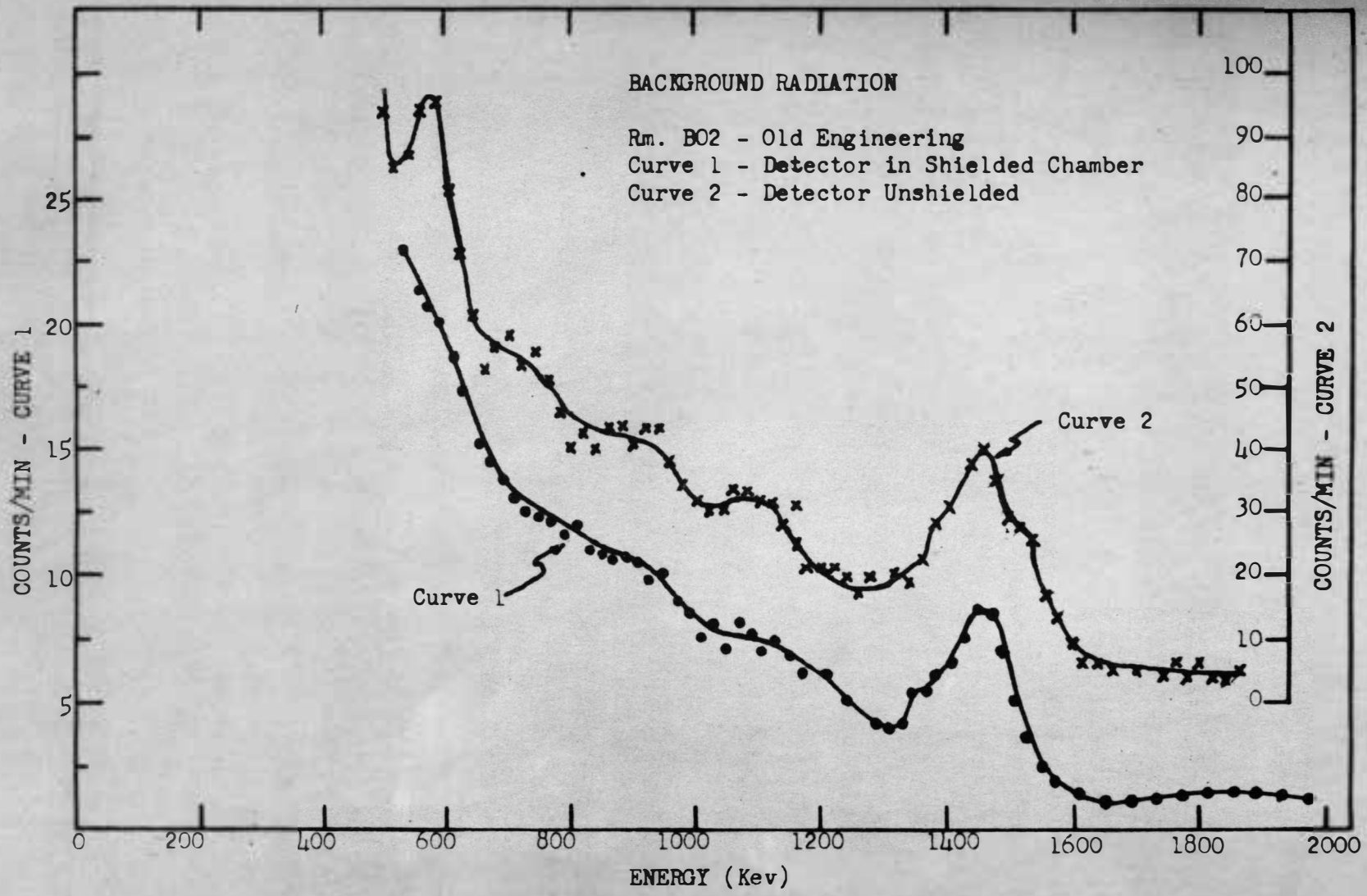

Figure 18. Background Radiation in B02, Old Engineering, obtained with 3 inch diameter x 3 inch thick NaI (Tl) crystal.

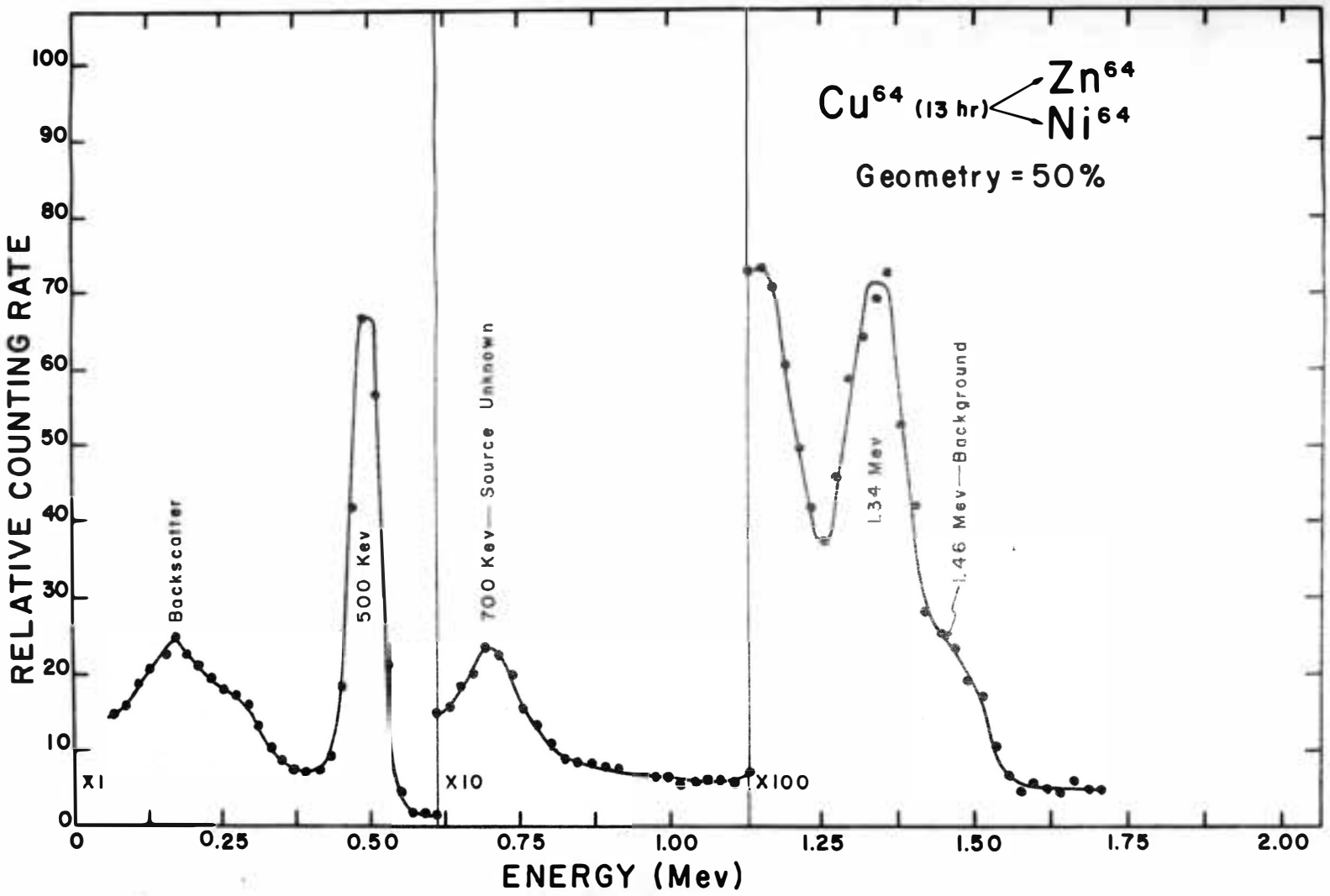

Figure 19. Cu^{64} gamma ray spectrum with radiation incident upon a 3 in. dia. by 3 in. thick NaI crystal.

3. TYPICAL GAMMA RAY SPECTRA

Spectra for a number of sources were obtained with the M.C.A. for three major purposes:

1) familiarization with analyzer operation

2) familiarization with spectrum interpretation

3) determination of experimental limitations of the equipment

Several of the spectra have already been referred to in previous sections. They were mainly for half-life sources that have interesting spectral characteristics. They are shown in Figures 3, 10, 11, 16, and 17. Certain of the peaks in these spectra were also used for calibration of the energy scales as was mentioned previously. Several other spectra are shown in Figures 14 and 19-22. These spectra were obtained from relatively short half-life sources that resulted from neutron capture by certain stable isotopes in the S.D.S.U. subcritical reactor. Use of these spectra in conjunction with activity vs. time curves may make it possible to calculate the neutron flux during irradiation, once the experimental efficiency of detection for the crystal is established.

Examination of the various gamma ray peak energies and comparison with accepted values indicate that experimentally determined energies are normally within one channel of the accepted values for each energy scale. A table of experimental gamma ray energies and resolutions for various prominent peaks in the spectra studied is shown in Figure 23. The aforementioned limits are sometimes exceeded slightly at the high end of an energy scale but it is felt that this can be attributed

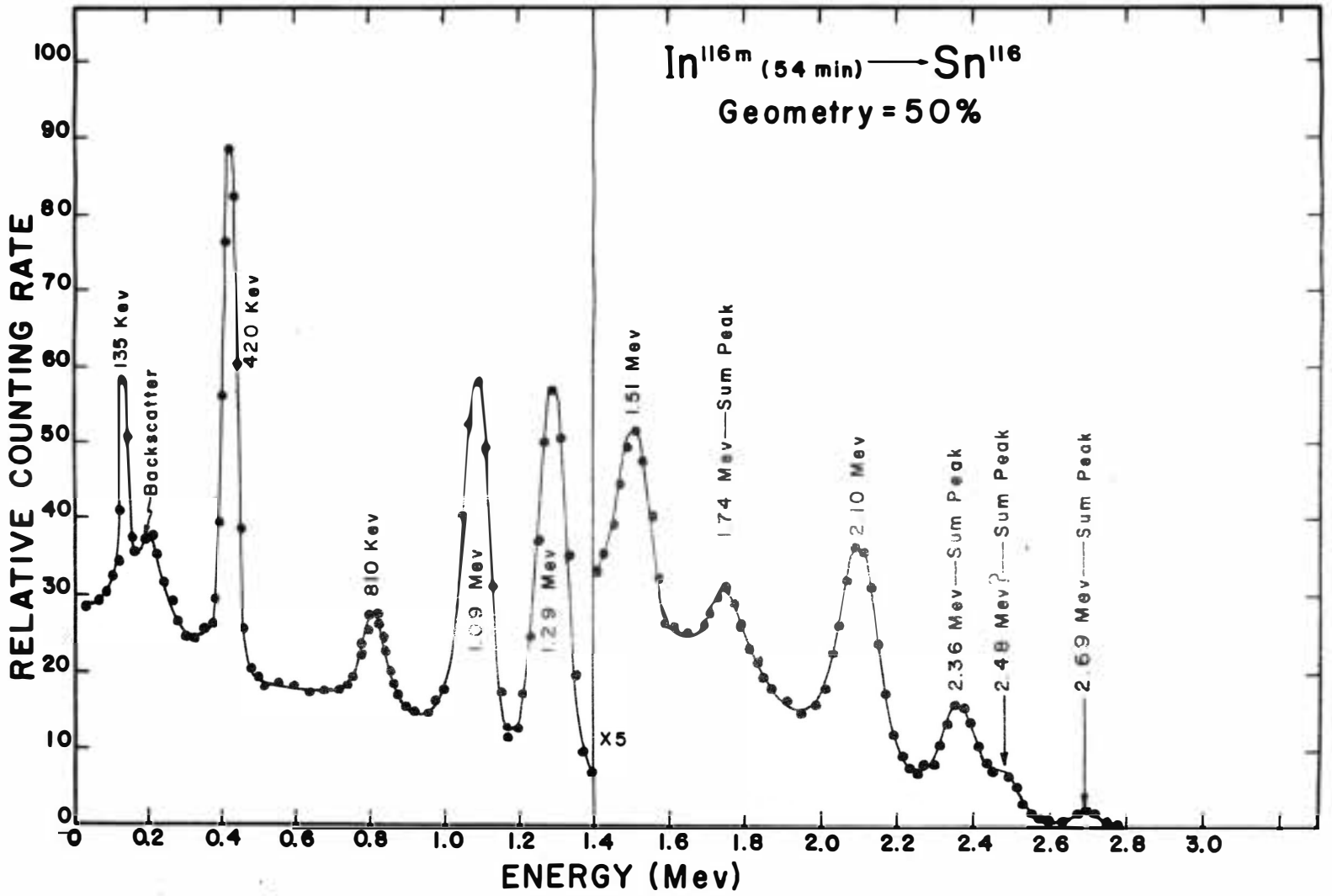

Figure 20. In^{116m} gamma ray spectrum with radiation incident upon a 3 in. dia. by 3 in. thick NaI crystal.

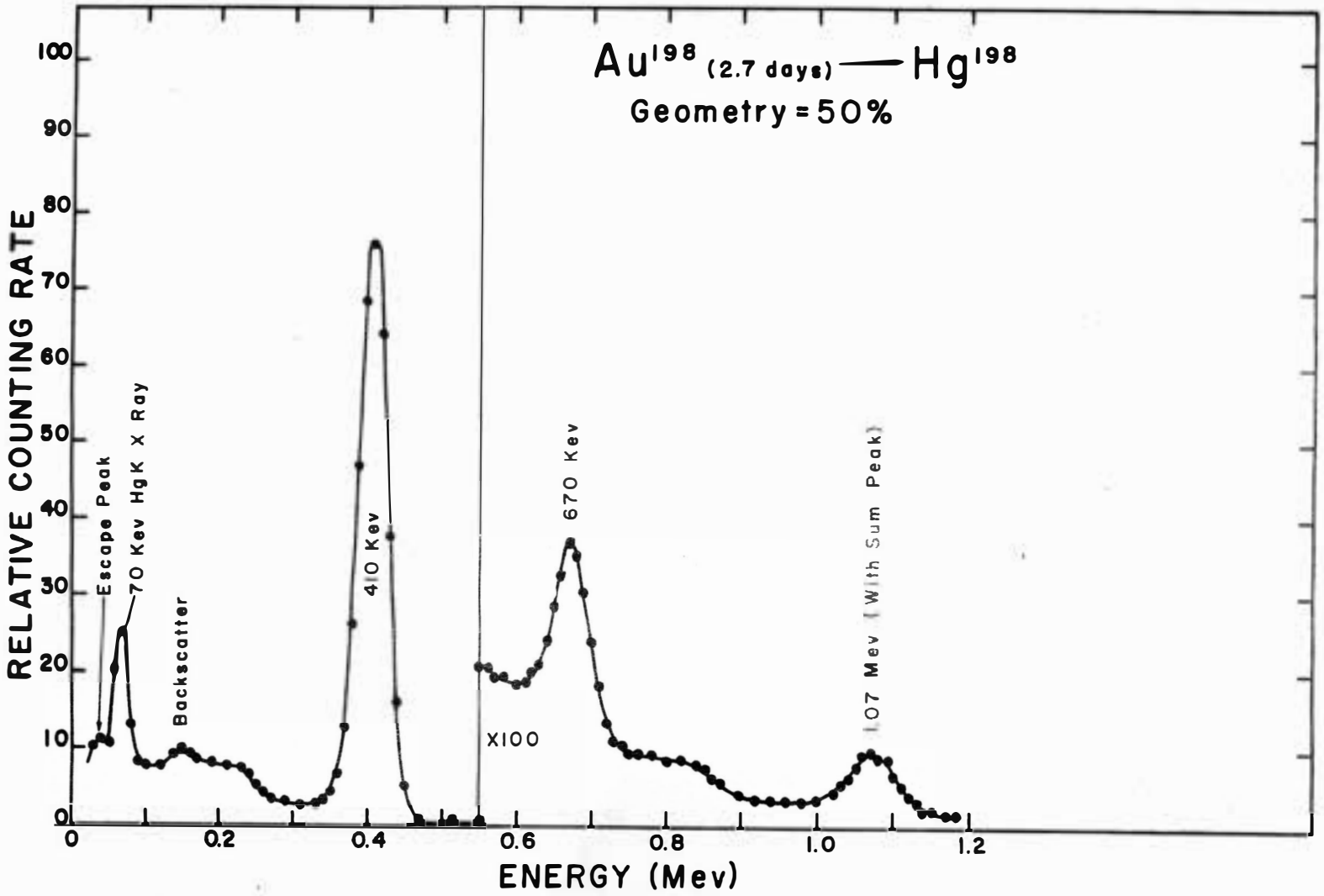

Figure 21. Au^{198} gamma ray spectrum with radiation incident upon a 3 in. dia. by 3 in. thick NaI crystal.

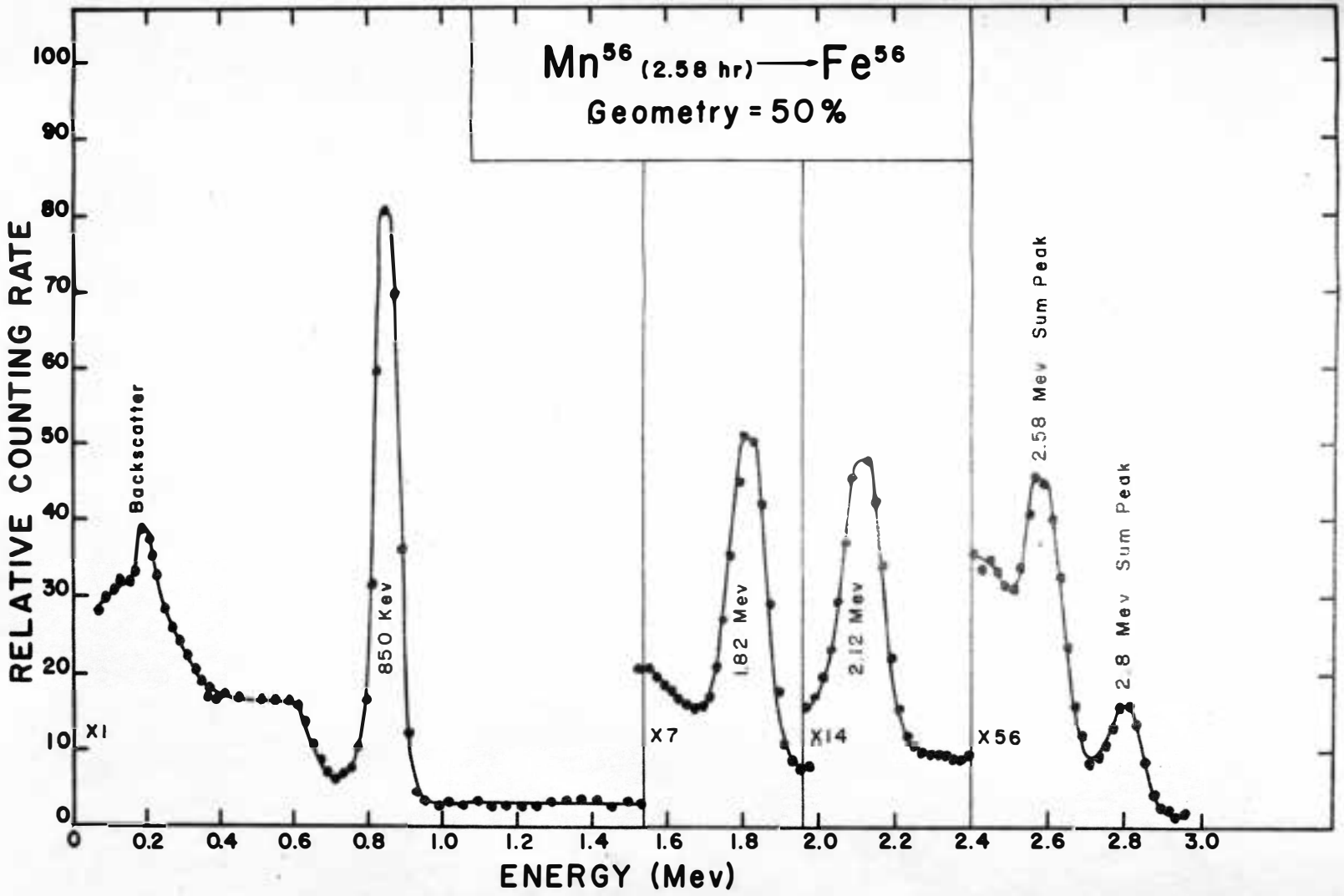

Figure 22. Mn^{56} gamma ray spectrum with radiation incident upon a 3 in. dia. by 3 in. thick NaI crystal.

Figure No.	Parent Isotope	Energy Scale	Gamma Ray Energy (Exp)	Gamma Ray Energy(Acc.)	Resolution (Exp.)
3	Sb^{125}	10 Kev/Ch.	170 Kev	175	
			*427	427	
10	Cs^{137}	10 Kev/Ch.	*660	662	8.4%
11	Cd^{109}	5 Kev/Ch.	90	87	17 %
14	Na^{24}	40 Kev/Ch.	1370	1380	
			2740	2760	6.2%
16	Co^{60}	20 Kev/Ch.	1170	1170	
			*1340	1330	8 %
			2480	2500	
17	Na^{22}	20 Kev/Ch.	* 505	511	11 %
			1290	1280	
19	Cu^{64}	20 Kev/Ch.	500	511	12 %
			1340	1340	
20	In^{116m}	10 Kev/Ch.	420	406	
		20 Kev/Ch.	1090	1085	
			1290	1274	
			2100	2090	
21	Au^{198}	10 Kev/Ch.	410	411	13 %
			670	680	
22	Mn^{56}	20 Kev/Ch.	850	840	8.5%
			1820	1800	
			2120	2120	

* Calibration Peaks

Figure 23. Table of experimental gamma ray energies and resolutions for prominent peaks shown in the designated figures. Accepted gamma ray energies are from Crouthamel, pp. 165-314.

to the use of a less tedious, but less precise, calibration procedure.

4. SOURCE CONSIDERATIONS

It has been implicit in the discussion thus far that the gamma rays were known to emanate from a given nucleus and that source activity was sufficient to give adequately resolved peaks in the spectrum. However , neutron activation of stable isotopes to produce radioactive sources can give rise to several complicating factors. There may be several nuclei that emit gamma rays in a radioactive decay chain, and more than one decay chain may be present. The original material may not be pure, and the impurities may be activated also with subsequent emission of gamma rays.

It may also happen that the activity of the source after irradiation is low. In this case, background radiation and Compton scattering can decrease peak resolution or even obscure low intensity peaks.

The methods for treating the above cases merit further discussion and the rest of this section is devoted to that end. Part of the discussion is general; that is, it is applicable to any method of nuclear particle energy determination. However, an appreciable part of the discussion has relevance only with respect to scintillation counters. This is the reason for inclusion of this section in Chapter I.

Interfering Activities From Source

The following method is used for minimizing impurity gamma ray spectra from the source. The source can be enriched in the desired isotope and purified to a great extent by chemical separation methods. In many cases, the trace impurities present have well known spectra. Hence, observation of source activity before removal of the impurities is advantageous since it helps determine what impurities are of significance.

When several excited nuclei, one from each radioactive decay chain produced during source irradiation, are the major activities for the source, consideration of the half life for each determines the proper approach to be used. If the nucleus under study has a half life appreciably longer than the other major nuclei, then it is only necessary to wait until the activities of those not under study have decreased appreciably. The more intense peaks for the nucleus under study will be immediately evident, and other less intense peaks may become evident as the overall activity drops. However, it may not be certain that these less intense peaks belong to the spectrum of the nucleus under study, since prominent peaks for minor activity nuclei may be present. At this juncture, it may be necessary to utilize chemical separation methods to minimize the undesired activities. For any other half-life possibilities, it is usually necessary to utilize chemical separation methods before studying the spectrum of a particular nucleus. In any case, if the spectra for any of the major activities not under study are known for the

particular experimental arrangement, then they can be fitted to the appropriate peaks in the composite spectrum and subtracted out.

When several nuclei belong to the same radioactive decay chain, repeated removal of the decay products helps one determine how the peaks are to be associated with the nuclei in the chain. This approach can be complicated, however, if there are more than two radioactive members in the chain. In any case, it may be difficult to determine how the low intensity peaks are to be associated with the nuclei. The magnitude of the difficulty will depend on the relationship among the activity half-lives.

Low Activity Sources

When the nucleus to be studied has low activity, it is imperative that the background radiation and the Compton scattering continuum for intense peaks be minimized. Their effects on spectrum interpretation were discussed in section two. However, only brief mention was made concerning minimization of these effects for better spectral resolution.

Background radiation can be lowered by shielding the source and detector from external surroundings. The shielding chamber in use for current experiments is a steel plate shell in the form of a one foot cube. Four inch thicknesses of iron are stacked on three sides of the shell while two inches of lead are stacked on top and two inches of iron on the bottom. The chamber door consists of two inch thick lead bricks stacked on a rolling platform. The spatial

distribution of the background radiation was investigated very roughly and the data is presented in tabular form in Figure 24. Note that no marked difference exists for the several cases. However, it may be desirable to shield the bottom more adequately in the future since the background radiation appears to be the most intense from this direction. Background spectra for both the shielded and unshielded case are shown in Figure 18. Note that shielding the detector lowers the background level by a factor of four in the energy range shown. Further decrease in background level can possibly be obtained by adding a few more inches of shielding. It has been mentioned in the literature that six inches of iron [15] or its equivalent is about the optimum shield thickness.

Improved spectral resolution can be obtained by optimizing detector efficiency and decreasing the probability for escape of the Compton scattered gamma rays. Thus, it is desirable to ascertain which factors affect detector efficiency and escape of degraded gamma rays. In the discussion that ensues, reference is made to the literature[16] and the reader can consult this text for greater detail.

It is helpful to define several terms that are frequently used when discussing efficiency.

a) Geometry is the fraction of the total radiation emanating from a point source that is incident on the detector face. In other words, the geometry of a point source at room temperatures is

---

[15] Crouthamel, op. cit., p. 82.

[16] Crouthamel, op. cit., p. 96.

Shielding	Background counts/min
a) No shielding, crystal in B02 Old Engineering	9280
b) Crystal in chamber with 1/4 in. thick steel walls, same location	7265
c) Same as in (b), except that 2 in. of lead added to front	6530
d) Same as in (b), except that 2 in. of lead added to top	6355
e) Same as in (b), except that 4 in. of steel added to side opposite crystal	6285
f) Same as in (b), except that 2 in. of lead added to side opposite crystal	6050
g) Same as in (b), except that 2 in. of lead added on back	6000
h) Same as in (b), except that 2 in. of lead added on bottom	5560
i) Full shielding, same as in (b) but with addition of 2 in. of lead on top and front, 4 in. of steel on both sides and in back, and 2 in. of steel on bottom	2105

Figure 24. Background counting rate of a 3 in. dia. by 3 in. thick crystal under various shielding conditions. Energy range from 1.0 Mev to 2.0 Mev

the fraction, Ω, of the total solid angle that the detector subtends at the source.

b) Incident intrinsic efficiency, $\epsilon_{(E)}$, is the fraction of the gamma radiation with energy, E, entering the detector that interacts in a measurable manner with the detector.

For a right cylindrical detector and a point source, the geometry is given by

$$\Omega = \frac{1}{2}\left(1 - \frac{Y}{\sqrt{Y^2+r^2}}\right)$$

The variables involved are shown on the diagram in Figure 25. The probability that a well-collimated, monoenergetic gamma ray will traverse a distance, x, in the detector with no interaction is $e^{-\mu x}$ where μ is the absorption coefficient of the detector. Then $1-e^{-\mu x}$ is the interaction probability, and use of this with the definition of the incident intrinsic efficiency, $\epsilon_{(E)}$, yields

$$\epsilon_{(E)} = \frac{1}{\Omega}\int (1 - e^{-\mu x})\, d\Omega$$

This can be re-expressed in terms of the variables previously defined in Figure 25.

$$\epsilon_{(E)} = \frac{1}{2\Omega}\left[\int_0^{\theta_1}(1 - e^{-\mu h \sec\theta})\sin\theta\, d\theta + \int_{\theta_1}^{\theta_2}(1 - e^{-\mu\{r\csc\theta - Y\sec\theta\}})\sin\theta\, d\theta\right]$$

Hence, μ, r, and h must be made large and Y made small for best efficiency.

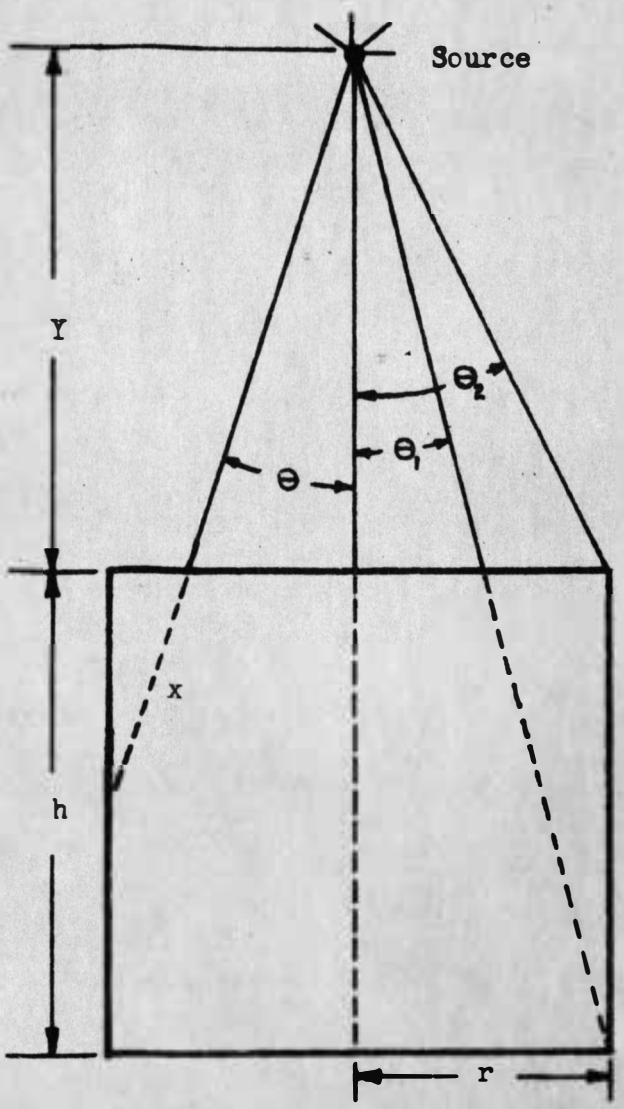

Figure 25. Schematic Diagram defining variables for intrinsic efficiency and geometry of a crystal with a point source. From Crouthamel, p. 98.

Values of μ are available for NaI crystals and Crouthamel[17] has tabulated the source intrinsic efficiency, $\Omega\epsilon_{(E)}$, vs. gamma ray energy for several combinations of Y, r, and h. Curves for the 3 inch diameter x 3 inch thick and the recently received 1.75 inch diameter x 2 inch thick crystal are presented in Figure 26.

The above discussion dealt with single interaction events between gamma rays and the detector. However, multiple scattering events at higher gamma energies are important factors concerning formation of the full energy peak. Theoretical techniques using a computer have been developed for computation of source full energy peak efficiencies, $\Omega\epsilon_{(E)}\ R_{(E)}$, where $R_{(E)}$ is the ratio of the full energy peak area to the total area of the spectrum for a mono-energetic gamma ray. Also, a number of experimental techniques[18,19] have been developed for the same purpose. Results of the above techniques can be summarized briefly by stating that detectors of large volume and greater density increase full energy peak efficiencies.

5. GAMMA RAY ENERGY DETERMINATION BY OTHER METHODS

At the beginning of this chapter, it was mentioned that a variety of methods other than scintillation counting exist for gamma

---

[17] Crouthamel, op. cit., p. 315.

[18] Crouthamel, op. cit., p. 103.

[19] M. Deutsch and O. Kofoed-Hansen, Experimental Nuclear Physics, p. 430, Wiley and Sons, New York, 1960.

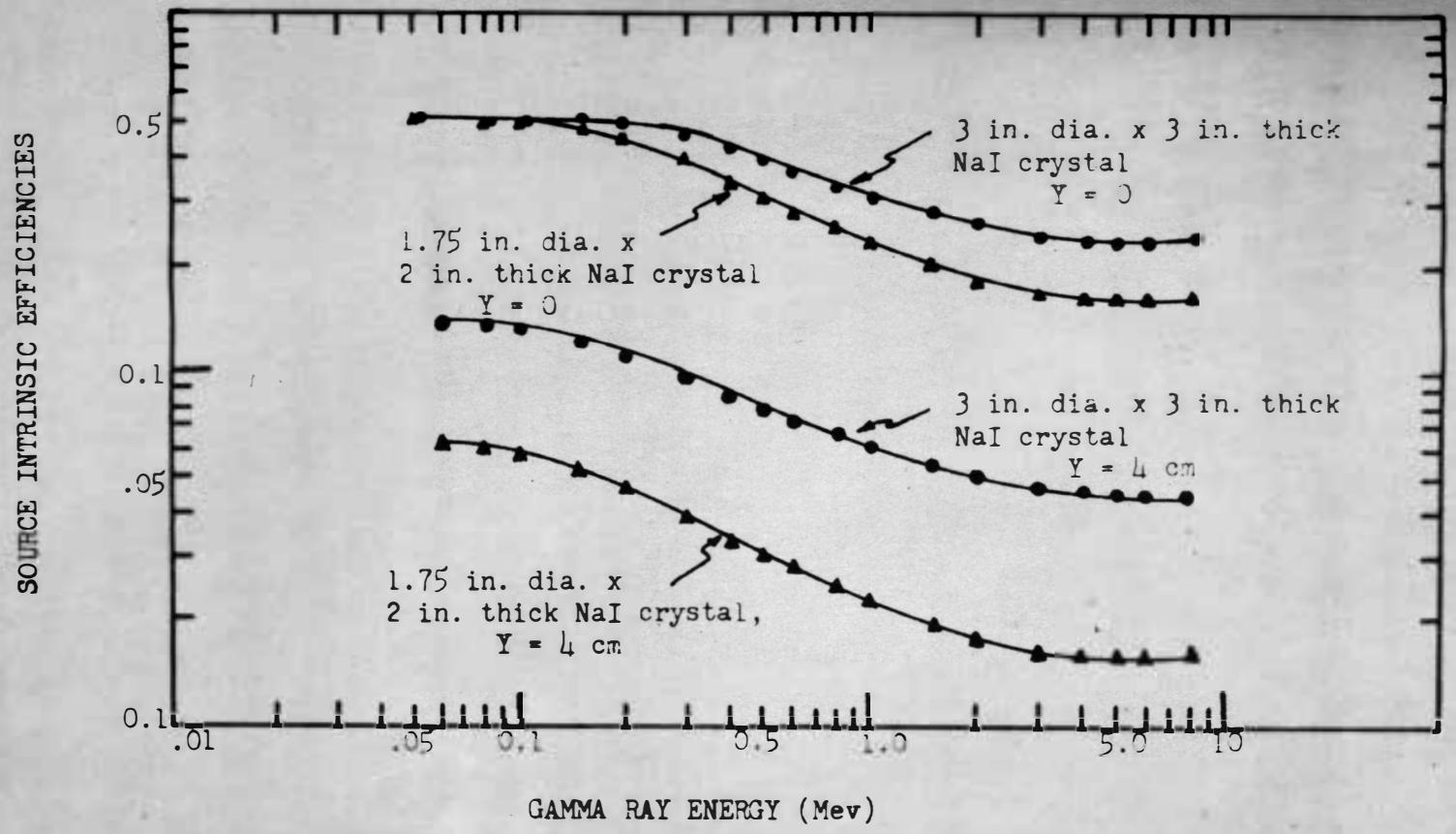

Figure 26. Calculated source intrinsic efficiencies for two NaI crystals vs. gamma ray energy at two different source distances. Data from Crouthamel, pp. 321. 329.

energy determination. Methods that merited further study with respect to project requirements are discussed below. Since many literature surveys are available[20,21] as well as many detailed articles on each of the methods, the discussion is concerned mainly with evaluation of these methods by the criteria listed at the beginning of the chapter.

Measurement of Absorption Coefficients

The absorption coefficient measurement method for determining gamma ray energies consists mainly of plotting gamma ray intensity vs. absorber thickness. This is done for a material whose absorption coefficient as a function of gamma ray energy is well known. For monoenergetic gamma rays, the beam intensity, I, as a function of absorber thickness is very nearly

$$I = I_0 e^{-\mu x}$$

Here I_0 is the beam intensity for no absorber, μ is the absorption coefficient, and x is the absorber thickness. The above expression is true only if the source is thin and the primary gamma rays are well-collimated before and after the absorber. This ensures normal incidence and minimizes detection of degraded gamma rays which are considered as removed from the beam. Since I, I_0, and x are experimental entities, μ can be calculated which, with the known absorption

---

[20] M. Deutsch and O. Kofoed-Hansen, op. cit., p. 266.
[21] D. E. Alburger, op. cit., p. 228.

coefficient curve, determines the gamma ray energy. A minor complication exists here since all μ vs. gamma energy curves have a minimum; hence, one μ value corresponds to two gamma energy values. This requires repetition of the above experiment for another known absorber.

The above method is not a judicious choice if the source has a complex gamma ray spectra. Also, collimation requirements make it necessary to use high activity sources. In any case, development of proportional counter techniques has rendered the absorption method virtually obsolete for gamma energy determination, and it is mentioned here for historical reasons only.

Curved Crystal Diffraction Method

After it was realized that gamma radiations were wavelike in nature, diffraction techniques were employed for precise gamma ray energy determinations. A method was developed by Du Mond and collaborators[22] which utilizes a curved quartz crystal transmission-type spectrometer. This device is shown schematically in Figure 27. A line source of gamma rays is made to move along a focusing circle whose diameter is determined by the requirement that the initially parallel crystal reflecting planes intersect at P after the crystal is bent. When the source is located at P, no reflection of gamma rays occurs at the crystal. However, as the crystal is moved away

[22] D. E. Alburger, op. cit., p. 242.

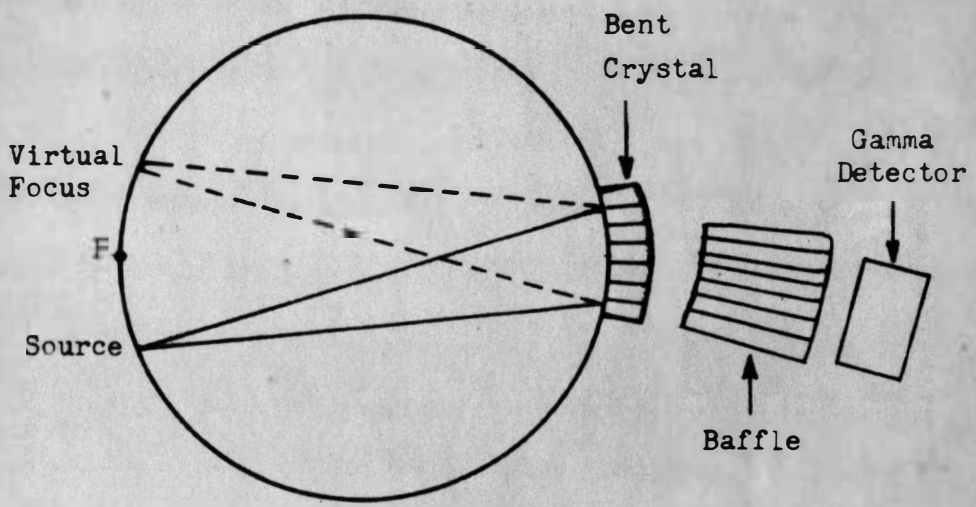

Figure 27. Curved crystal gamma ray spectrometer.
From Alburger, p. 242.

from P, sufficient reflection from the crystal takes place when the Bragg condition is satisfied; namely

$$n\lambda = 2 d \sin\theta$$

Here λ is the wavelength of the gamma ray, d is the spacing between the crystal reflecting planes, θ is the angle that the incident gamma ray makes with the reflecting planes, and n is the order number. Thus there are 2 gamma ray components transmitted through the crystal: the unreflected component which emanates from the source; and a reflected component which appears to come from a virtual source on the focusing circle. The main problem in the instrument design is to detect only the reflected component. This is accomplished by the use of a lead baffle shielding the counter, where orientation of the baffle is always such that the slots point toward the virtual source. Then a plot of counting rate vs. diffraction angle reveals the gamma peaks at their corresponding Bragg angle. Here, one must remember that reflections of order higher than one can occur.

The instrument line width for the above device is approximately $\Delta\lambda = 7 \times 10^{-13}$ cm. This corresponds to about 1% at 1 Mev and about 0.1% at 100 Kev. This is markedly superior to that obtained with proportional counter methods. However the small angle of reflection (less than 0.5° at 1 Mev) makes it necessary to have small aperture for the baffle slots. Further, the reflectivity of the crystal varies approximately as the inverse of the squared gamma energy. Thus, the source under study must have a very high activity. This limits the

practically useful range of the curved crystal diffraction method to less than 1 Mev and restricts its use to energy standard measurements for the most part.

Gas Filled Type Proportional Counter

Certain types of nuclear radiation produce a number of ion-electron pairs in proportion to their energies during passage through a gas. If the electrons so produced are then subjected to an appropriate electric field, they will give rise to electron avalanches that grow in an exponential fashion. The number of electrons arriving at the collector will still be in proportion to the ionizing nuclear radiation energy provided that the electric field magnitude is not so great as to cause gas discharge. Thus one has a method for determining the nuclear radiation energy causing the initial ionization. This method, with experimental modifications, is called the gas-filled proportional counting method.

The gas-filled proportional counter works well for charged particles that produce ion-electron pairs along their overall path. Resolution, resolving time, etc. are more than adequate for these cases. However the gas-filled detector is not very practical for gamma rays because of the long mean free path of gamma rays in gases. In fact, detection of gamma rays depends mostly on the ejection of Compton electrons from the walls of the gas-filled counter. These Compton electrons have a short range in the wall material; hence, only a thin layer at the inner surface of the wall contributes to

the gas amplification. In any case, gamma ray detection efficiency is less than 1% for 1 Mev energies and resolution is poor. However, gas filled type proportional counters are adequate for detection of electromagnetic radiation below about 100 Kev and have two to three times better resolution than scintillation spectrometers have in this energy region. For this reason, gas-filled proportional counters are often used to supplement scintillation counters in gathering spectral data.

Conversion Electron Analysis with Magnetic Spectrometers

Gamma ray energy measurement is also possible by studying electrons emitted from the source during internal conversion and electrons ejected from an external absorber by the gamma rays under study. External absorbers are commonly known as converters or radiators. External conversion depends upon the nature of the gamma ray - converter interaction. Consequently, electrons resulting from Compton scattering, the photoelectric effect, and pair production have all been studied.

The external and internal conversion electrons are usually analyzed with any one of a wide variety of magnetic electron spectrometers. The designs of these spectrometers[23] have been discussed in great detail in the literature. There are, in general, two broad types of spectrometers: prismatic; and axial focusing. Major

[23]M. Deutsch and O. Kofoed-Hansen, op. cit., p. 455.

designs of the prismatic type are the uniform field semicircular focusing device, the double focusing spectrometer, and the multi-section, or "orange" spectrometer. For these designs, the electrons under analysis travel in roughly circular orbits perpendicular to the field. Analysis is accomplished by noting that the radius of an electron orbit depends on electron momentum and magnetic field strength. Major designs of the axial focusing type are the thin and thick magnetic lenses, the solenoid uniform field instrument, and intermediate image spectrometers. For these designs, electrons move in more or less helical paths when traversing the spectrometer and are focused to one or more source images along the axis. Analysis is accomplished by noting that the electron image position is a function of electron momentum and magnetic field strength.

In general, the resolutions obtainable with electron magnetic spectrometers rank among the best in gamma ray spectrometry. The line width values range from about 2% for axial focusing designs to as low as 0.2% for a double focusing instrument. However, this narrow line width is obtainable only for very low electron transmission rates. As an example, intermediate image spectrometers operate with about 6% transmission while double-focusing spectrometers operate with transmissions less than 1%. Thus, conversion electron methods with magnetic spectrometers are not very practical for study of low activity sources. Further, all the "source" problems discussed with regard to beta-spectrometry in the next chapter arise and must be considered in spectrum interpretation. Experimental procedure is

also more cumbersome since the electron analysis must be accomplished in high vacuum.

Gamma ray energy determination by analyzing electrons emitted by the source during internal conversion is accomplished by first measuring electron energies with a magnetic spectrometer. When the data is plotted, peaks in the counting rate are revealed which correspond to the internal conversion electron energies. Then the known binding energies for the appropriate atomic sub-shells are added on to the corresponding peak energies to obtain the competing gamma transition energies. Here one must correct for source thickness when determining peak energies. Peak energy determination is also more difficult for those sources having a continuous β -ray spectrum. Often the internal conversion electron spectrum is superimposed on the continuous beta-ray spectrum, and this can lower the resolution and obscure low intensity peaks.

Gamma ray energy determination by analyzing photoelectrons ejected from a converter proceeds in a manner similar to that discussed in the preceding paragraph. The exception is that the known binding energies added on to the electron energy peaks are those for the appropriate atomic sub-shells of the converter material. Here one must correct for converter thickness when determining the photo-electron peak energies. The photo-electron spectrum is complicated by the presence of Compton electrons which, in general, lower the resolution and obscure low intensity peaks.

Gamma ray energy determination can be made by observing the electron spectrum resulting from Compton scattering of gamma rays by a converter. As discussed previously in this chapter, a maximum exists on the amount of gamma energy that can be transferred to a relatively free electron in the converter. This leads to a sharp cut-off in the Compton electron continuum for each gamma ray. The cut-off bears a one-to-one relationship to the incident gamma energy; hence the incident gamma energy is determined when the Compton cut-off energy is measured. Here again one must correct for converter thickness when determining the electron energies.

Another method that utilizes Compton electrons is that in which the angle of Compton scattering is specified by strong collimation. Analysis of the Compton electron energies at the specified angle yields counting rate peaks that have one-to-one relationships with the corresponding incident gamma ray energies.

Gamma energies greater than 1.02 Mev can be determined by analyzing the negatron-positron spectra ejected from the converter after pair production interactions. This requires a special arrangement called the magnetic pair spectrometer which is shown schematically in Figure 28. Here positrons and negatrons are subjected to the same magnetic field and are detected only in the case of coincidence by counters suitably placed at the respective focus points. The placement of the coincidence system is based on the following reasoning. The incident gamma energy, E_γ, is given by

$$E_\gamma = T_+ + m_0c^2 + T_- + m_0c^2$$

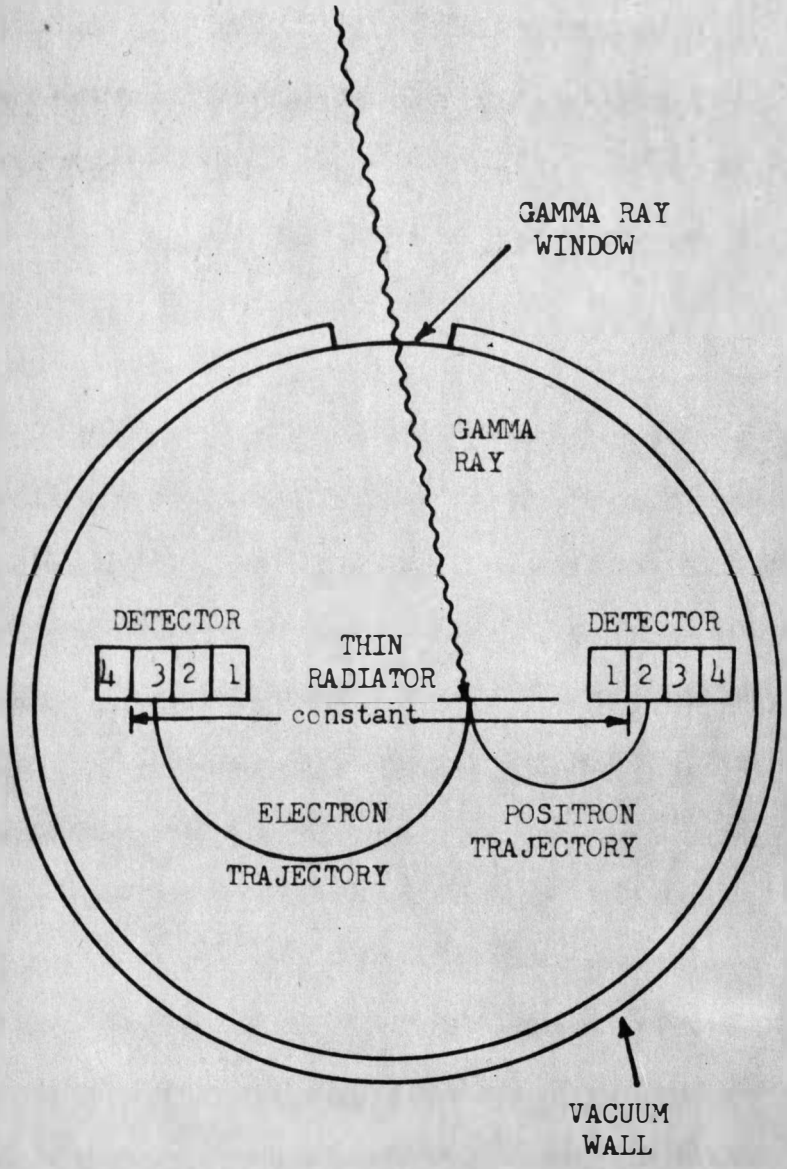

Figure 28. Schematic diagram for a semicircular focusing magnetic pair spectrometer.

where T_+ and T_- are the observed kinetic energies for the positron and negatron respectively and $m_o c^2$ represents electron rest energy. The total energy of each particle can be expressed in terms of linear momentum, p, by

$$T_\pm + m_o c^2 = \left[(m_o c^2)^2 + p_\pm^2 c^2 \right]^{\frac{1}{2}}$$

thus

$$E_\gamma = \left[(m_o c^2)^2 + p_+^2 c^2 \right]^{\frac{1}{2}} + \left[(m_o c^2)^2 + p_-^2 c^2 \right]^{\frac{1}{2}}$$

When $E_\gamma \gg m_o c^2$, the sum of p_+ and p_- is constant to a first approximation. Hence, the sum of the radii of curvature for each electron pair is approximately constant. The coincidence arrangement detects only those positrons and negatrons that are separated by this constant.

Semiconductor Detectors

In the past ten years, use of semi-conductor materials for nuclear radiation has increased greatly. Three major types of semiconductor detectors[24] have arisen thus far: the diffused junction detector; the surface barrier junction detector; and the lithium-drifted junction detector. The first two are very similar and differ only in the technique of fabricating the p-n junction. Here p-n

---

[24] W. J. Price, Nuclear Radiation Detection, p. 212, McGraw-Hill Book Co., New York, 1964.

refers to an originally intrinsic semiconductor base that has two different regions after suitable treatment. One region contains a majority of electron acceptor impurity atoms (p type) while the other region contains a majority of electron donor impurity atoms (n-type). When the p-n junction is operated at reverse bias, a thin charge depletion region results that is very resistive to the establishment of steady-state currents. However, if a nuclear radiation produces a number of electron-hole pairs in the depletion region, the lifetimes of the pairs may be long enough such that the charges are swept out of the depletion region by the imposed electric field and are detected as a charge or voltage pulse. The pulse is proportional to the energy of the incident radiation provided the number of pairs depends on the available energy and that the average energy expended per electron-hole pair creation is independent of the characteristics of the incident radiation.

Junction type detectors can also be fabricated by an ion-drift method. This method depends upon the tendency of ionized donors, or acceptors, to drift appreciably when the temperature of the material is raised. Lithium, a donor impurity, is diffused onto one surface of a p-type silicon block. When the temperature of the block is in the range, 100°C to 400°C, lithium ion drift predominates over natural diffusion of electrons that are donated to the conduction band by initially neutral lithium atoms. Application of reverse bias to the junction at these elevated temperatures results in an intrinsic region that is 0.5 cm to 1 cm thick. This is generally

thicker than the depletion regions for surface barrier and diffused junction detectors. When the junction is returned to operating temperatures, and reverse bias is applied again, residual charge carriers are swept from the intrinsic region. An approximately constant electric field is then established across the intrinsic region, and electron-hole pairs produced there by nuclear radiation can be collected.

In view of the above discussion and other more detailed discussions in the literature, one can designate the more important properties of a good semi-conductor detector:

1) high resistivity at operating temperatures
2) high mobility and long carrier lifetimes for electrons and holes produced by nuclear radiation
3) the capability of supporting high bias voltages
4) sufficient cross-sectional area and maximum thickness of the sensitive region

Improvement of certain of these properties can lead to more stringent requirements on the others. For instance, increasing the sensitive region thickness leads to the requirement of higher mobilities and longer carrier lifetimes. Also, increase in the cross-sectional area leads to higher resistivity requirements in order that leakage current be minimized. The need for higher resistivity to decrease leakage current (improve resolution) has led to the operation of detectors at liquid nitrogen temperatures in many instances.

The diffused junction and surface barrier junction detectors work very well with heavy, charged particles since these particles can be stopped within the depletion layer. However, the use of these detectors for gamma ray and high energy beta ray detection is not very practical because of the greater penetrating power of these rays.

Lithium drifted junction detectors with silicon bases have been used for detection of beta rays with good results. External and internal conversion electron spectra taken with these detectors have typical line widths of 1% to 3% near 1 Mev at dry ice temperatures.

Lithium drifted junction detectors with germanium bases have been utilized for gamma ray detection. Gamma ray energies up to 150 Mev have been measured with typical line widths of 2% to 3% at liquid nitrogen temperatures. At room temperature, low energy gamma ray line widths are only slightly better than those obtained by scintillation techniques.

Improvement of semiconductor detectors with regard to higher atomic number for base materials, thicker sensitive regions, and higher resistivity, higher mobility materials may result in a good gamma ray detector for moderate energies. At the present time, however, lithium drifted junction detectors with a germanium base can only be used to supplement scintillation counters.

CHAPTER II

BETA RAY SPECTROMETRY

A number of methods for obtaining beta ray spectra have been described in the literature.[25] Those methods that merited further study with respect to current experiments and for historical reasons are:

1) range measurements in cloud chambers or photographic emulsions
2) electron magnetic spectrometer analysis
3) gas-filled type proportional counters
4) scintillation type proportional counters
5) semiconductor detectors

For current experiments, the main criteria for evaluating these methods were: resolution; detection efficiency and source activity requirements; experimental complexity; and cost and availability.

Evaluation of the above methods indicated that an anthracene crystal scintillation detector is an adequate choice at the present time. For this reason, a discussion of the scintillation method for beta ray spectrometry will ensue next, and the discussion of the other methods will be deferred until later in this chapter.

---

[25] M. Deutch and O. Kofoed-Hansen, op. cit., p. 450.

1. SCINTILLATION COUNTERS

Beta Ray Scintillation Crystals

A fundamental requirement for the scintillation crystal is that it fully convert the beta-ray energy to photons in the ultra-violet and visible regions. Just how fully this conversion takes place is dependent upon how successful the crystal is in stopping the beta rays within its sensitive volume.

The situation for beta rays is somewhat different than that for gamma ray detection, since there is no need to convert the primary energy to photoelectric electrons, Compton electrons, or electron-positron pairs, which then optically excite the crystal. However, whereas the secondary electrons during gamma ray conversion are liberated and absorbed again within the crystal, the beta rays normally enter the crystal from a different medium. This can result in appreciable backscatter of the incident beam if the atomic number of the crystal is too large. For this reason, organic, plastic, and liquid scintillators are used for beta ray spectrometry. Backscatter from inorganic crystals is nearly 90%, the case for NaI crystals, while that for anthracene crystals is 10% or lower.

It was noted in Chapter I, section 1, that the instrumental line width of a scintillation spectrometer is roughly inversely proportional to the square root of the average light yield per scintillation. Thus, the crystal with the greatest light yield should be used if other negative factors are not of significance. Anthracene

has the greatest light yield among the organic, plastic, and liquid scintillators and is frequently used for beta ray detection. However, plastic and liquid scintillators are often used in cases where it is necessary to have irregularly shaped detectors, and where the requirements on resolution and detection efficiency are not critical.

All of the organic, plastic, and liquid phosphors are particularly suitable for experiments involving coincidence counting because of their short light decay constants. The liquid and plastic scintillators have decay constants on the order of five nanoseconds, and anthracene's decay constant is approximately 30 nanoseconds.[26] For purposes of comparison, the decay constant for NaI is approximately 250 nanoseconds.

In view of the above discussion, it appears that anthracene is a judicious choice for a beta ray scintillation crystal at present. The detection efficiency and light yield for anthracene is superior to that for plastic and liquid scintillators. Furthermore, anthracene's decay constant is more than adequate for any beta-gamma coincidence experiments that may be performed.

Pulse Height Reproduction and Analysis

The pulse height reproduction and analysis chain for beta rays is the very same as that employed for gamma rays. In fact, it was only necessary to substitute a 1½" diameter x 3/16" thick anthracene crystal in place of an NaI crystal on the single channel analyzer

[26] Harshaw Scintillation Phosphors, op. cit., p. 10.

chain. The method of pulse reproduction and analysis has already been covered in Chapter I. Thus, it will suffice here to discuss only the instrumental line widths obtainable with anthracene crystals and the calibration methods used for beta ray analysis.

It has already been mentioned that the instrumental line width is roughly inversely proportional to the square root of the average light yield per scintillation. Since anthracene's light yield per scintillation is approximately half that for NaI, the best instrumental line widths obtainable with anthracene are approximately 1.5 times larger than those obtainable with NaI. Typical values for anthracene are from 12% to 20%. Experimental values for resolution have not been obtained yet, since the resolution requirements for beta-gamma coincidences and continuous beta spectra are not critical. Furthermore, no thin beta sources of special designs that emit internal conversion electrons are in use at present. It may be necessary to determine the experimental resolution at a later date if it happens that the nucleus under study undergoes internal conversion.

The calibration technique utilized for single channel analysis of beta rays is similar to that employed for gamma rays. A source of special design that has a continuous beta spectrum with a well known end-point energy is analyzed, and the high voltage and gain settings are varied to place the spectrum endpoint at the desired baseline setting. This defines a particular energy scale for the analyzer, and the conversion from baseline setting to energy can be

made for any other source analyzed with the same scale. Two calibration sources presently in use are Co^{60} and a Sr^{90}, Y^{90} decay chain. If it becomes necessary to study nuclei which undergo internal conversion, then the calibration technique can be improved by utilizing thin sources with well-known internal conversion electron spectra.

2. EXPERIMENTAL BETA RAY SPECTRA

Interpretation of Beta Ray Spectra

The prominent characteristics for the experimental beta ray spectra are most effectively discussed with reference to spectra in which they occur. The continuous beta ray spectra for two Co^{60} sources are shown in Figure 29. Curve 2 is for a specially prepared source that is used primarily for beta energy scale calibration. Curve 1 is for the beta ray source used in the beta-gamma coincidence experiments discussed in the next chapter. Note that the curves are very similar with the exception that the counting rate for curve 1 is much greater. Both curves exhibit a continuous beta spectrum with a single maximum above a baseline setting of 200. The marked increase in counting rate below the noted baseline setting is not well understood at present. That it is due to primary beta rays is certain, for absorption of the primary betas in a 1/4 inch iron shield lowers the counting rate over the entire scale to nearly background. Possibly this increase is caused by bremsstrahlung that is produced as the primary betas pass through the very thin aluminum

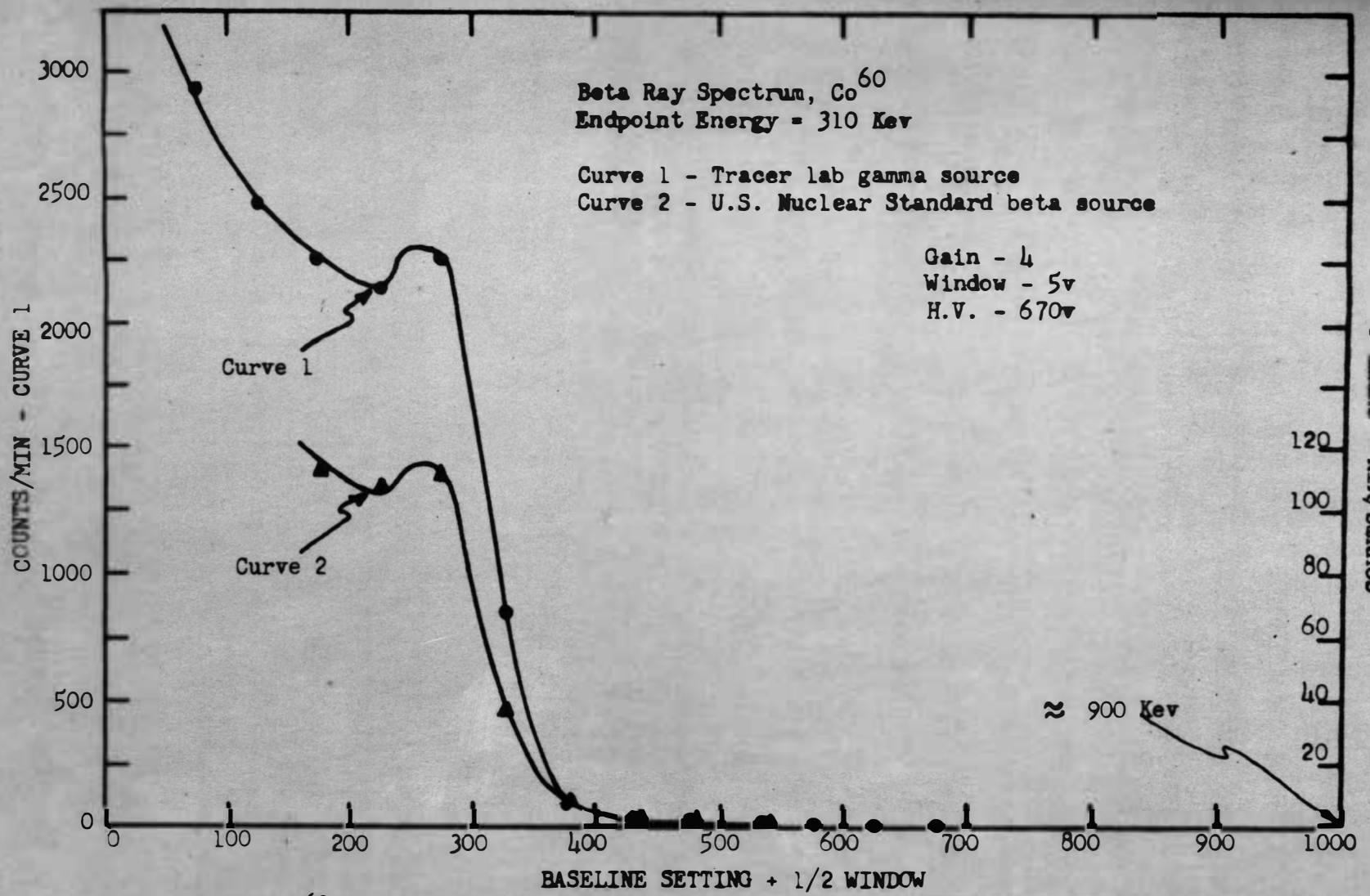

Figure 29. Co^{60} beta ray spectrum with radiation incident upon 1.5 in. dia. by 3/16 in. thick anthracene crystal.

window covering the anthracene crystal.

Compton scattering of source gamma radiation by the anthracene crystal can also lead to a marked increase in counting rate at baseline settings close to zero. This is illustrated in Figure 13. Experimentation with sources that emit gamma rays at 700 Kev or less did indeed reveal an appreciable counting rate at low baseline settings. Here the betas were removed from consideration by shielding the anthracene crystal from the source with 1/4 inch of iron and 1/4 inch of aluminum. However, for Co^{60}, the characteristic gamma radiation does not interact significantly with the crystal, since the counting rate drops to nearly background if only the betas are removed from consideration. Furthermore, it is impossible to interpret the low energy region for the Sr^{90}, Y^{90} source on the basis of Compton scattering of gamma rays by the crystal, since this source emits no characteristic gamma radiation. The Sr^{90}, Y^{90} beta ray spectrum is shown in Figure 30.

When gamma rays interact with the anthracene crystal also, summing of any coincident beta and gamma interactions can occur. This shifts the spectrum towards higher energies and also distorts the spectrum somewhat. This is of no major significance with regard to beta-gamma coincidence experiments that use separate detectors for the betas and gammas. However, this spectrum distortion may present problems in those cases where internal conversion occurs.

Beta radiation from a Cs^{137} source used primarily for gamma detector calibration was analyzed with the anthracene crystal. This

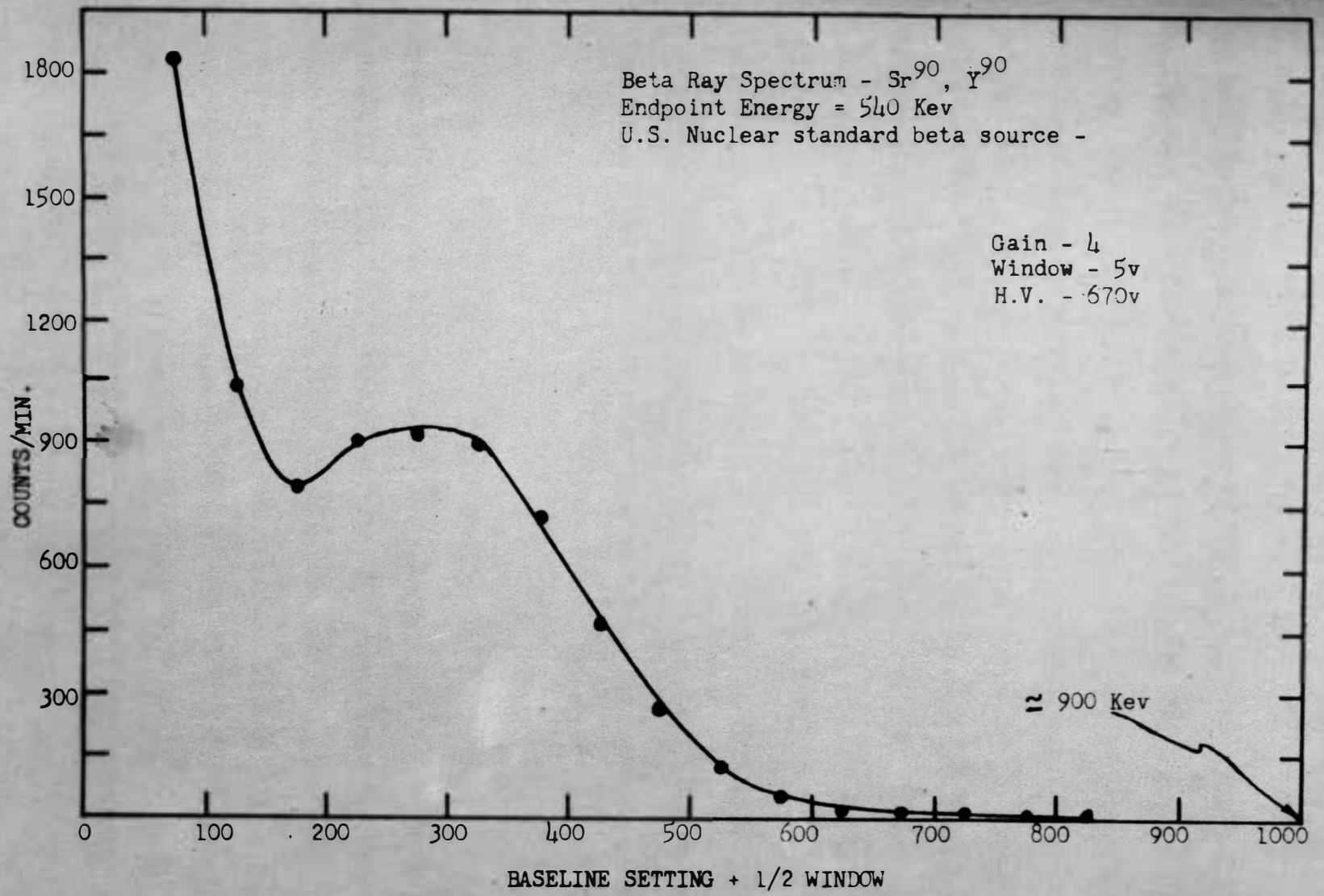

Figure 30. Sr^{90},Y^{90} beta ray spectrum with radiation incident upon 1.5 in. dia. by 3/16 in. thick anthracene crystal.

source emits internal conversion electrons with energies of approximately 625 Kev and a continuous beta spectrum with an endpoint energy of approximately 514 Kev.[27] Consequently, the Cs^{137} beta spectrum should have the form illustrated in Figure 31. It is apparent that the experimental Cs^{137} beta spectrum shown in Figure 32 deviates from the known form markedly. Another experimental beta-ray spectrum for Cs^{137} at a higher gain is shown in Figure 33. Here a continuous spectrum is evident, but no clear separation of the known continuous beta spectrum and the internal conversion electron peak is noticeable.

The marked departure of the experimental Cs^{137} beta spectrum can possibly be attributed to the fact that the Cs^{137} source is relatively thick. For thick sources, absorption and scattering of betas takes place within the source. This reduces the total number of betas emitted and shifts the spectrum towards the low energy end of the scale. For this reason, beta sources are usually in the form of a thin film deposited on a backing material of low atomic number.

The experimental beta ray spectrum for Au^{198} is shown in Figure 34. Au^{198} is known to have a continuous beta spectrum for which the 99% branch has an endpoint energy of 960 Kev. Consequently, the experimental counting rate should begin to rise above background in Figure 34 at a baseline setting of approximately 650. However, it is apparent that this does not happen until a baseline setting

---

[27] The 514 Kev endpoint energy is that for the 99% branch. A 1% branch also exists and has an endpoint energy of 1.18 Mev.

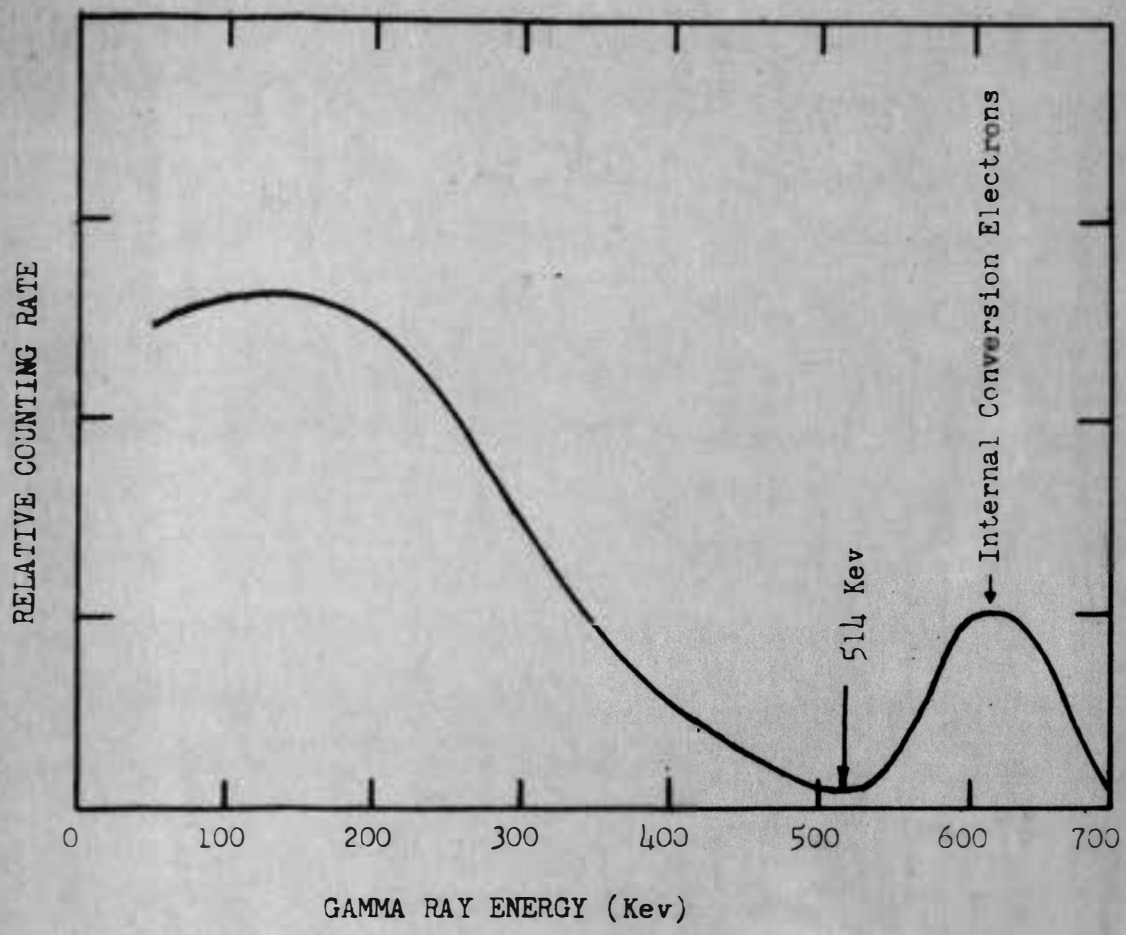

Figure 31. Schematic diagram of Cs^{137} beta ray spectrum with radiation incident upon an anthracene crystal.

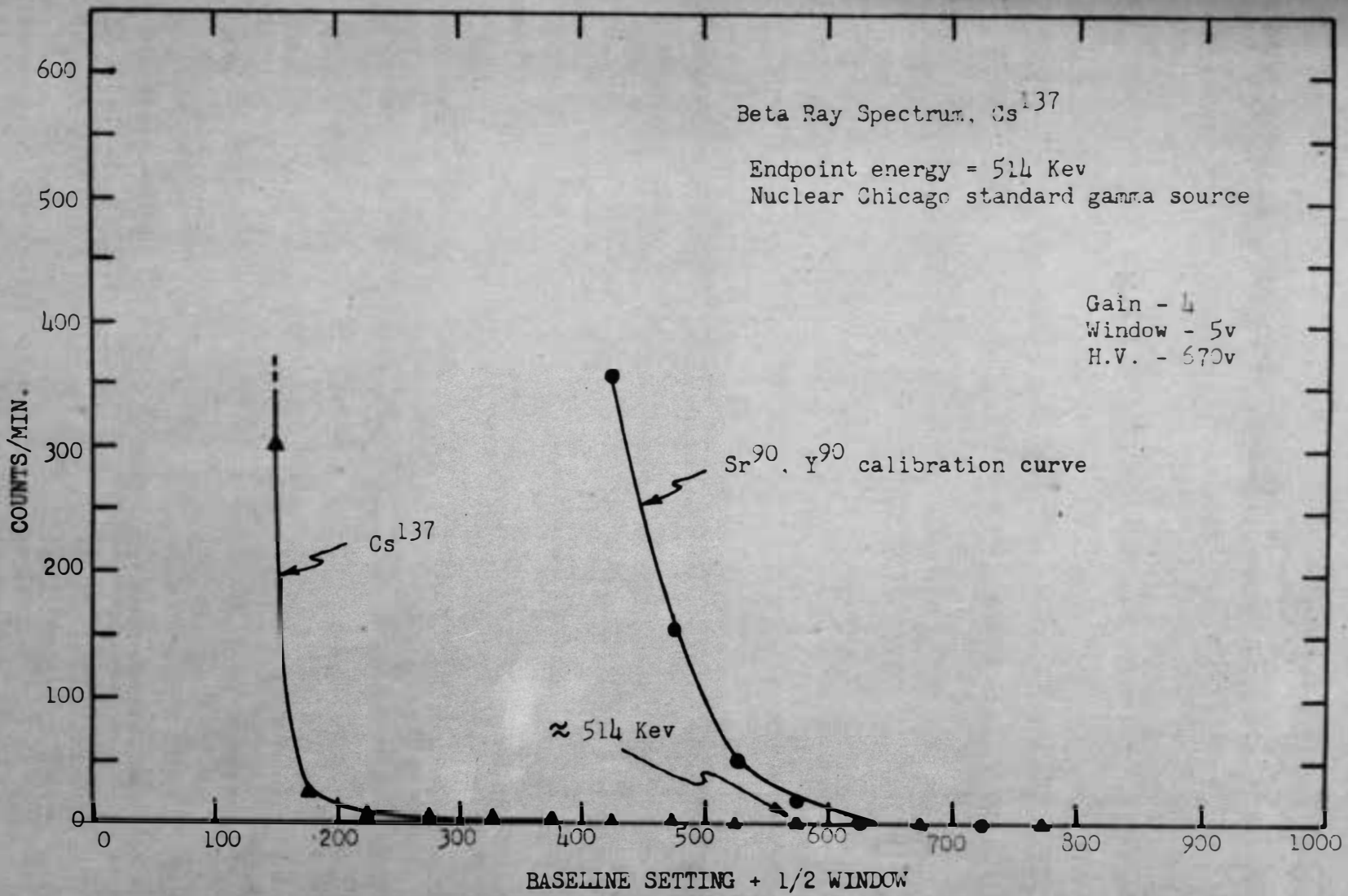

Figure 32. Cs^{137} beta ray spectrum with radiation incident upon 1.5 in. dia. by 3/16 in. thick anthracene crystal.

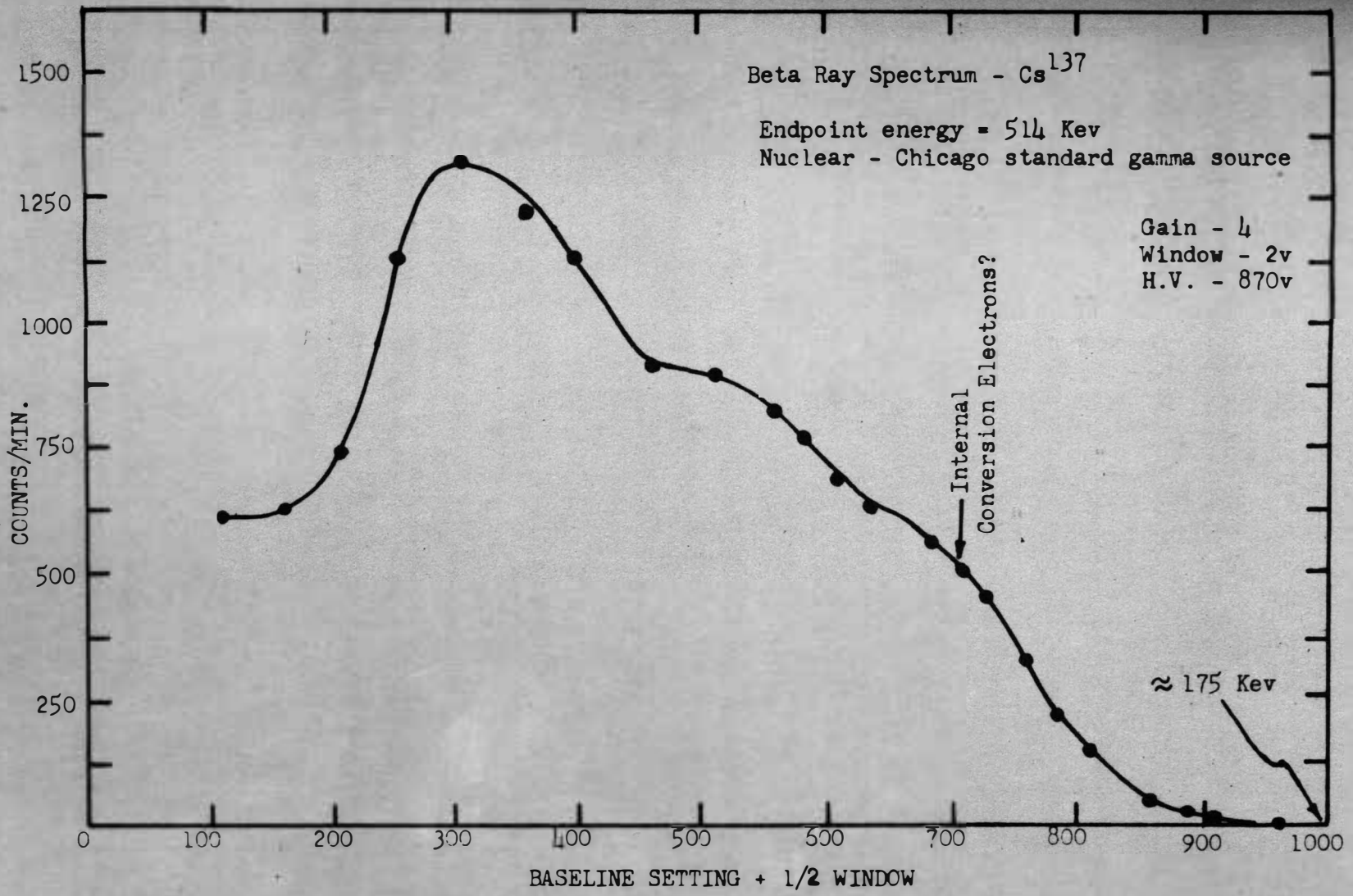

Figure 33. Cs^{137} beta ray spectrum at high gain. Radiation incident upon 1.5 in. dia. by 3/16 in. thick anthracene crystal.

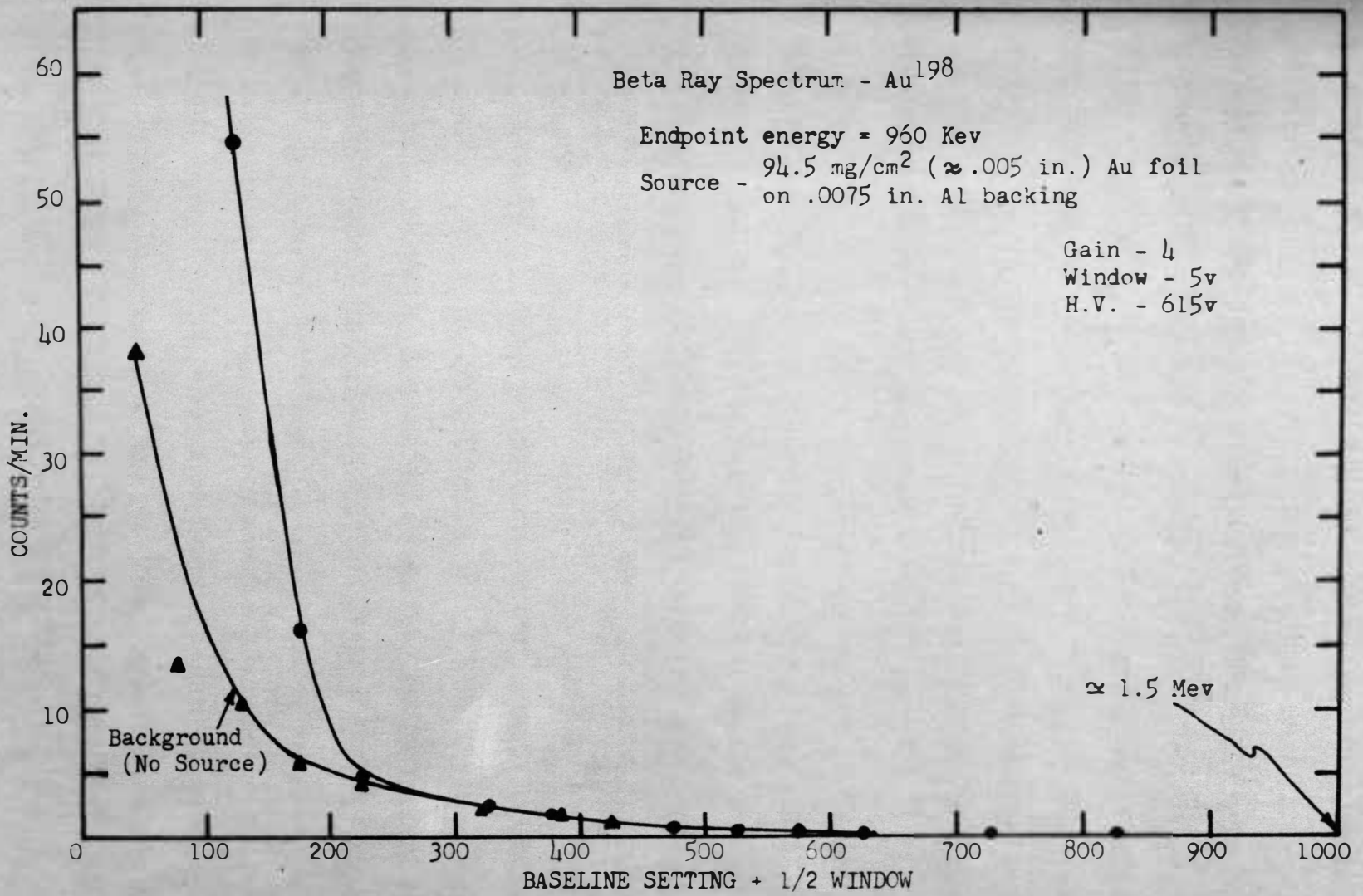

Figure 34. Au^{198} beta ray spectrum with radiation incident upon 1.5 in. dia. by 3/16 in. thick anthracene crystal.

of approximately 200. In part, the deviation from known form probably results from use of a relatively thick source by beta-ray spectrometry standards. However, the Au^{198} source has a relatively large surface area; hence, a significant number of higher energy beta rays with little or no energy loss should have been detected by the crystal. Since no counting above background was in evidence for baseline settings near 600, it is possible that the anthracene crystal is not of sufficient thickness for proportional conversion of high energy beta rays.

Scattering by the source backing can also lead to error in the observed beta spectrum. For example, it has been reported in the literature that the beta counting rate is increased by as much as 60%[28] because of backscatter from a thick lead backing.

Future Beta Ray Spectra

It is evident from the preceding discussion that the preparation of a beta source is much more critical than is the case for a gamma ray source. While the source utilized for present beta-gamma coincidence experiments exhibited no spectrum distortion, future applications will require the use of specially prepared beta sources. The main purpose for beta-gamma coincidence experiments is to determine those gamma rays that are in coincidence with a particular beta branch. If it is experimentally difficult to discern the different

---

[28] M. Deutsch and O. Kofoed-Hansen, Op. cit., p. 439.

beta branches because of a distorted spectrum, then the proper coincidence experiments cannot be performed.

It was pointed out in the preceding discussion that the anthracene crystal may not be of sufficient thickness to stop beta rays with energies greater than approximately 600 Kev. In view of this, a crystal of 1/2 inch thickness has been ordered for future work. This should be of sufficient thickness to stop beta rays with energies of approximately 2 Mev or less.

3. OTHER METHODS OF BETA RAY SPECTROMETRY

It was mentioned at the beginning of this chapter that a number of methods for obtaining beta ray spectra were of interest. Those methods, other than scintillation techniques, that merited further study with respect to project requirements are discussed below. Since many of these methods utilize the same devices that are employed in gamma ray spectrometry, the reader is referred to Chapter I, section 5, for the discussion of these devices. The ensuing discussion consists mainly of evaluation of these methods with respect to current experiments.

Beta Ray Energy Determination by Range Measurements

Energy measurements for beta rays can be made by using a calibrated absorber as in the case for gamma rays. However, the path of the beam through the absorber is not straight but exhibits a tortuous track with considerable branching from the main track.

Subsequently, the actual track length of a beam in a cloud chamber or in an electron-sensitive emulsion is normally measured and correlated with an energy by an empirical range-energy relationship. This method has poor resolution because of the variable nature of the branching.

Cloud chamber and emulsion techniques are also used for electron energy measurement in another method. In this case, the total number of droplets or grains along the track are counted. Since the droplet count in a cloud chamber should in principle yield the total number of ion-pairs formed, one can determine the total energy expended from a knowledge of the energy necessary to create an ion-pair. The total number of grains along a track in an emulsion is known to be a function of electron energy. However, correlation of total grains developed with electron energy is complicated since the energy loss per grain depends on electron energy and emulsion composition.

The above methods are not normally used for beta spectra analysis because of their low resolution and their tedious experimental procedure. They are used extensively in high-energy experiments with cosmic rays and accelerators, since other methods do not extend to this range, or are not convenient to use.

Electron Magnetic Spectrometer Analysis

Magnetic spectrometer analysis of electrons has already been discussed in Chapter I. In summary, the resolution for magnetic

spectrometers is superior to that obtainable with other methods; thus, magnetic spectrometers are normally used where high precision measurements are necessary. However, the poor transmission for magnetic spectrometers limits their use to analysis of sources with high activity. Furthermore, the experimental equipment is cumbersome since analysis must be done in a vacuum.

Gas-Filled Proportional Counters

Gas-filled proportional counters are frequently used for detection of beta rays with energies of approximately 1 Mev or less. However, detection at the higher energy end is possible only if gas pressures on the order of 50 atmospheres are used and if the counter is placed in a magnetic field of a few thousand gauss. The high pressures result in high operating voltages and extreme requirements on gas purity. Furthermore, instrumental corrections are of paramount importance at the higher energies.

The gas-filled proportional counters have an advantage over scintillation counters whenever the electrons to be analyzed have very low energies. Gas-filled counters have been used with acceptable resolutions at energies as low as 250 ev while the scintillation counters have acceptable resolutions only above 20 Kev.

Semiconductor Detectors

Lithium-drifted semiconductor detectors may be of great utility in the future for high resolution beta ray spectroscopy. Resolutions

of 0.5% to 1.0% at 200°K have been obtained with 600 Kev electrons.[29] These compare favorably with values obtained with medium resolution magnetic spectrometers. Semiconductor detectors have an advantage over magnetic spectrometers in that they are more amenable to convenient experimental arrangements. Also, they can be used with sources of somewhat lower activity than those used with magnetic spectrometers.

Semiconductor detectors have the disadvantage that the sensitive area of beam interception is small. Thus, their use for analysis of sources with low activity is questionable. Semiconductor detectors have a further disadvantage in that they must be cooled to dry ice and liquid nitrogen temperatures for many applications.

---

[29] Practical Guide to Semiconductor Detectors, Technical Measurement Corporation, North Haven, Conn., 1965.

CHAPTER III

COINCIDENCE COUNTING EXPERIMENTS

If a source has rather complex beta ray and gamma ray spectra, then it is desirable to discern the various beta-gamma and gamma-gamma coincidences that exist. Detection of these coincidences facilitates construction of an energy level scheme for the nucleus under study. Hence, an experimental investigation of present equipment capability for detection of the above coincidences was in order, and the pertinent experiments and results are discussed below.

The basic experimental arrangement for beta-gamma and gamma-gamma coincidence counting experiments is shown in block form in Figure 35. Two separate detector chains are utilized and in the case of beta-gamma coincidence counting, the beta crystal is coupled to the single channel analyzer (S.C.A.) chain. This arrangement was chosen since it is desirable to use multi-channel analysis for all gammas in coincidence with a particular beta branch. Furthermore, the present beta crystal cannot be coupled to the multi-channel analyzer (M.C.A.), since it was made by a different manufacturer and its preamplifier output does not match the M.C.A. circuitry. The M. C. A. contains the necessary coincident gate circuitry; hence, the S.C.A. output must be used to produce the gate pulse for the M.C.A. coincidence input. The waveshape required for the coincidence gate input is shown in Figure 36a. The waveshape for the S.C.A. outputs are shown in Figure 37. It is evident that the S.C.A. outputs do

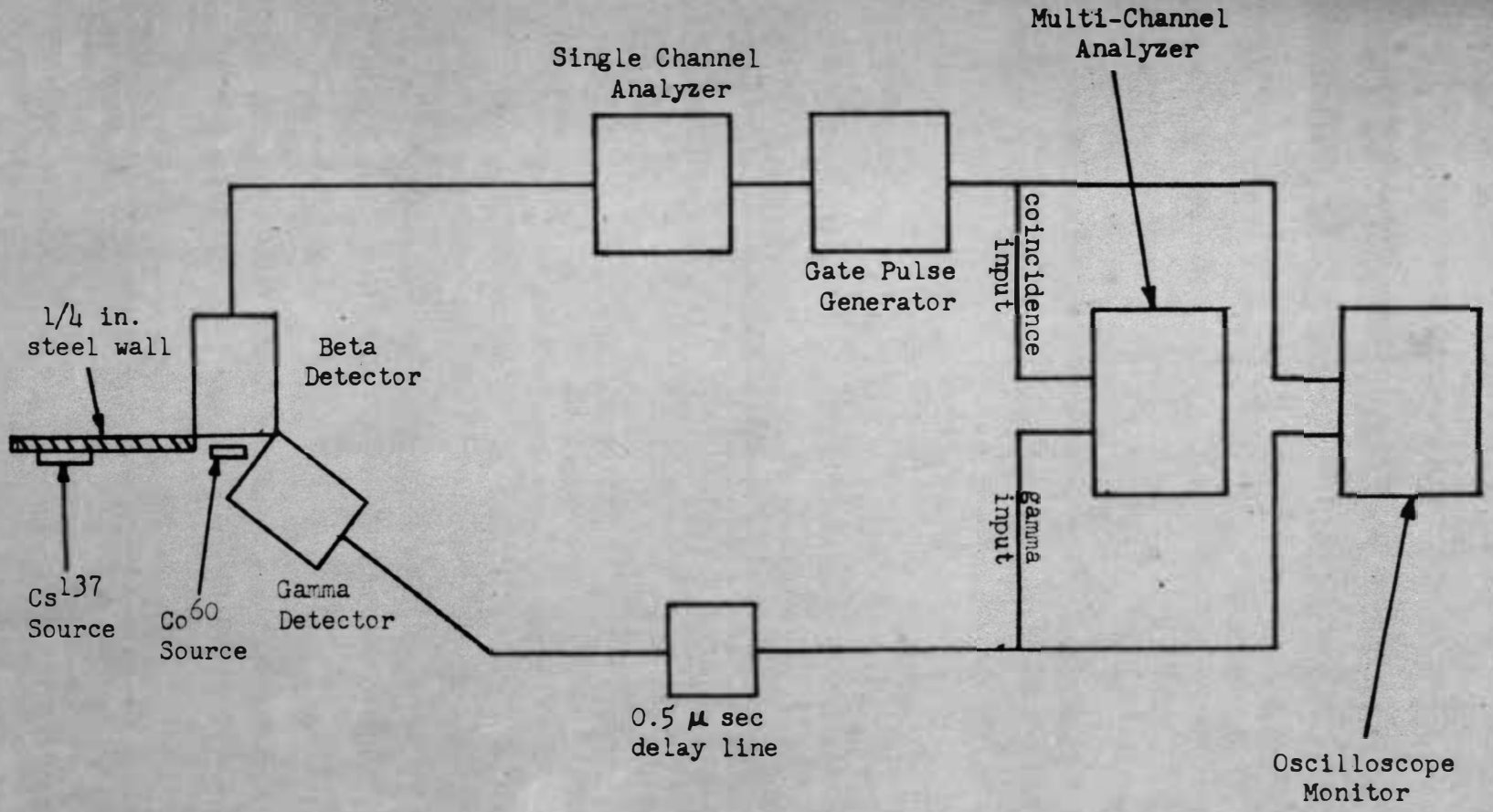

Figure 35. Block diagram of experimental coincidence detection system.

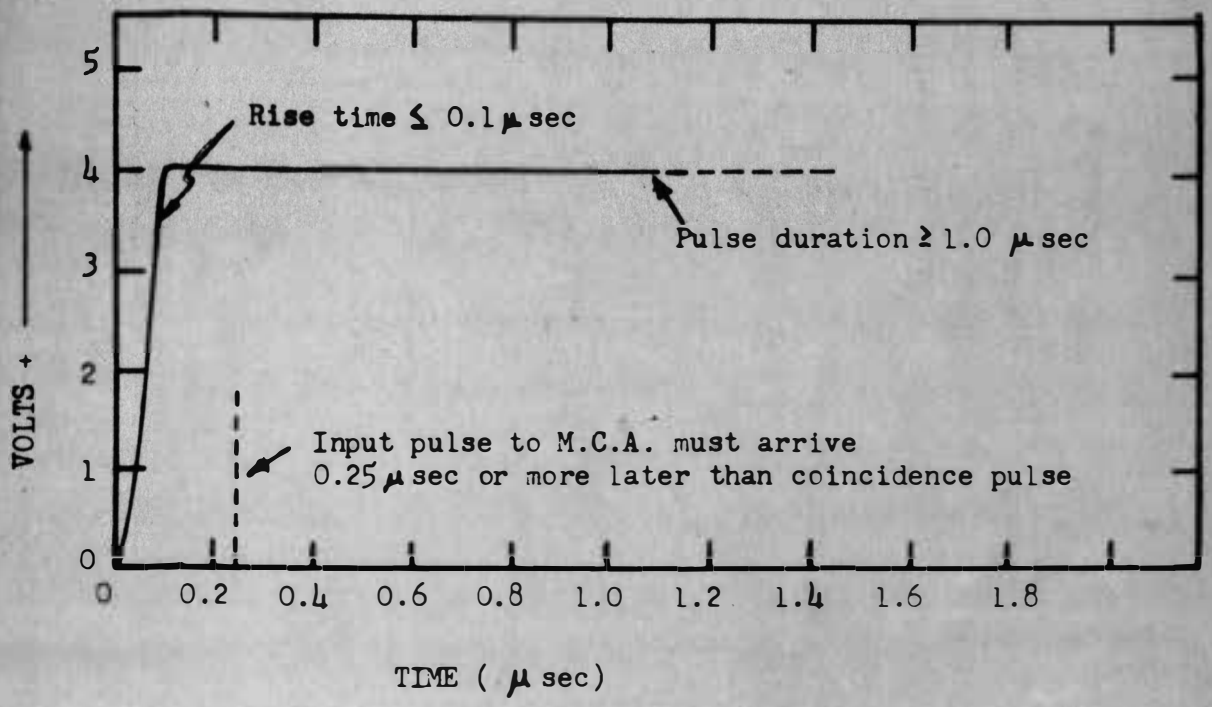

Figure 36a. Waveshape requirement for multi-channel analyzer coincidence gate pulse.

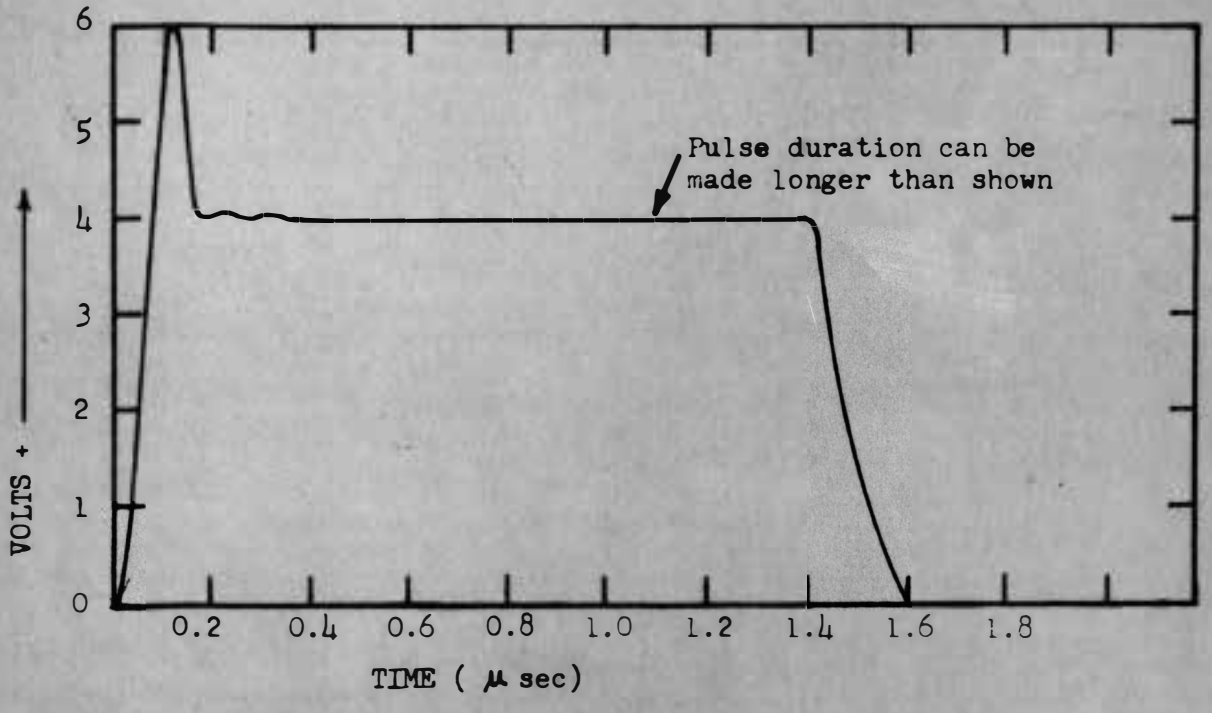

Figure 36b. Output pulse from 535 Tektronix oscilloscope gate pulse generator after voltage amplitude adjustment. Pulse generator triggered by single channel analyzer outputs shown in Figure 37.

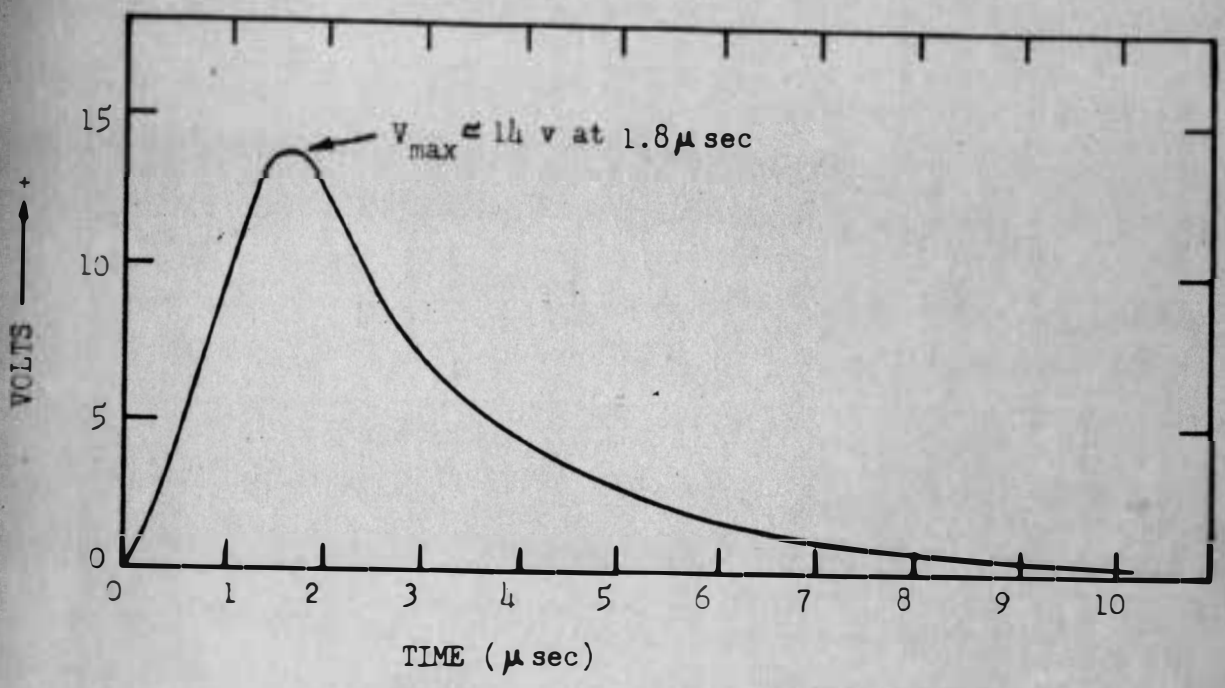

Figure 37a. Window output (C.R. out) pulse of single channel analyzer.

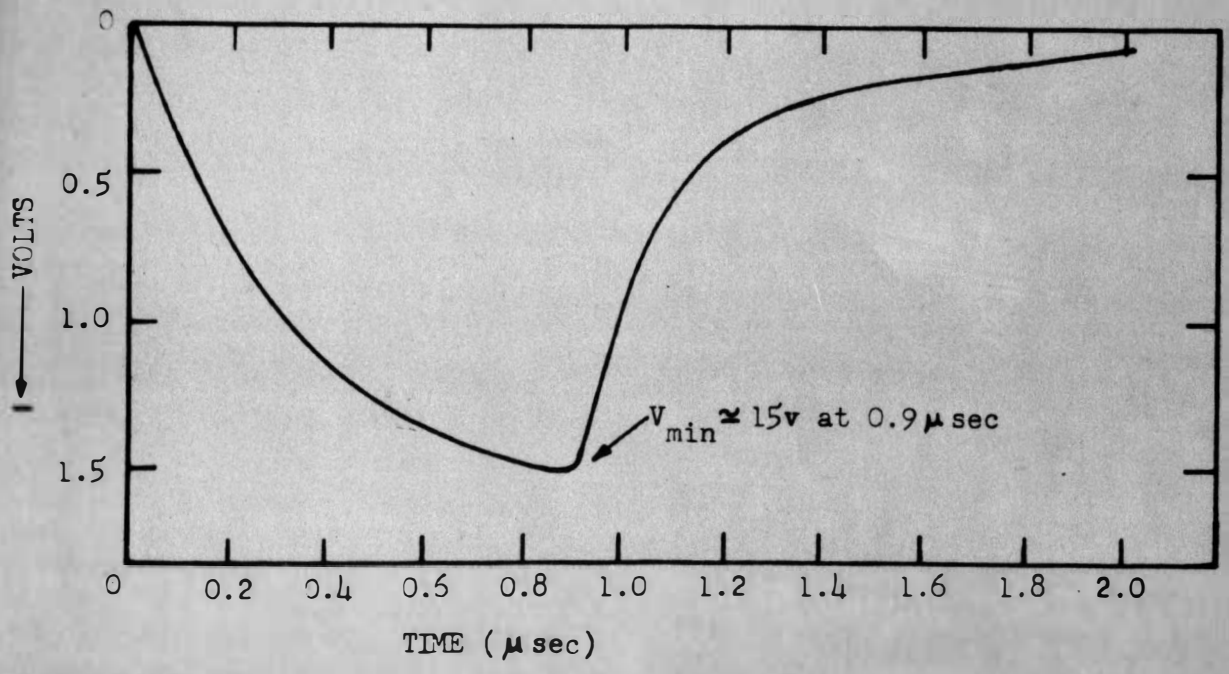

Figure 37b. Integral output (Int. out) pulse of single channel analyzer.

not have the required waveshape; hence, they are used to trigger the square wave gate pulse generator of a 535 Tektronix 535 oscilloscope. The 535 gate pulse after voltage amplitude adjustment is shown in Figure 36b. This pulse meets the coincidence input requirements, but has an extraneous spike on the pulse front that results from improper impedance matching. The spike is of no significance with regard to coincidence detection; however, it should be removed for future experiments since it gives rise to "noise" counts in the M.C.A. channels. Also, if the spike exceeds approximately 10 volts, then it interferes with the normal operation of the pre-set timer and data print-out. A variable time delay is used for the gamma detector input to the M.C.A. for reasons that are discussed below. A 546 Tektronix oscilloscope is used to monitor the input pulse shapes and timing.

1. BETA-GAMMA COINCIDENCE COUNTING

A simple experiment was devised to test the capability of the above arrangement for detection of beta-gamma coincidences. Here, a Co^{60} source was placed between the gamma and beta detectors to provide the necessary beta-gamma coincidences. A Cs^{137} source was also used to provide gammas that were definitely not in coincidence with the Co^{60} betas. The geometry for each source was adjusted until the counting rates for Co^{60} gammas and Cs^{137} gammas were approximately equal when no coincidence requirements were imposed on the Co^{60} gammas. The equality is evident in the composite "singles" spectrum shown

in Figure 38. Also, the Cs^{137} source was shielded from the beta crystal by air and 1/4 inch steel plate. This reduced the beta crystal counting rate due to Cs^{137} alone to nearly background.

No beta-gamma coincident counting was evident in the above experiment for Co^{60} when the S.C.A. window output was used to trigger the 535 gate pulse. Since the betas and gammas from Co^{60} are definitely emitted in coincidence, the lack of observed coincidences must have been due to electronic difficulties. These difficulties were the consequence of two circumstances:

1) The coincidence circuitry requires that all gamma pulses arrive at least 0.25 microseconds later than the corresponding beta gate pulse.
2) The coincidence gate pulses actually arrived from 1.3 to 1.5 microseconds later than the corresponding gamma pulses as shown in Figure 39.

The time delay mentioned in (2) was caused mainly by an inherent delay in the S.C.A. circuitry. The delay, approximately 1.0 microsecond in duration, is introduced by the method of pulse height analysis. Subsequently, no further experiments using the S.C.A. window output were performed since the longest time delay available for gamma pulses was 0.5 microseconds.

The beta-gamma coincidence experiment described above was performed with the S.C.A. integral output triggering the 535 coincidence gate pulse. Here the baseline was set at 220 (see Figure 29) to exclude low energy counts, all of which may not have been caused

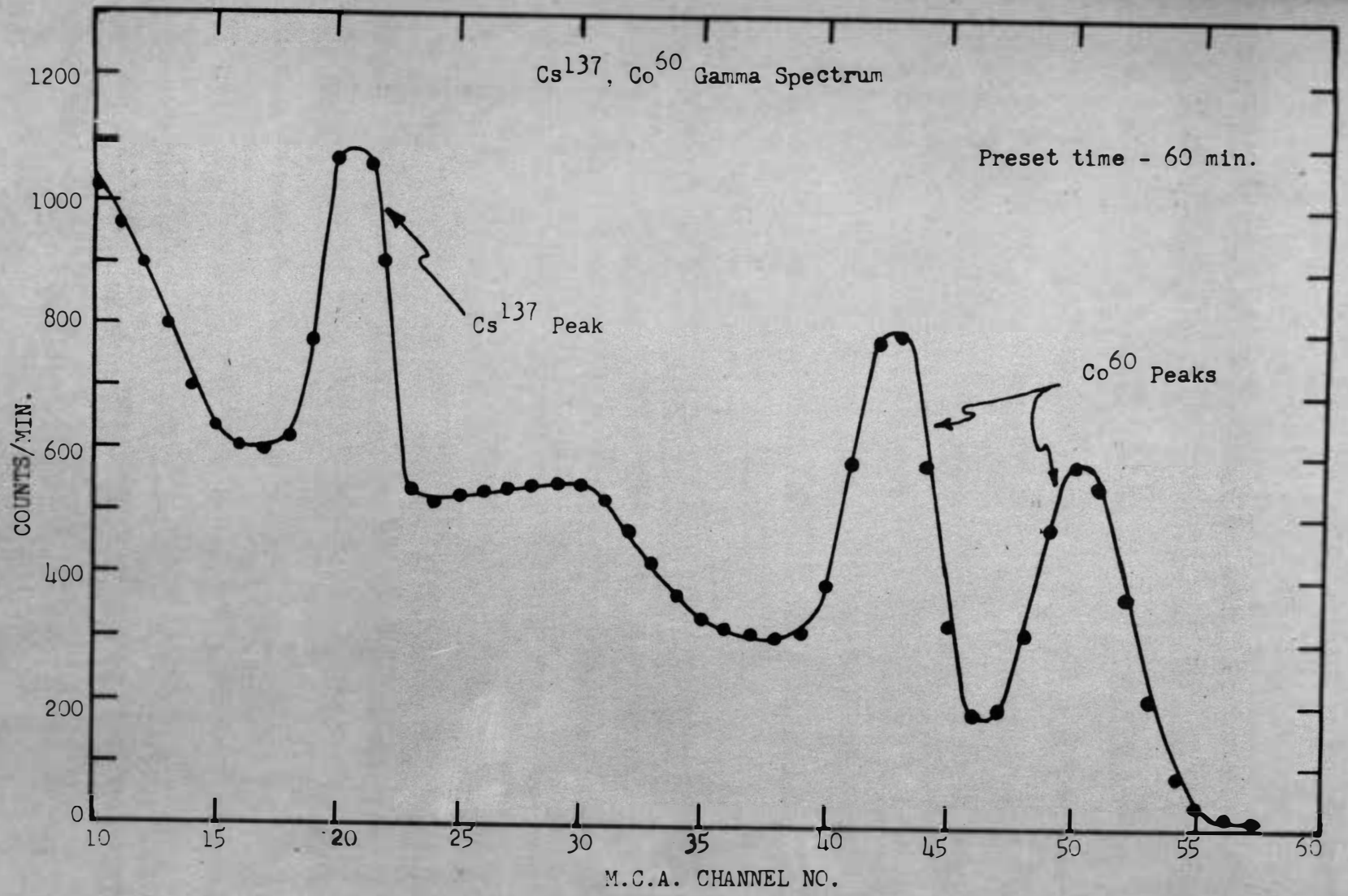

Figure 38. Composite singles gamma spectrum for Co^{60} and Cs^{137} sources used for beta-gamma coincident experiments. Gammas detected by 1.75 in. x 2.0 in. NaI crystal.

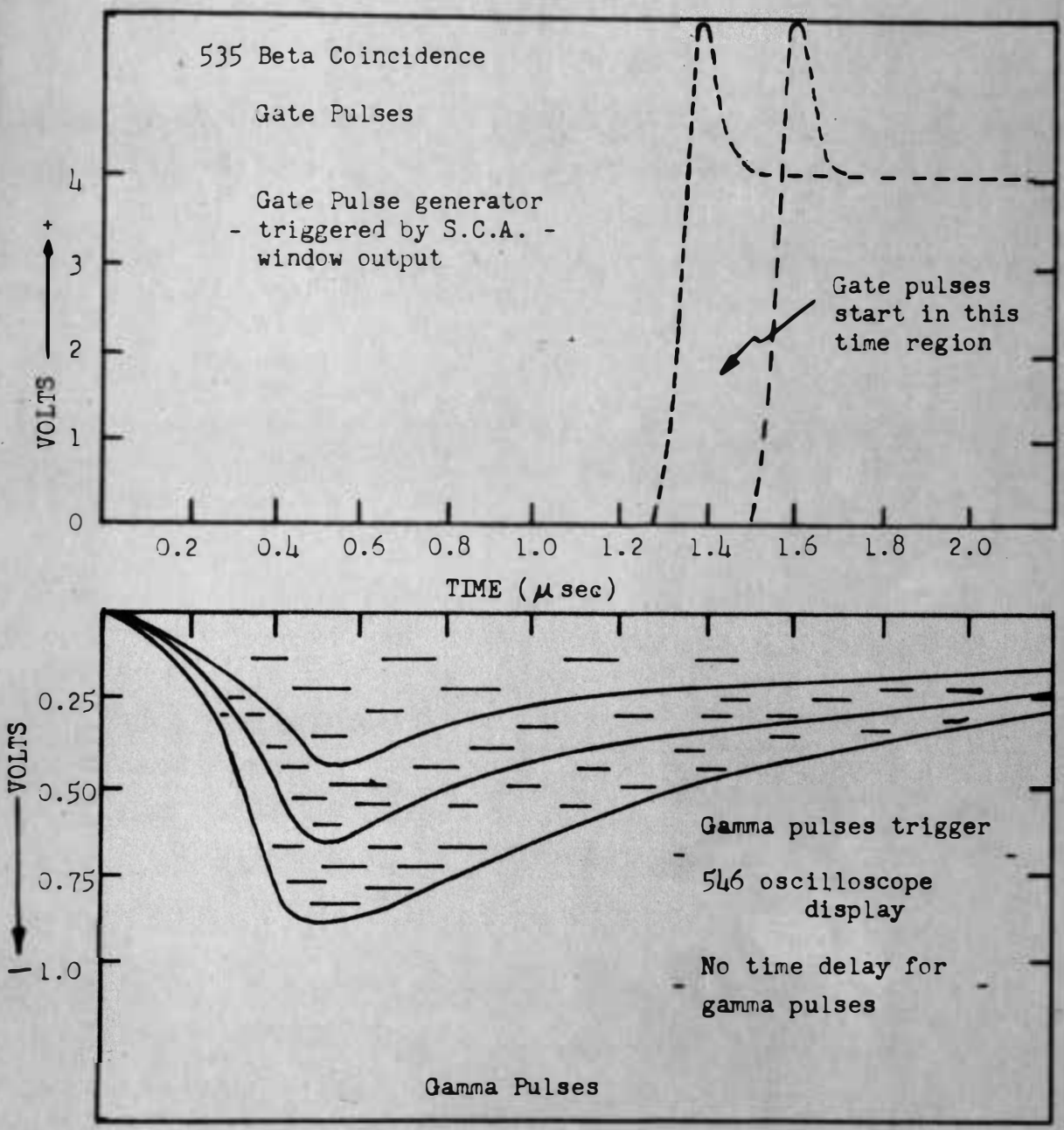

Figure 39. Comparison of the 535 beta coincidence gate pulse triggered by the single channel analyzer window output with undelayed gamma signals from 1.75 in. by 2.0 in. NaI crystal.

by Co^{60} betas. The S.C.A. integral output does not have the inherent time delay problem discussed previously, since pulses appearing at this point in the circuit are those that exceed the baseline setting but have not yet been analyzed. However, the integral output was used here only to permit further study of the coincidence counting apparatus. In actual application where a source may have several beta branches with continuous spectra, it will be mandatory to use the window output in order to discriminate among the beta branches.

Some coincident counting was indeed evident when the gamma pulses were delayed 0.5 microseconds. The spectrum for the gammas in coincidence with Co^{60} betas is shown in Figure 40. Ideally, the coincidence spectrum should exhibit complete suppression of the Cs^{137} gamma peak, except for random coincidences, and exhibit counting rates for the Co^{60} gamma peaks that are approximately 25% of the counting rates noted in the singles spectrum of Figure 38. The Cs^{137} peak is indeed suppressed in the coincidence spectrum of Figure 40. However, the Co^{60} gamma counting rates were much less than expected.

The possibility that the Co^{60} peaks in Figure 40 were due to random coincidences was ruled out, since the Co^{60} and Cs^{137} source geometries were initially adjusted to yield approximately equal counting rates at the gamma detector. Hence, a Cs^{137} peak of nearly the same height as the Co^{60} peaks would appear also in Figure 40 if the Co^{60} peaks were caused by random coincidences alone. Furthermore, a calculation of the number of random coincidences that occur was made by utilizing the equation

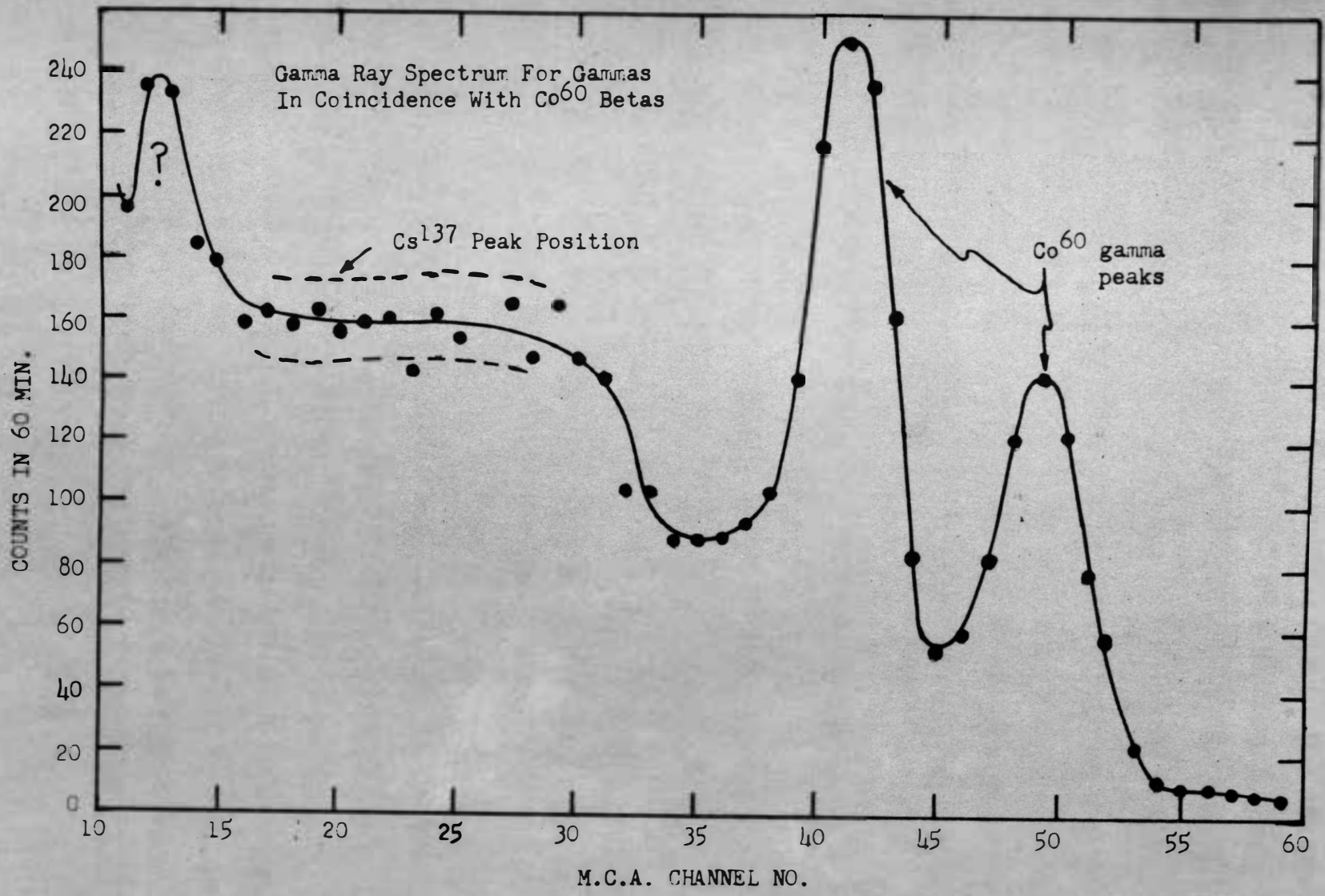

Figure 40. Gamma ray spectrum for gammas in coincidence with Co^{60} betas. 1.75 in. x 2.0 in. NaI gamma crystal views both a Co^{60} and a Cs^{137} source.

$$C_R = \tau \bar{N}_B \bar{N}_\gamma$$

Here C_R is the number of random coincidences per second, τ is the time in seconds during which the coincidence circuit accepts pulses, $\bar{N}_B$ is the average value of the observed counts/sec. at the beta detector, and $\bar{N}_\gamma$ is the average value of the observed counts/sec. at the gamma detector. Representative numbers for this experiment were: $\bar{N}_B$ = 70 counts/sec; $\bar{N}_\gamma$ = 50 counts/sec; and τ = 1.25 microseconds. Substitution of these numbers in the above expression yielded 16 counts/60 min. for the random coincidence counting rate. Note that this is appreciably less than the observed rate for Co^{60} beta-gamma coincidences in Figure 40. Also, the number of random coincidences between Cs^{137} gammas and Co^{60} betas was determined experimentally. The data shown in Figure 41 was obtained by viewing the Cs^{137} source with the gamma detector only and the Co^{60} source with the beta crystal only. One could expect that this was the random coincidence counting rate for Co^{60} gammas as well, since the counting rates for the two sources at the gamma detector were approximately equal.

An investigation of the rather slow coincidence counting rate was performed, since the 0.5 microsecond delay for gamma pulses was more than sufficient to meet the 0.25 microsecond lag requirement mentioned previously. An oscilloscope display revealed that the beta gate pulses occurred in a time period from 0.1 microsecond behind to approximately 0.15 microseconds ahead of the gamma pulse as is shown in Figure 42. This extra time delay beyond that inherent

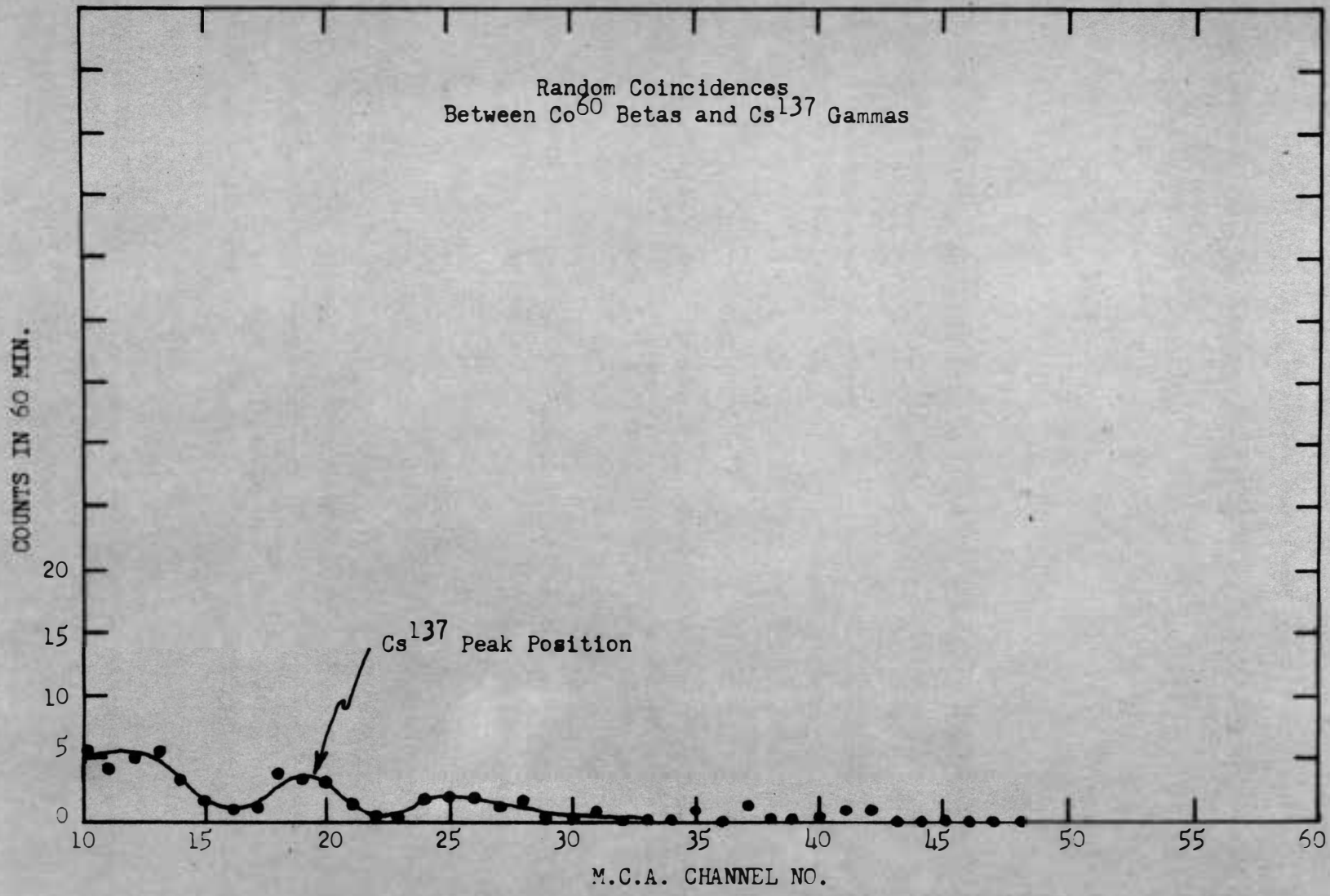

Figure 41. Random coincidence spectrum with Co^{60} viewed by only the beta detector and Cs^{137} by only the gamma detector. Gamma crystal was 1.75 in. x 2.0 in. NaI crystal.

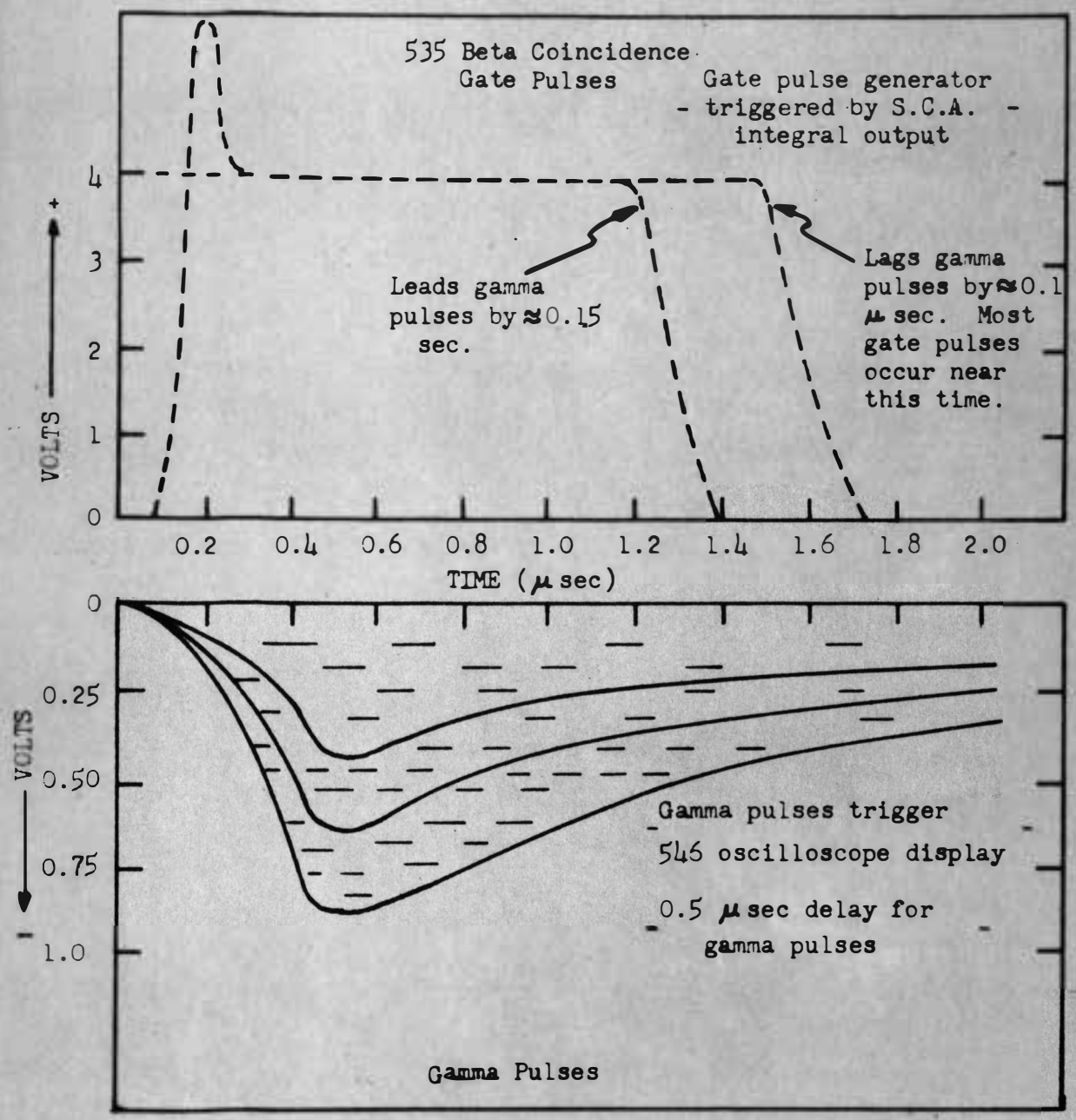

Figure 42. Comparison of the 535 beta coincidence gate pulse triggered by the single channel analyzer integral output with delayed gamma signals from 1.75 in. by 2.0 in. NaI crystal.

delay discussed previously was mainly the result of two factors:

1) Approximately 0.1 microsecond is necessary for the beta pulse front to rise to baseline voltage. This case is illustrated in Figure 43.
2) The start of the 535 oscilloscope gate pulses after arrival of the S.C.A. integral output pulses is variable and can be delayed more or less by adjustment of the 535 triggering level. The gate pulses lag by 0.2 microseconds or more as shown in Figure 44.

The first factor could not be rectified since it arises from the method of pulse shaping for the S.C.A. linear amplifier. The time lag caused by the second factor could only be minimized by proper adjustment of the 535 triggering level. Here, drift in the triggering level was not helpful.

In summary, beta-gamma coincident counting for Co^{60} was definitely observable if the integral output of the S.C.A. was used to trigger the 535 gate pulse generator. However, the counting rate was much less than expected, and the slow counting rate was the result of time delays inherent in the S.C.A. and the method of gate pulse generation. Hence, the difficulty here was pulse timing, as was the case for experiments utilizing the S.C.A. window output. The remedy is the same for both cases; more time delay of the gamma pulses is necessary.

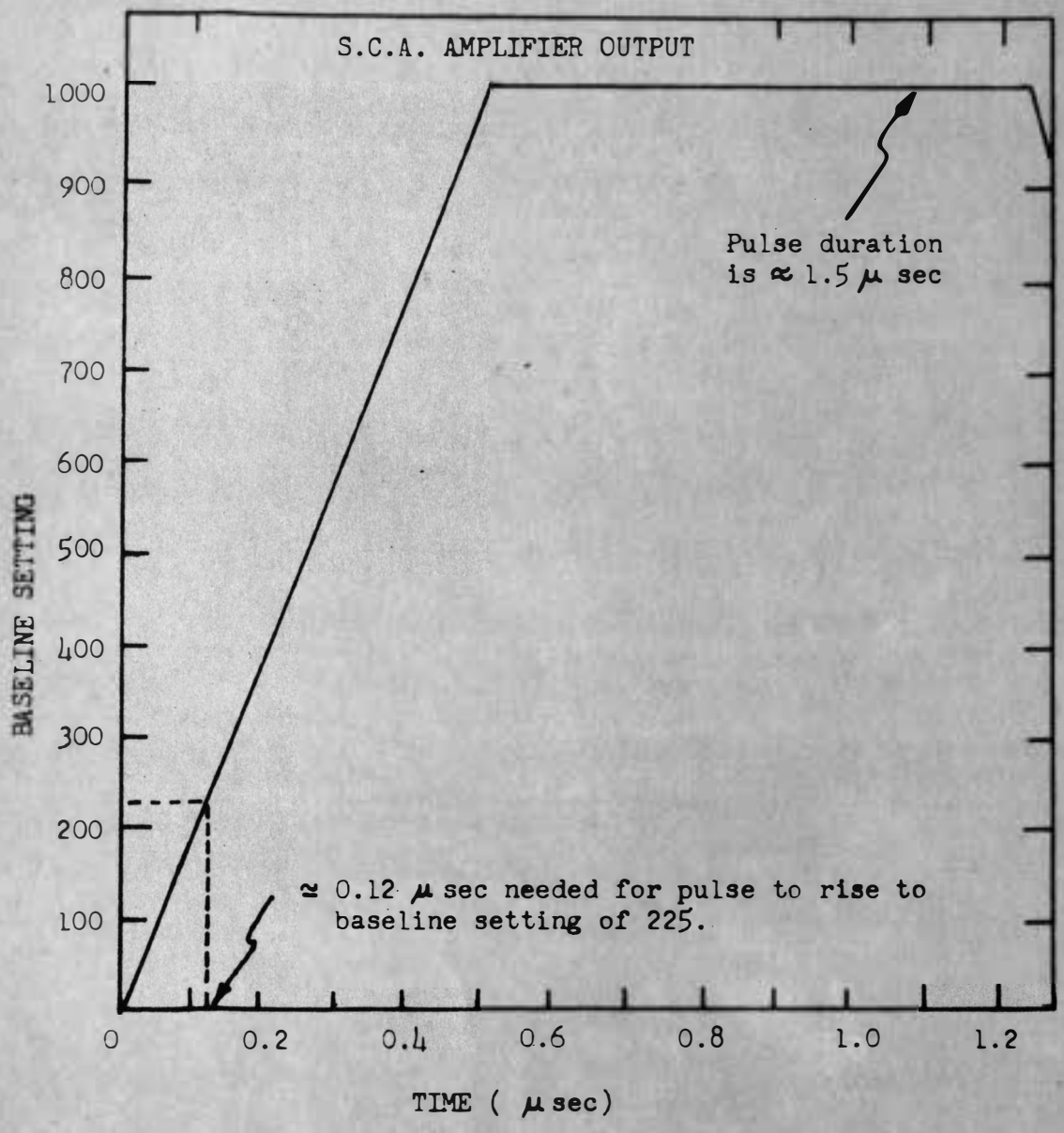

Figure 43. Illustration of output pulse waveshape for linear amplifier of single channel analyzer.

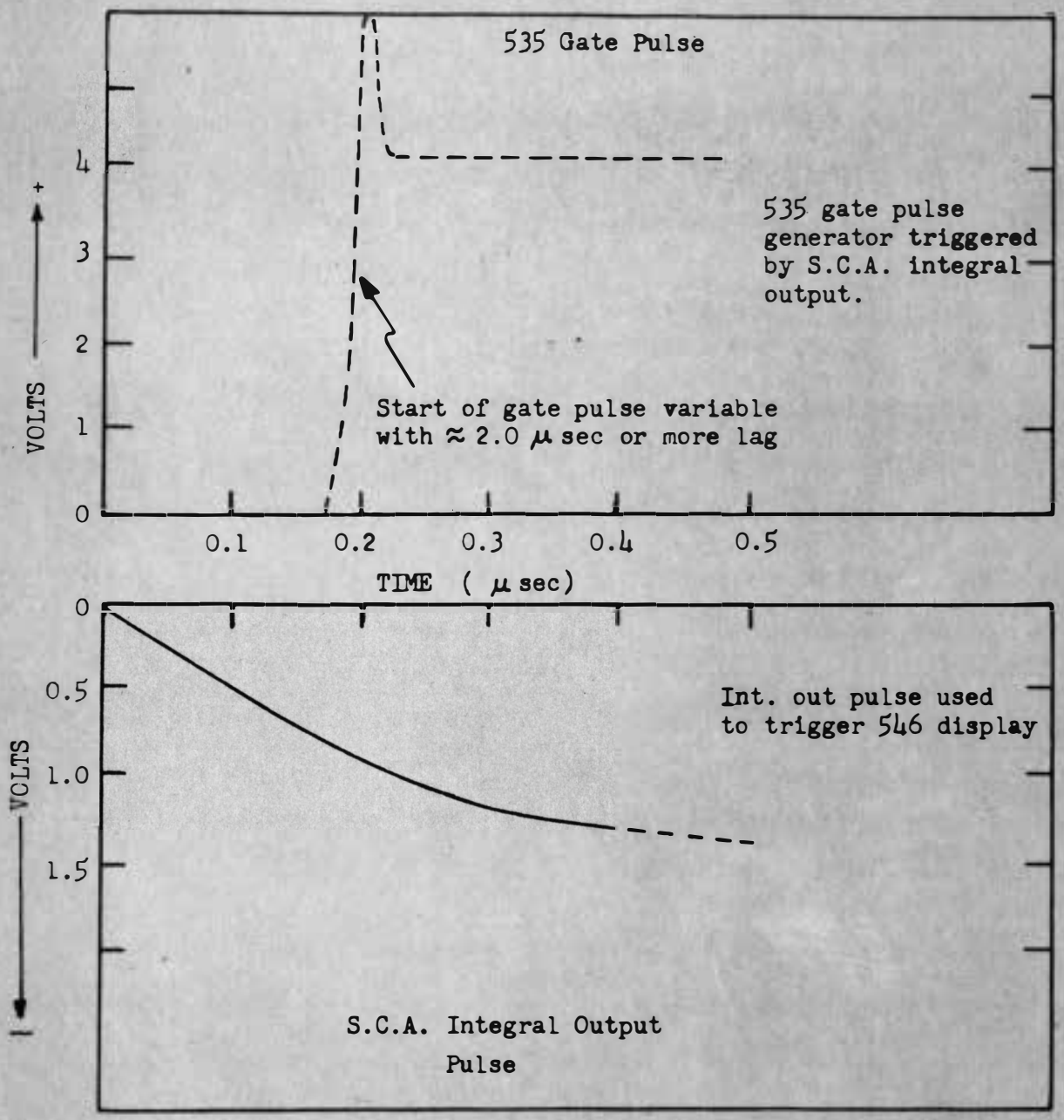

Figure 44. Comparison of 535 beta gate pulse triggered by the S.C.A. integral output pulse with the S.C.A. integral output pulse.

2. GAMMA-GAMMA COINCIDENCE COUNTING

For gamma-gamma coincidence counting, it is necessary to use the window output of the S.C.A. in order to select a given gamma ray and discern the gammas in coincidence with it. Hence, no experiments of this nature were performed because of the previously mentioned time delay in the S.C.A. window output.

Angular correlation experiments fall under the general heading of gamma-gamma coincidence counting. Consequently, no experiments of this nature have been performed thus far. Here, it is also necessary to accurately position one detector at given angles with the other detector, and a device to accomplish this has not been designed and built thus far.

3. FUTURE COINCIDENT COUNTING EXPERIMENTS

A variable time delay of sufficient magnitude has been ordered such that the S.C.A. window output can be used in the coincidence arrangement described above. The extra delay for the gamma pulses coupled with possible minor modifications in gate pulse generation should permit acceptable coincidence counting for future applications.

Another more elaborate coincidence scheme, termed slow-fast coincidence counting, is often used where short coincidence resolving times are necessary. A typical slow-fast coincidence counting system is shown in block form in Figure 45. Part of the necessary circuitry for this type of system is presently available at S.D.S.U. in the form of two-channel coincidence analyzer built by Tracerlab. The

above system, or some variation of this system, merits further study for future experiments.

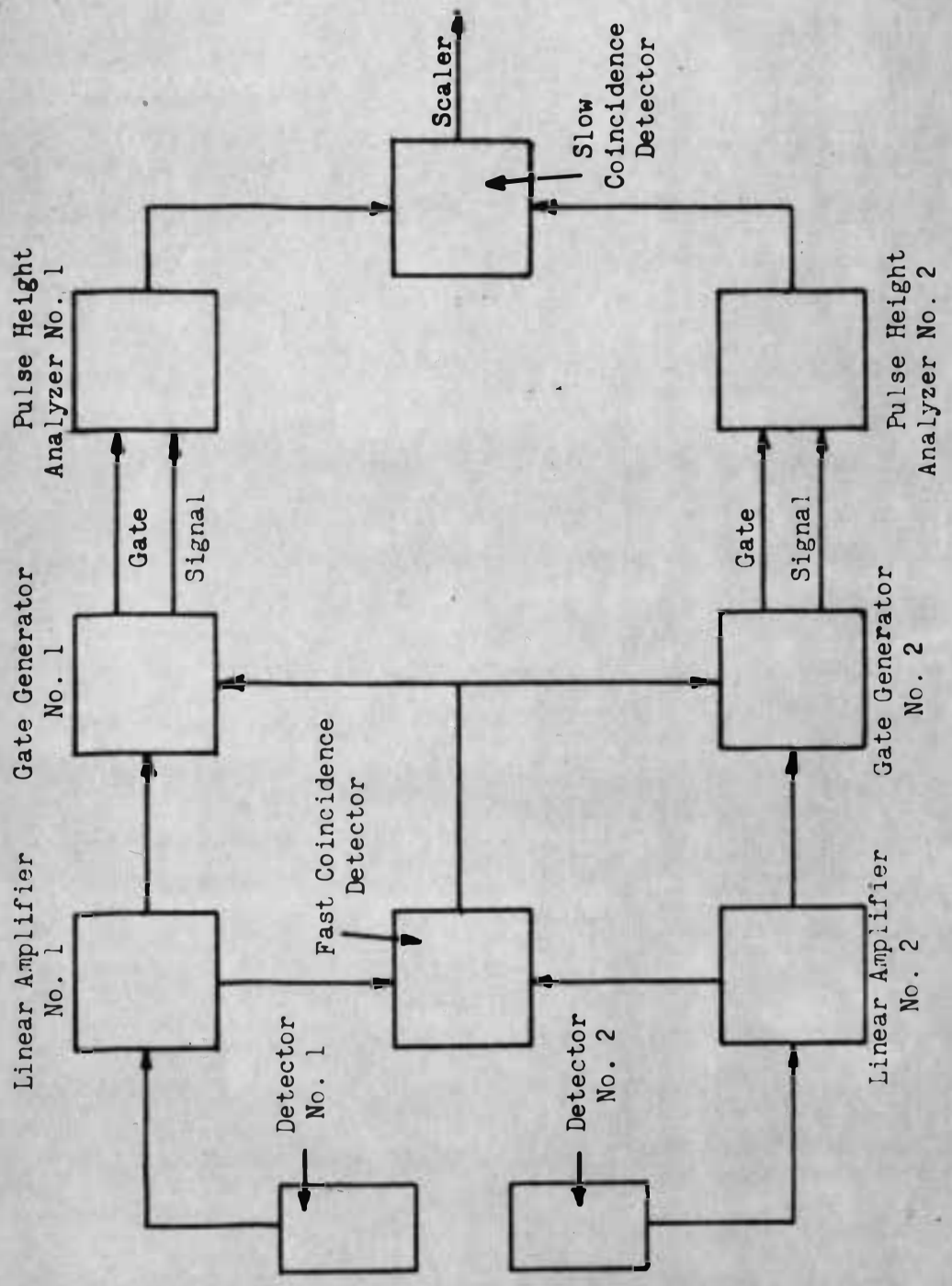

Figure 45. Block diagram of typical fast-slow coincidence system.

CHAPTER IV

FUTURE APPLICATIONS

Three isotopes have been considered for study with the experimental methods described in the first three chapters. They are Gd^{162}, Nd^{152}, and Yb^{178}. These isotopes can be produced from the corresponding stable isotopes by double neutron capture. However, this requires a large neutron flux and a large neutron capture cross section for the intermediate isotope in order that the resultant isotope have sufficient activity.

The above isotopes were chosen since the intermediate isotope did have a large capture cross section. Hence, irradiation with a large neutron flux, such as that available in a reactor at Argonne Laboratory, should yield sources with acceptable activity.

Calculations were made concerning the Gd^{162} activity and the major interfering activity after a given irradiation period. These calculations and other work concerning preparations for measurement of the Gd^{162} half-life are discussed in the following section. No calculations have been made thus far concerning the other two isotopes.

1. PRELIMINARY STUDIES FOR Gd^{162}

Gd^{162} Activity Calculation

The double neutron capture reaction that is used to produce Gd^{162} and the accompanying radioactive decay chains are shown below.

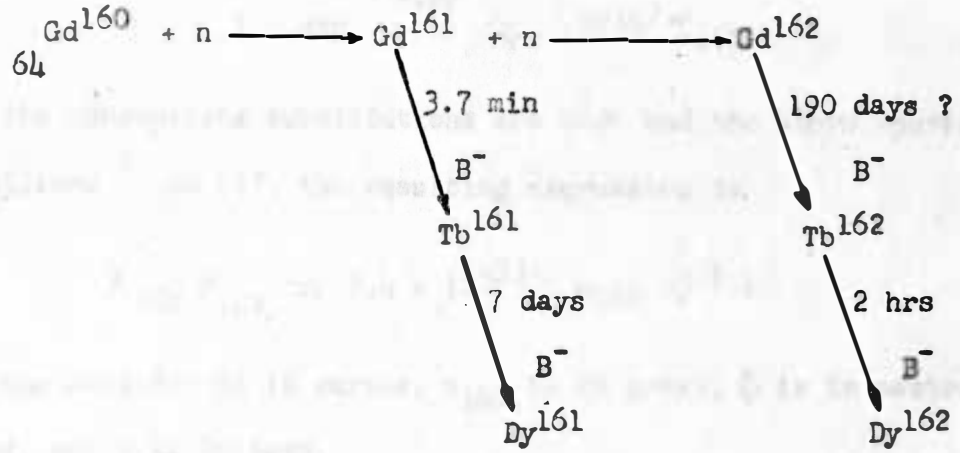

The Gd^{162} activity after a given neutron irradiation period can be calculated from the expression,

$$\lambda_{162} N_{162} = \frac{m_{160}}{A} N_o \phi^2 \sigma_{160} \sigma_{161} \frac{\tau_{161}}{.693} \left(1 - \exp^{\frac{-.693t}{\tau_{162}}}\right) \quad (1)$$

Here $\lambda_{162} N_{162}$ is the Gd^{162} activity, m_{160} is the mass of Gd^{160}, A is the atomic weight of Gd^{160}, N_o is Avagadro's number, ϕ is the neutron flux, σ_{160} and σ_{161} are the neutron capture cross sections of Gd^{160} and Gd^{161} respectively, τ_{161} and τ_{162} are the half lives of Gd^{161} and Gd^{162} respectively, and t is the time of neutron irradiation. The values for the capture cross sections and the Gd^{161} half-life are known: σ_{160} = 0.8 barns; σ_{161} = 10^5 barns; and τ_{161} = 3.7 min. The half-life of Gd^{162} is uncertain[30], but for the purpose of this calculation, τ_{162} = 190 days. Also, t is much less than τ_{162} in practice, and the following approximation can be made.

---

[30] K. T. Faler and J. M. Hollander, University of California Radiation Laboratory 3710, Dec '56 - Feb '57.

$$1 - \exp \frac{-.693t}{\tau_{162}} \approx .693t/\tau_{162}$$

When the appropriate substitutions are made and the above approximation is utilized in eq (1), the resulting expression is

$$\lambda_{162} N_{162} \approx 9.4 \times 10^{-33} \; m_{160} \; \phi^2 \; t \qquad (2)$$

Here the activity is in curies, m_{160} is in grams, ϕ is in neutrons/cm^2sec, and t is in days.

The source chosen was 100 mg of gadolinium which is 94% enriched in Gd^{160}. The largest neutron flux available in CP-5 reactor at Argonne National Laboratory is approximately 7×10^{13} neutrons/cm^2 sec. For Gd^{160} irradiation, the neutron flux chosen was $\phi = 7 \times 10^{13}$ neutrons/cm^2sec. The irradiation time chosen was t = 1 day. Calculation of Gd^{162} activity according to (2) yields $\lambda_{162} N_{162} = 4.5$ microcuries. This is adequate for use with the detection system described in earlier chapters.

Tb^{161} Activity Calculation

It is necessary to determine the magnitude of the Tb^{161} activity after the chosen irradiation period, since it will be present as a major interfering activity during the study of Gd^{162} decay. The Tb^{161} activity can be calculated from the expression,

$$\lambda_{Tb} N_{Tb} = \frac{m_{160}}{A} N_o \sigma_{160} \phi \left(1 - \exp \frac{-.693t}{\tau_{Tb}}\right) \qquad (3)$$

Here $\lambda_{Tb} N_{Tb}$ is the Tb^{161} activity, τ_{Tb} is the Tb^{161} half-life, and all other symbols have the same significance as previously.

The half-life of Tb^{161} is known, τ_{Tb} = 7 days, and the value of σ_{160} has been specified previously. Equation (3) can then be written in an intermediate form

$$\lambda_{Tb} N_{Tb} = 8.15 \times 10^{-14} \; m_{160} \; \phi \left(1 - \exp^{-.099t}\right) \qquad (4)$$

Here $\lambda_{Tb} N_{Tb}$ is in curies, m_{160} is in grams, ϕ is in neutrons/cm^2sec, and t is in days. When the values previously chosen for m_{160}, ϕ, and t are substituted into (4), the resultant activity is 54 millicuries.

It is evident upon comparison of the Gd^{162} and Tb^{161} activities that the Tb^{161} activity will obscure the Gd^{162} activity for some time after irradiation. But Tb^{161} has a relatively short half life, and the activities will be of the same magnitude after approximately 14 Tb^{161} half lives. For this reason, the source must "cool" for over three months.

Tb^{162} Activity Considerations

It was noted previously that Gd^{162} decays into Tb^{162} which has a half life of approximately 2 hours. Hence, the Tb^{162} activity is nearly the same as the Gd^{162} activity several hours after irradiation. Thus, it will be necessary to chemically separate Tb^{162} from the source periodically in order to temporarily suppress the Tb^{162} activity. An ion exchange separation method[31] has been developed, and it appears

---

[31] Private communication from L. D. Mc Isaac, Phillips Petroleum Co., Idaho Falls, Idaho.

to be sufficient to allow temporary suppression of the Tb^{162} activity.

Gd^{162} Half Life Measurement

The half life of Gd^{162} has been reported in the literature as greater than one year[32], and also as 190 days. Because of this uncertainty, it will be necessary to make an accurate half life measurement for Gd^{162}. In preparation for this task, a procedure was developed for measurement of half lives on the order of one year. This was accomplished by determining the Cd^{109} decay half life for which the accepted value is 470 days. The experimental decay curve for Cd^{109} decay is shown in Figure 46. The corresponding half life was determined to be 473 days. These results indicate that half lives on the order of one year can be measured rather accurately by following the decrease in activity for about 5% of a half life.

Since the decrease in activity during a 3 or 4 day interval is small for one year half-life source, it is mandatory to have good counting statistics. The data points for the Cd^{109} half-life curve represent approximately 450,000 counts. Thus, decreases of approximately 2% in activity can be observed. Fluctuations of the preset timer on the multi-channel analyzer probably caused the significant departure of the first few points from the indicated curve. This

---

[32] Chart of the Nuclides, Knolls Atomic Power Laboratory, Distributed by General Electric Co., Schenectady, New York, 7th edition, Rev to June, 1964.

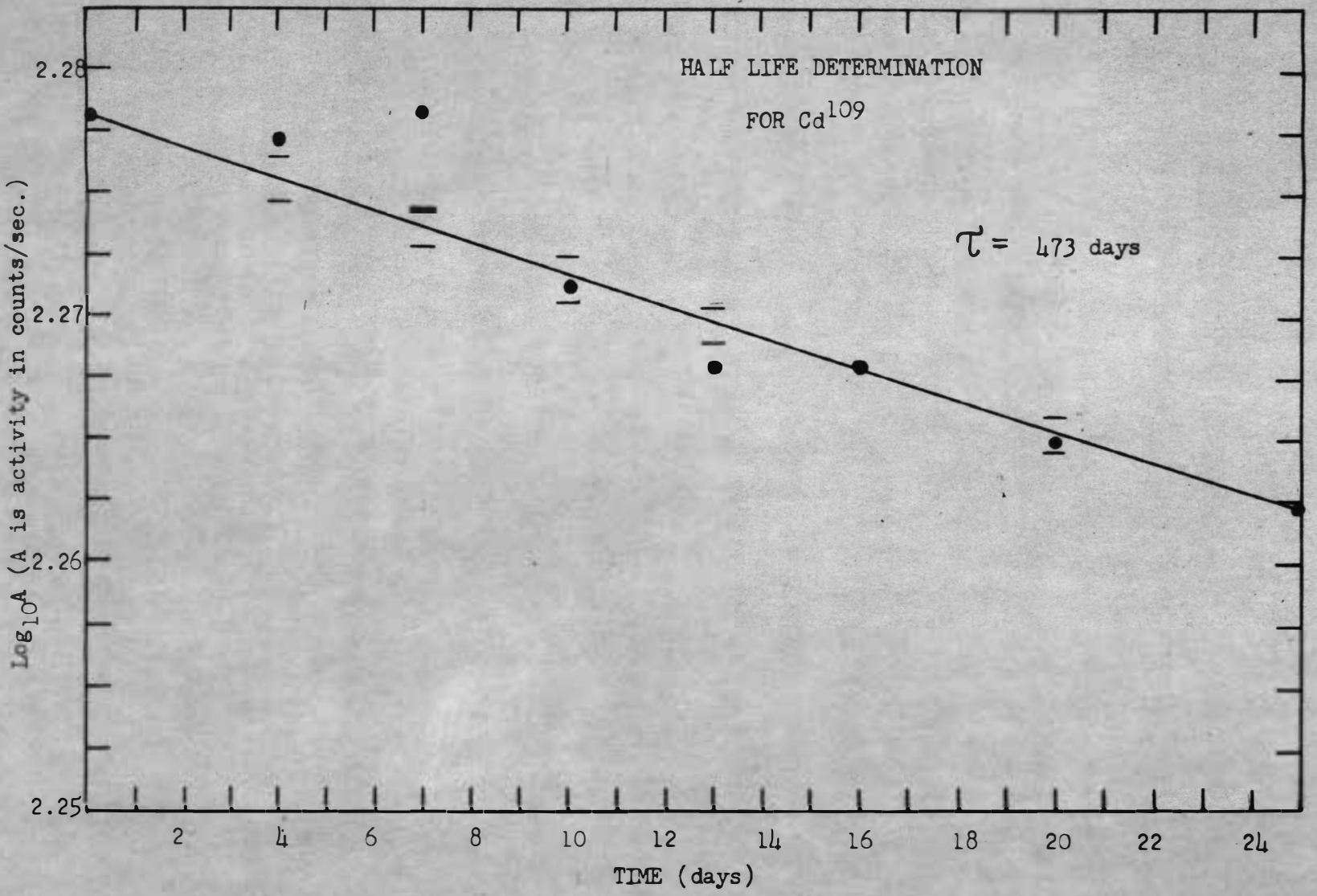

Figure 46. Graph of logarithm of Cd^{109} activity vs. observation time of activity. Curve is used to determine Cd^{109} half life.

problem was circumvented for later data points by plotting the average of three time trials. This will be a desirable procedure for future half life experiments if the source half life and activity permit a member of trials for each data point.

CONCLUSIONS

The experimental method for obtaining gamma ray spectra is satisfactory for future application. This is witnessed by the fact that peak location accuracies and peak resolutions are of the same order as the best values reported in the literature for methods using scintillation crystals.

The experimental method for obtaining beta ray spectra is not completely satisfactory at present. However, satisfactory beta ray spectra can probably be obtained in future applications by using specially prepared thin sources and a thicker anthracene crystal.

Slow rate coincident counting with the single channel analyzer integral output, but so far no coincident counting with the single channel analyzer window output, can be observed with the present coincidence arrangement. Satisfactory coincidence counting can probably be obtained with this arrangement if there is additional time delay of the gamma pulses.

Calculation of the Gd^{162} activity after neutron irradiation indicates that the Gd^{162} activity will be sufficient for experimental purposes. However, high Tb^{161} activity will make it necessary to "cool" the source for over three months.

Half-life measurement experiments indicate that an accurate measurement of the Gd^{162} half-life should be possible by following the activity decrease for about 5% of a half life.

BIBLIOGRAPHY

D. E. Alburger, "The Detection of Gamma Rays and the Measurement of Gamma Ray Spectra", Nuclear Spectroscopy B, Edited by Fay Ajzenberg-Selove, Academic Press, New York, 1960.

R. L. Chase, Nuclear Pulse Spectrometry, McGraw-Hill Book Co., Inc., New York, 1961, Chapters 3, 4, and 5.

C. E. Crouthamel, Beta and Gamma Ray Spectroscopy, Pergamon Press, New York, 1960.

M. Deutsch and O. Kofoed-Hansen, "Gamma Rays", also "Beta Rays", Experimental Nuclear Physics, vol. III, edited by E. Segre, John Wiley and Sons, Inc., New York, 1959.

Harshaw Scintillation Phosphors, The Harshaw Chemical Co., Cleveland, Ohio, 1962.

I. Kaplan, Nuclear Physics, Addison-Wesley Publishing Co., Inc. Reading, Massachusetts, 1963.

Practical Guide to Semiconductor Detectors, Technical Measurements Corp., North Haven, Connecticut, 1965.

W. J. Price, Nuclear Radiation Detection, McGraw-Hill Book Co., New York, 1964.